NASA CR-137844
MDC E1415 VOL. III

NASA CONTRACTOR REPORT

NASA CR-137844
MDC E1415 VOL. III

(NASA-CR-137844) PLANETARY/DOD ENTRY TECHNOLOGY FLIGHT EXPERIMENTS. VOLUME 3: PLANETARY ENTRY FLIGHT EXPERIMENTS HANDBOOK Final Report, 1 Apr. 1975 - 29 Feb. 1976 (McDonnell-Douglas Astronautics Co.) 98 p HC $5.00 CSCL 03B/13

N76-28245

Unclas
47942

PLANETARY/DoD ENTRY TECHNOLOGY FLIGHT EXPERIMENTS

Planetary Entry Flight Experiments Handbook

By H.E. Christensen, R.J. Krieger, W.R. McNeilly and H.C. Vetter

Prepared by

MCDONNELL DOUGLAS ASTRONAUTICS COMPANY — EAST

St. Louis, Missouri 63166 (314) 232-0232

for Ames Research Center

NATIONAL AERONAUTICS AND SPACE ADMINISTRATION ● WASHINGTON, D.C. ● FEBRUARY 1976

NASA CR-137844
MDC E1415 VOL. III
29 FEBRUARY 1976

PLANETARY/DoD ENTRY TECHNOLOGY FLIGHT EXPERIMENTS

COPY NO. 34

Planetary Entry Flight Experiments Handbook

By H.E. Christensen, R.J.Krieger,
W.R. McNeilly and H.C. Vetter

Prepared Under Contract No. NAS 2–8678 by

MCDONNELL DOUGLAS ASTRONAUTICS COMPANY – EAST

Saint Louis, Missouri

for

NATIONAL AERONAUTICS AND SPACE ADMINISTRATION

FOREWORD

This final report was prepared by McDonnell Douglas Astronautics Company-East (MDAC-E) for NASA Ames Research Center Contract NAS2-8678, Planetary/DoD Entry Technology Flight Experiments. It covers the period 1 April 1975 to 29 February 1976. This effort was performed for the National Aeronautics and Space Administration, Ames Research Center, under the direction of the Thermal Protection Branch with Dr. Phillip R. Nachtsheim as Contract Technical Monitor and with the cooperation of Capt. R. J. Callahan of SAMSO and R. C. Loesch of Aerospace Corporation as advisors for the DoD portion of the study.

The report consists of four volumes:

Volume I - Executive Summary

Volume II - Planetary Entry Flight Experiments

Volume III - Planetary Entry Flight Experiments Handbook

Volume IV - DoD Entry Flight Experiments

TABLE OF CONTENTS

List of Pages

Title Page

i through ii

1 through 84

1.0 INTRODUCTION

Purpose - This handbook presents a summary of these study results considered useful for advanced mission planning of Shuttle launched entry technology experiments. The information is intended for use by an independent investigator to identify and plan experiments involving earth flight simulation of the outer planet entry environment.

Scope - Advanced planning for planetary entry technology experiments requires a knowledge of both planetary environment requirements and earth flight simulation capabilities. Hence this handbook has been organized to systematically present these data in parametric form so that a comparison of requirements and capabilities can be readily accomplished.

The environment produced by entry into Jupiter and Saturn atmospheres are summarized. Worst case design environments are identified and the effect of entry angle, type of atmosphere and ballistic coefficient variations are presented.

The range of environments experienced during earth entry is parametrically described as a function of initial entry conditions. The sensitivity of these environments to vehicle ballistic coefficient and nose radius are also shown.

An elliptical deorbit maneuver strategy is defined in terms of the velocity increment required versus initial entry conditions and apoapsis altitude. Mission time, ground track and out of plane velocity penalties are also presented.

Performance capability of typical Shuttle launched boosters are described including the initial entry conditions attainable as a function of payload mass and apoapsis altitude.

Units - The International System (SI) of Units is used throughout this handbook. Conversion factors to English units are documented in Reference 1 (NASA SP-7012). An abbreviated list of conversion factors for quantities commonly used in this handbook are presented in Figure 1-1.

CONVERSION FACTORS

To convert from	to	Multiply by
	HEATING RATE	
$Btu/foot_2^2$-second	watts/meter^2	+04 1.134 893
Btu/foot^2-second	kilowatts/centimeter^2	-03 1.134 893
watts/meter^2	$Btu/foot_2^2$-second	-05 8.811 403
kilowatts/centimeter^2	Btu/foot^2-second	+02 8.811 403
	TOTAL HEAT/AREA	
$Btu/foot_2^2$	joules/meter^2	+04 1.134 893
Btu/foot^2	joules/centimeter^2	00 1.134 893
joules/meter^2	$Btu/foot_2^2$	-05 8.8114
joules/centimeter^2	Btu/foot^2	-01 8.8114
	THRUST	
pound (force)	newton	00 4.448 221 615
newton	pound (force)	-01 2.248 089 431
	SPECIFIC IMPULSE	
second ($lbf\text{-}sec/lb_m$)	meters/second	00 9.80667
meters/second	second ($lbf\text{-}sec/lb_m$)	-01 1.01971
	BALLISTIC COEFFICIENT	
pounds (mass)/foot^2	kilograms/meter^2	00 4.882 242 764
kilograms/meter^2	pounds (mass)/foot^2	-01 2.048 238 992
slugs/foot^2	kilograms/meter^2	+02 1.570 874 634
kilograms/meter^2	slugs/foot^2	-03 6.365 880 372
	MASS	
pound	kilogram	-01 4.535 9237
kilogram	pound	00 2.204 6226

FIGURE 1-1

To convert from	to	Multiply by
	LENGTH	
feet	meters	-01 3.048
feet	centimeters	+01 3.048
feet	kilometers	-04 3.048
meters	feet	00 3.28084
centimeters	feet	-02 3.28084
kilometers	feet	+03 3.28084
inches	meters	-02 2.540
inches	centimeters	-01 3.9370
meters	inches	+01 3.9370
centimeters	inches	-01 3.9370
nautical mile	meters	+03 1.8520
nautical mile	kilometers	00 1.8520
meters	nautical mile	-04 5.399 568
kilometers	nautical mile	-01 5.399 568
	AREA	
$foot^2$	$meter^2$	-02 9.290 304
$foot^2$	$centimeter^2$	+04 9.290 304
$meter^2$	$foot^2$	+01 1.076 391
$meter^2$	$foot^2$	-03 1.076 391
$inch^2$	$meter^2$	-04 6.4516
$inch^2$	$centimeter^2$	00 6.4516
$meter^2$	$inch^2$	+03 1.548 946
$centimeter^2$	$inch^2$	-01 1.54 946
	VOLUME	
$feet^3$	$meter^3$	-02 2.831 684 659
$feet^3$	$centimeter^3$	+04 2.831 684 659
$meter^3$	$feet^3$	+01 3.531 466 672
$centimeter^3$	$feet^3$	-05 3.531 466 672

FIGURE 1-1 (CONT)

2.0 PLANETARY ENTRY ENVIRONMENT

Introduction - The environments, experienced during entry into the atmosphere of typical outer planets, are presented in this section. These environments constitute the basic requirements for the design of earth flight simulation experiments. The information shown represents a summary compilation of available data. A more detailed explanation of the analytical basis for these data can be found in the references listed in Section 6.

Entry environments are described primarily in terms of heating parameters although pressure and deceleration loads data are also provided. The heating environment is emphasized because it is substantially more severe than any encountered to date. Compared with earth entry, outer planet entry is characterized by high velocity, high convective and radiative fluxes and relatively short entry time. Further, the heating environment is dominated by shock layer radiation as opposed to convective dominated earth entry.

Heating environment descriptions are presented for stagnation point conditions only. They do not include the effect of re-radiation from the heat shield surface or that of mass injection into the boundary layer. As such, these data represent a measure of the incident environment but not a rigorous definition of the total, net flux absorbed by the heat shield. Further, this level of definition reflects the only body of available information large enough to cover the full range of mission and vehicle uncertainties.

Worst case design environments are tabulated for each outer planet. However, emphasis is placed on parametrically describing the environment as a function entry angle, type of atmosphere and entry vehicle ballistic coefficient. Parametric data is considered more useful for purposes of advanced planning. It allows evaluation of future changes in mission and vehicle uncertainties and provides insight into how closely a given parameter should be simulated.

2.1 Jupiter Entry Environment - The assumptions used to establish the maximum Jupiter entry environment are presented in Figure 2-1 along with a summary of the resulting design point environment. The effect of entry angle, atmosphere model and ballistic coefficient variations on peak radiative flux, convective flux and pressure level are shown in Figures 2-2, 2-3 and 2-4.

The mission and configuration assumptions of Figure 2-1 were derived from available results of current outer planet probe studies. The selection of entry angle and atmosphere model are of particular interest because of the uncertainty associated with each parameter.

The initial entry angle corresponds to a shallow entry mission nominally targeted for a relative angle of -9.5 degrees (-7.5 degrees inertial). A typical entry angle uncertainty of ± 1.5 degrees was applied to identify a worst case design condition of -11 degrees. This small uncertainty allows targeting for shallow entry and reflects the accurate knowledge of Jupiter ephemeris and physical data obtained from recent Pioneer missions.

Atmospheric composition uncertainties were taken into account by parametrically considering the cool, nominal and warm models defined in Reference 4. The nominal model was assumed to establish the maximum design conditions. Ordinarily a cool atmosphere would be used since it results in a more severe environment. However, Pioneer 11 flight data indicates that the cool model is no longer valid and that the nominal atmosphere as currently defined represents a realistic worst case.

Jupiter entry produces the most severe heating environment of any planet considered. This is primarily due to a very high entry velocity (47 km/sec) which is a fundamental result of Jupiter's massiveness and hence very high gravitational field. Additional factors include a steep atmospheric density gradient (large inverse scale height) induced by the high gravity and a high vehicle ballistic coefficient resulting from the large mass of a thick heat shield. However, the peak stagnation pressure and "g" loads are relatively moderate. This is a result of the rather shallow initial entry angle.

JUPITER DESIGN ENVIRONMENT

MISSION ASSUMPTIONS	
RELATIVE ENTRY VELOCITY	47 km/SEC
RELATIVE ENTRY ANGLE	-11 DEG
ATMOSPHERE MODEL	NOMINAL
CONFIGURATION ASSUMPTIONS	
NOSE RADIUS	.22 m
NOSE RADIUS/BASE RADIUS	.50
BALLISTIC COEFFICIENT (AVERAGE)	136 kg/m^2
ENVIRONMENT PARAMETERS*	
PEAK RADIATIVE FLUX	38 kW/cm^2
PEAK CONVECTIVE FLUX	19 kW/cm^2
TOTAL HEAT LOAD	440 kJ/cm^2
HEAT PULSE DURATION	14 SEC
PEAK PRESSURE	10 ATM
PEAK DECELERATION	300 g

*STAGNATION POINT, NONBLOWING

FIGURE 2-1

JUPITER RADIATIVE FLUX ENVIRONMENT

- o V_{REL} = 47 km/sec
- o ALT = 450 km
- o R_N = .22m
- o R_N/R_B = .50
- o STAGNATION POINT
- o NON BLOWING

(a) EFFECT OF MISSION UNCERTAINTIES

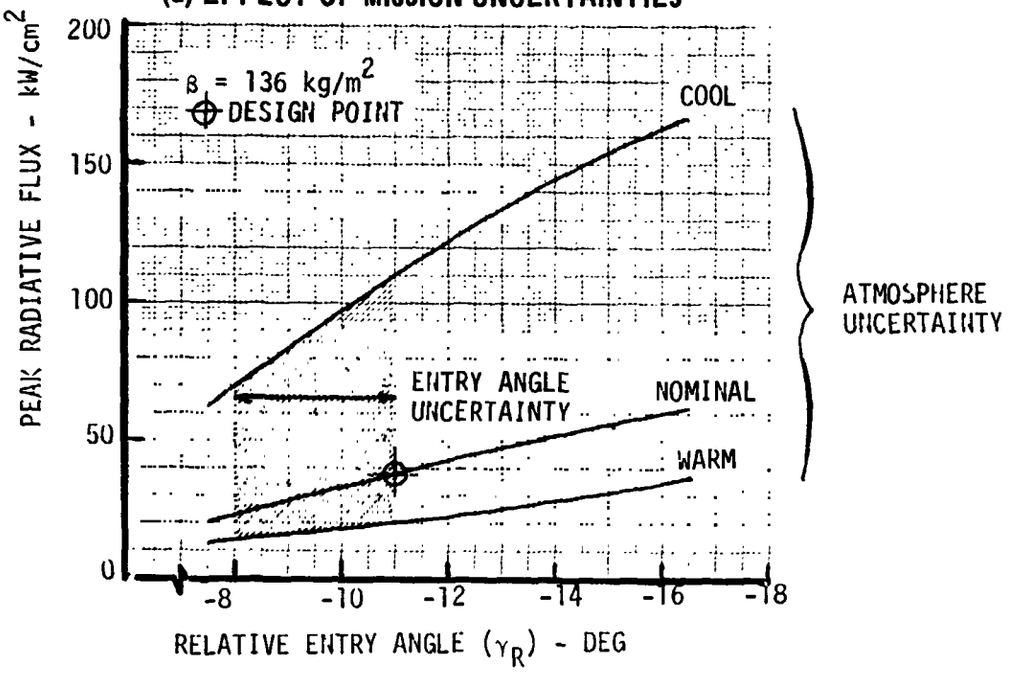

(b) EFFECT OF BALLISTIC COEFFICIENT

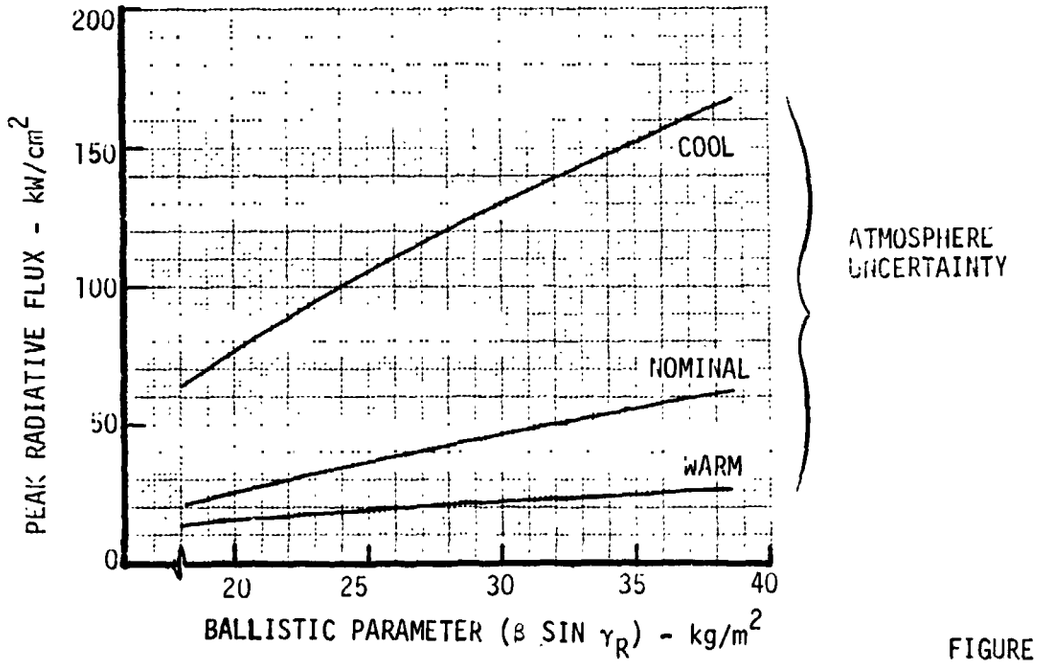

FIGURE 2-2

JUPITER CONVECTIVE FLUX ENVIRONMENT

- o V_{REL} = 47 km/sec
- o ALT = 450 km
- o R_N = .22 m
- o R_N/R_E = .50
- o STAGNATION POINT
- o NON BLOWING

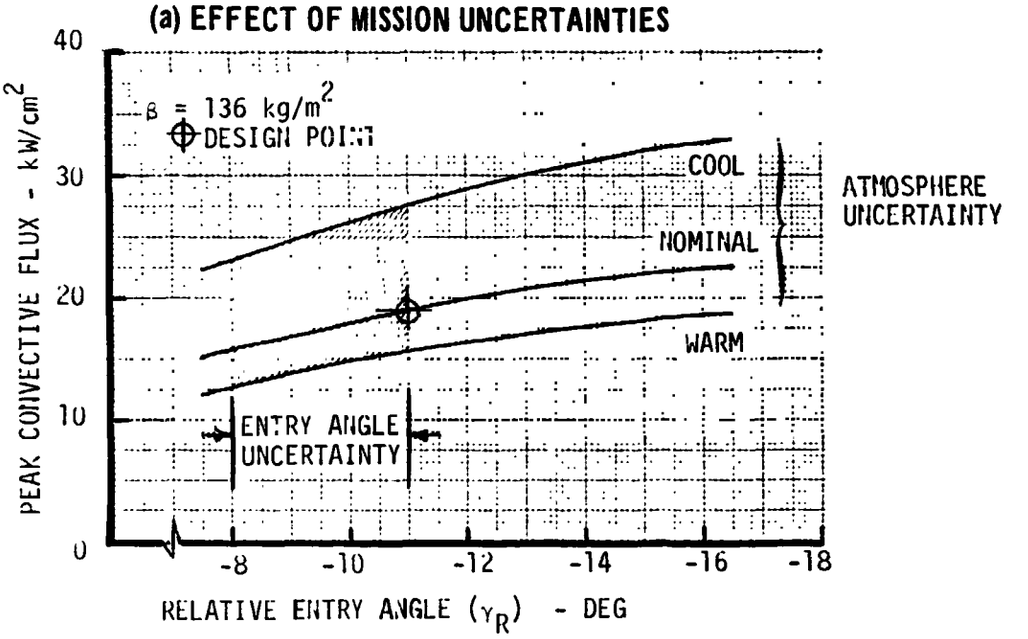

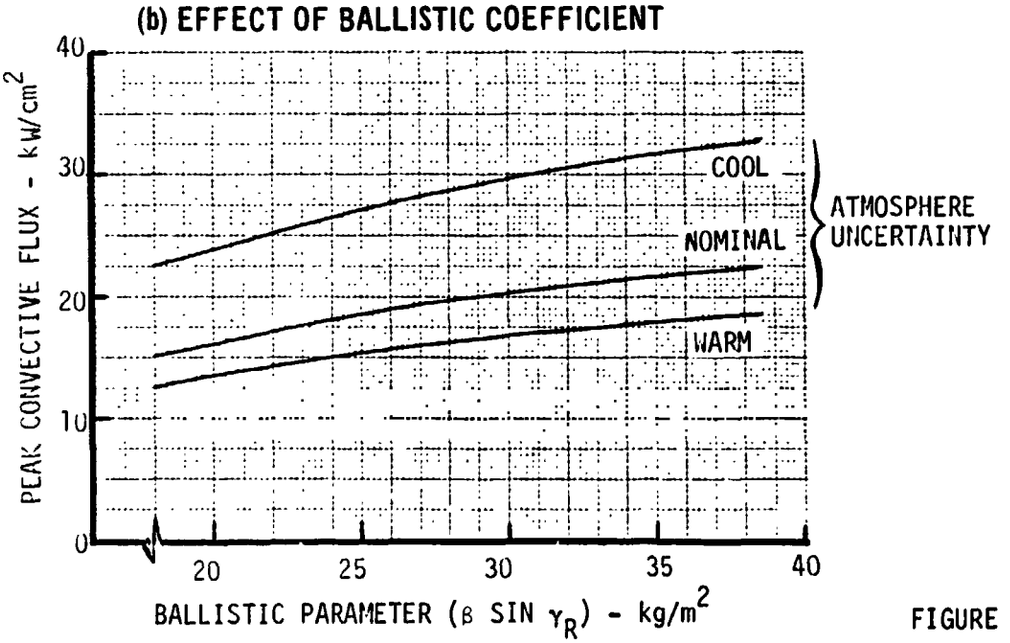

FIGURE 2-3

JUPITER PRESSURE ENVIRONMENT

- o V_{REL} = 47 km/sec
- o ALT = 450 km
- o R_N = .22m
- o R_N/R_B = .50
- o STAGNATION POINT
- o NON BLOWING

(a) EFFECT OF MISSION UNCERTAINTIES

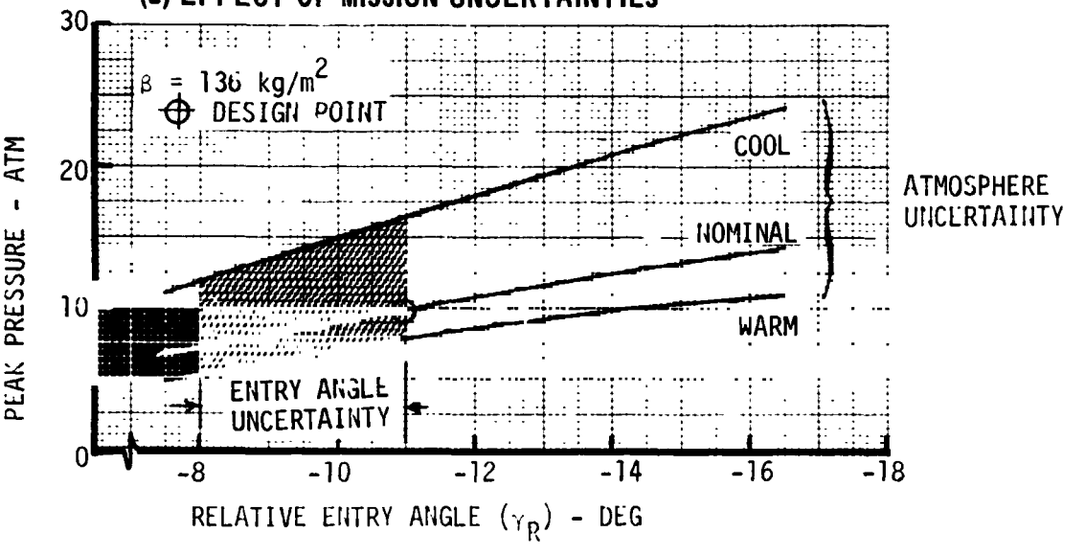

(b) EFFECT OF BALLISTIC COEFFICIENT

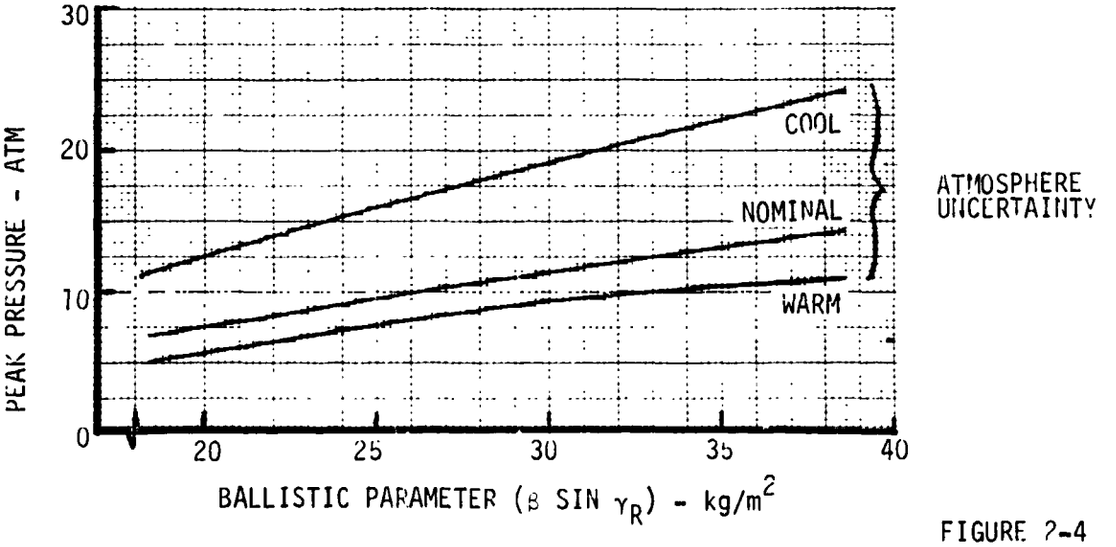

FIGURE 2-4

2.2 Saturn Entry Environment - The assumptions and resulting maximum design point environment associated with entry into the atmosphere of Saturn are presented in Figure 2-5. The influence of entry angle, atmosphere model and ballistic coefficient variations on peak radiative flux, convective flux and pressure level are shown in Figures 2-6, 2-7 and 2-8.

The Figure 2-5 assumptions represent mission and vehicle characteristics determined during past Saturn/Uranus entry probe studies. These data also reflect an uncertainty in the knowledge of Saturns location and physical nature. Unlike Jupiter, Saturns ephemeris and physical properties have not yet been defined by flyby missions. The earliest opportunity for such refinement will be the planned Pioneer 11 flyby in 1979. As a result, there is a large uncertainty in entry angle (± 10 degrees) which contributes to the rather steep (-48 degrees) design entry. Similarly, the most conservative atmosphere model (cool) is used for design purposes.

Saturn entry produces the highest stagnation pressures and deceleration loads of any planet considered. This is a direct result of selecting a steep entry into a cool atmosphere for purposes of design. The heating environment, however, is less severe than that encountered during a shallow Jupiter entry. This is primarily due to a lower entry velocity (32 km/sec).

2.3 Uranus Entry Environment - At present, the Uranus entry environment is considered best described by assuming it the same as Saturn. Available data is insufficient for a separate Uranus presentation because of special problems involved in selecting an atmosphere model. The current cool atmosphere, which results in radiative heating of Jupiter proportions, is now considered invalid because of excessively high helium content relative to solar abundance. Use of the nominal atmosphere model eliminates the radiative component altogether. Hence, until more accepted atmosphere models become available and used in entry heating analysis, the Saturn environment is considered the best available approximation.

SATURN DESIGN ENVIRONMENT

MISSION ASSUMPTIONS	
RELATIVE ENTRY VELOCITY	32 km/sec
RELATIVE ENTRY ANGLE	-48 DEG
ATMOSPHERE MODEL	COLD
CONFIGURATION ASSUMPTIONS	
NOSE RADIUS	.22 m
NOSE RADIUS/BASE RADIUS	.50
BALLISTIC COEFFICIENT	120 kg/m^2
ENVIRONMENT PARAMETERS	
PEAK RADIATIVE FLUX	20 kW/cm^2
PEAK CONVECTIVE FLUX	13 kW/cm^2
TOTAL HEAT LOAD	74 kJ/cm^2
HEAT PULSE DURATION	10 sec
PEAK PRESSURE	19 ATM
PEAK DECELERATION	700 g

FIGURE 2-5

SATURN RADIATIVE ENVIRONMENT

- V_{REL} = 32.0 km/sec
- ALT = 600 km
- R_N = .22m
- R_N/R_B = .5
- STAGNATION POINT
- NON BLOWING

(a) EFFECT OF MISSION UNCERTAINTIES

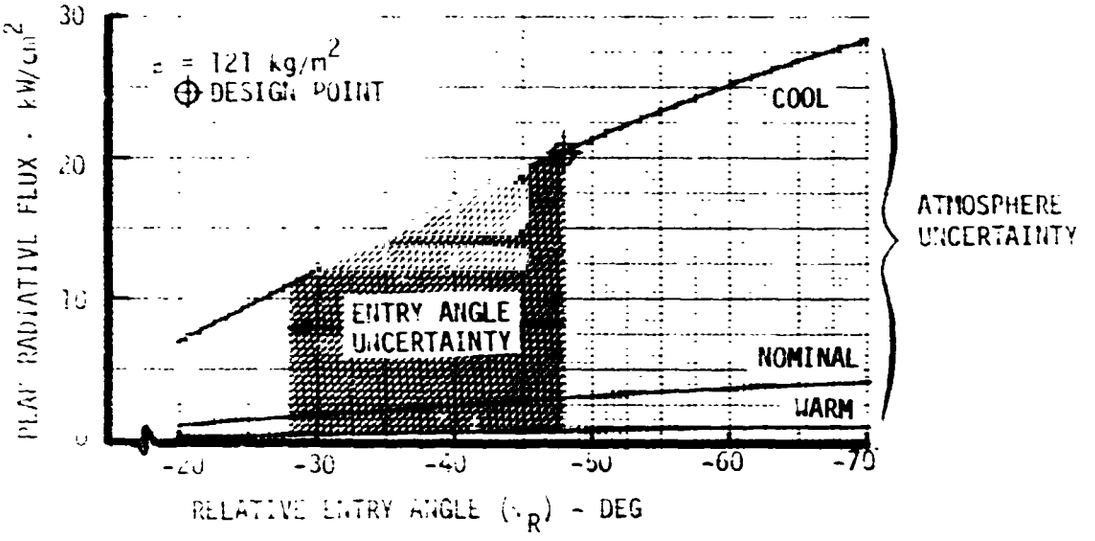

(b) EFFECT OF BALLISTIC COEFFICIENT

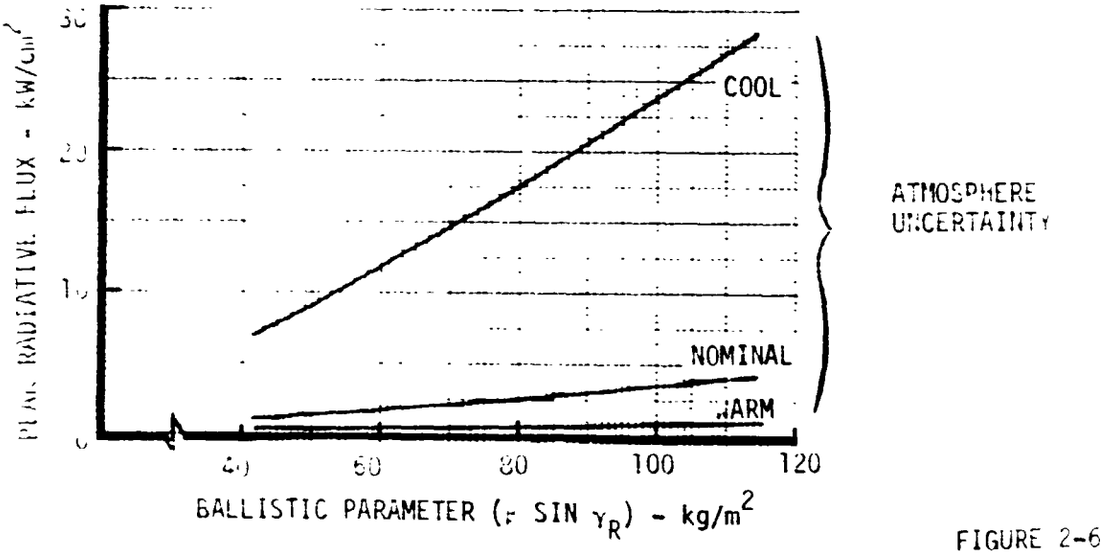

FIGURE 2-6

SATURN CONVECTIVE FLUX ENVIRONMENT

- o V_{REL} = 32.0 km/sec
- o ALT = 600 km
- o R_N = .22m
- o R_N/R_E = .5
- o STAGNATION POINT
- o NON BLOWING

(a) EFFECT OF MISSION UNCERTAINTIES

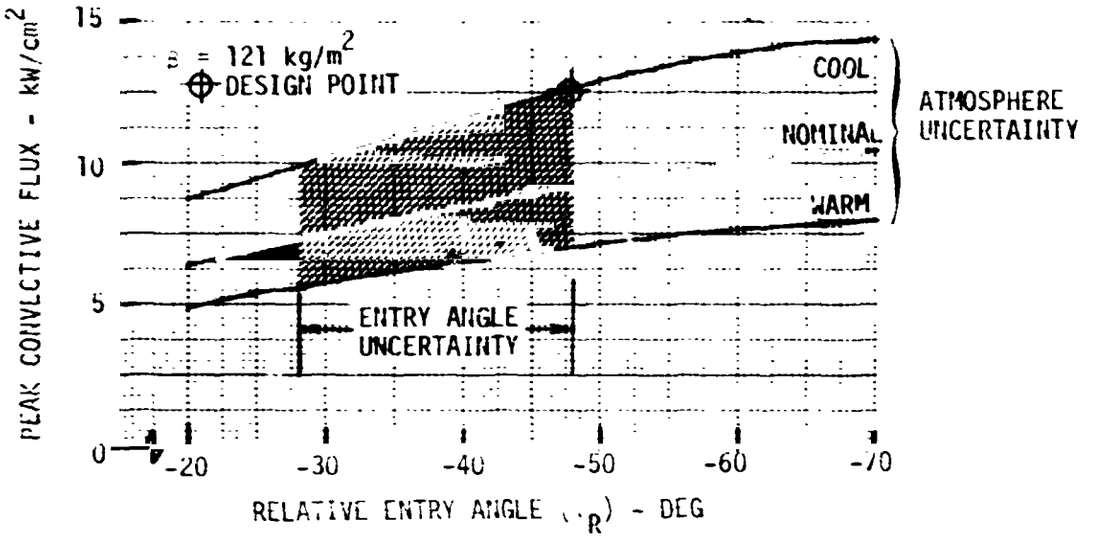

(b) EFFECT OF BALLISTIC COEFFICIENT

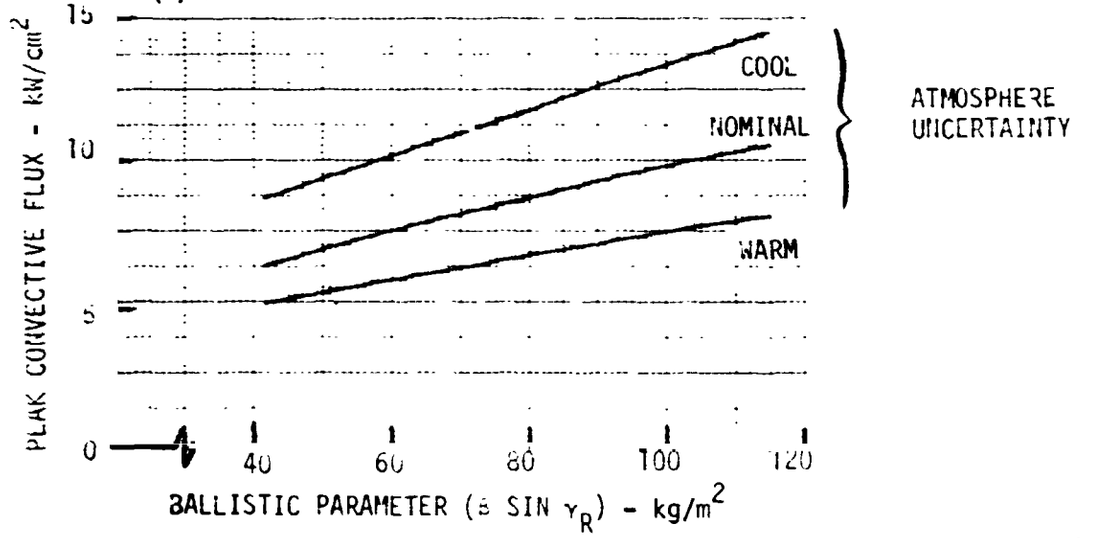

FIGURE 2-7

SATURN PRESSURE ENVIRONMENT

- o V_{REL} = 32.0 km/sec
- o ALT = 600 km
- o R_N = .22m
- o R_N/R_E = .5
- o STAGNATION POINT
- o NON BLOWING

(a) EFFECT OF MISSION UNCERTAINTIES

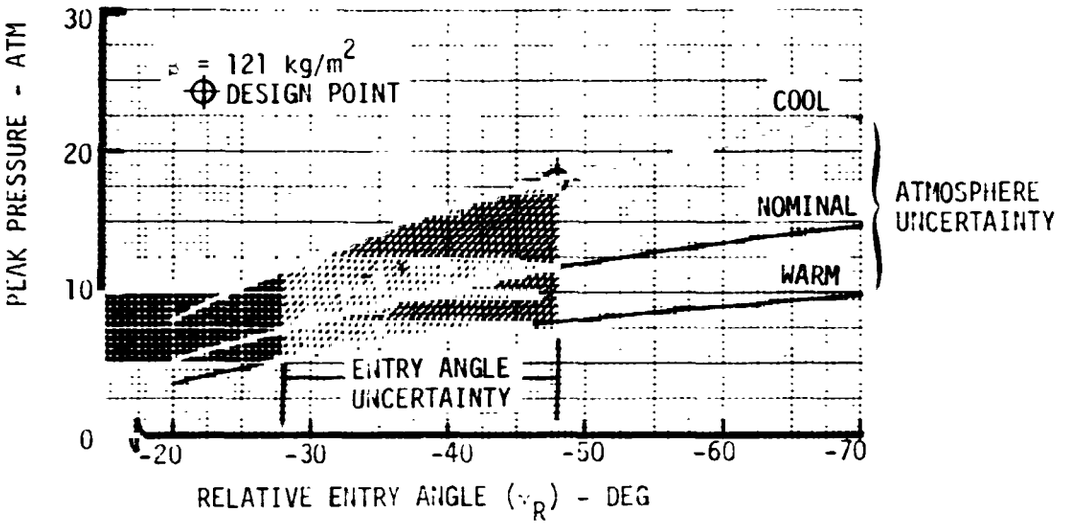

(b) EFFECT OF BALLISTIC COEFFICIENT

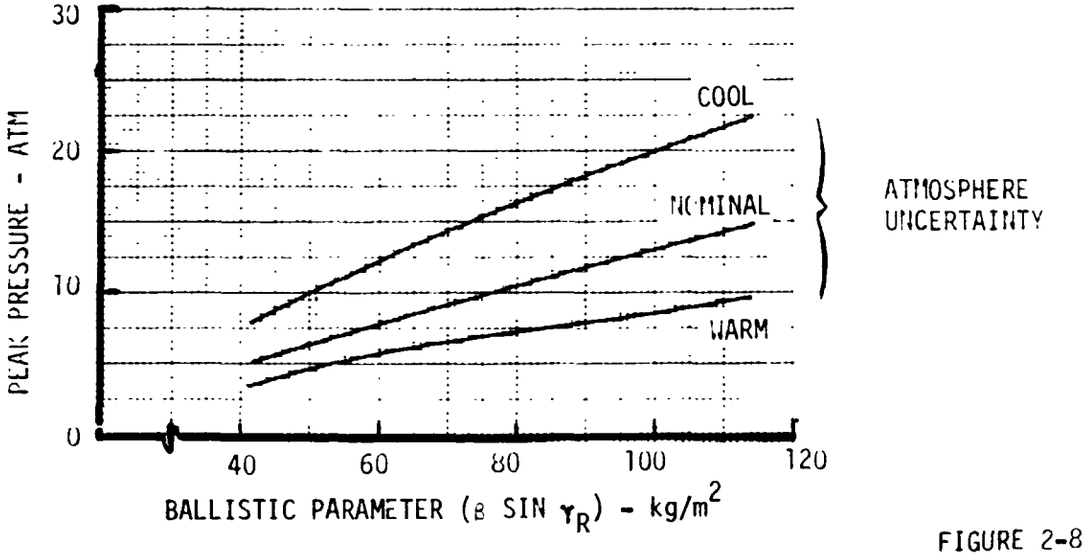

FIGURE 2-8

3.0 EARTH ENTRY ENVIRONMENT

This section presents a description of the environments that can be produced by high speed entry into the earth's atmosphere. Data are shown for the range of initial entry conditions generally attainable by Shuttle launched boosters. This information is intended to identify the capability of earth flights to simulate planetary entry environments and to determine the required initial entry conditions.

The environmental parameters shown are intentionally the same as those used in Section 2.0 to describe the planetary entry environment. Stagnation point heating characteristics are emphasized but do not include the effect of re-radiation or boundary layer mass injection.

The range of initial earth entry velocity needed to simulate planetary heating is much lower than actual planetary mission entry velocities. This is due to differences in atmosphere composition. The outer planet atmospheres are composed primarily of hydrogen-helium mixtures at about the solar abundance ratio, whereas the earth atmosphere is nearly 21 percent oxygen and 79 percent nitrogen. From basic thermodynamics it is known that the low molecular weight gases, hydrogen and helium, have a much higher heat capacity than air. Thus simulation of similar shock layer temperatures or heating rates in air require a much lower entry speed than that of planetary entries. The higher molecular weight of air also results in a steeper atmospheric density gradient which enhances simulation of the peak environment conditions but reduces the heating duration.

A three degree of freedom point mass trajectory computer program was used to compute earth entry trajectories. The earth model was a spherical rotating earth. All trajectories began at 121.92 km with the inertial velocity and flight path angle defined. In addition to computing altitude, velocity, flight path angle, latitude, longitude and heading as a function of reentry time, the program also determined the trajectory conditions at peak stagnation point radiative heat flux, dynamic pressure, and deceleration. This was accomplished by automatic monitoring of these parameters as the trajectory was computed. Once a peak value was passed, the trajectory parameter immediately preceeding the peak were stored. Upon completion of a trajectory, smaller time step trajectory segments were computed about the peak values to provide a precise definition of the peak values. The dynamic pressure and decleration result from the solution to the equations of motion. The stagnation point convective heat flux (kW/cm^2) was determined by the following equation:

$$\dot{q}_c = 0.01464 \frac{\rho^{1/2} V^{3.15}}{R_N^{1/2}}$$

where ρ = atmospheric density (kg/m^2)

V = velocity (km/sec)

R_N = nose radius (meters)

This equation was evaluated at each point on the computed trajectory and integrated over the full trajectory to give the total convective heating at the stagnation point. The stagnation point radiative heat flux was determined from a table look-up of data for a cooled shock layer from Reference 8. These data provide stagnation point radiative heat flux as a function of altitude, nose radius, and velocity. A table look-up of radiative heat flux was performed at each point on the trajectory and the values integrated to give stagnation point total radiative heating.

3.1 Reference Vehicle Environment - Detailed entry environment descriptions are presented for a cone/hemisphere shaped entry body having a ballistic coefficient (β) of 120 kg/m^2 and a nose radius (R_N) of .22 m. A single reference vehicle configuration was chosen to allow a full yet concise presentation of the various environment and entry conditions parameters. The selected configuration is typical of outer planet probes currently under study.

Figures 3-1 through 3-3 are computer output summaries that detail the peak stagnation point values of radiative flux, convective flux and pressure/"g" loads. Data is presented as a function of initial entry conditions and describes the flight conditions at which the peak value of each environment parameter occurs.

Each summary is composed of 48 cases which are subdivided into 6 groups of 8 cases each. As shown in the second and third columns, each of the 6 groups correspond to a different entry velocity while the 8 cases within each group represent a different entry angle. Note that these initial entry conditions are given as inertial coordinates. This is done for ease of comparison with the booster capability information presented in Section 4.

The fourth through eighth columns provide a definition of that point in the mission at which the peak environment parameter occurs. The time shown refers to the length of time it takes to pass from an altitude of 122 km (400,000 ft) to the peak environment point. The individual values of altitude, relative flight conditions and free stream density are based on a due east entry into a 1962 U.S. Standard Atmosphere and a spherical, rotating earth.

The ninth through twelvth columns list the magnitude of the environmental parameters of interest. Peak values are indicated by enclosure in a rectangular box. For example, Figure 3-1 presents the peak level of radiative flux. The corresponding levels of convective flux, pressure and "g" loads do not represent maximum values but rather the magnitude of these parameters that exist at the time of peak radiative heating. Similarly Figure 3-2 shows peak convective flux while Figure 3-3 indicates maximum pressure levels and "g" loads. Note that in each table, peak radiative flux values in excess of about 50 kW/cm^2 are extrapolated. This refers to the limitations of the basic computer input data. Values so noted should be treated with caution.

The final three columns show the total stagnation point heat load. Radiative and convective components are listed as well as the sum total. These are total mission values and hence are the same on each table.

Graphical presentations of these data are also shown. Figures 3-4 through 3-9 illustrate the effect of initial entry conditions on peak heating rates, pressure, "g" loads and total heat load. Figure 3-10 indicates the duration of the radiative and convective heat pulse. Figures 3-11 through 3-14 show the initial entry angle and velocity combinations necessary to achieve a given maximum level of heat flux, pressure and "g" loads.

CONDITIONS AT PEAK RADIATIVE HEAT FLUX FOR EARTH ENTRY OF A HIGH SPEED – LOW β(120 kg/m^2) VEHICLE

CASE NO	I-VEL. (KM/S)	I-GAM (DEG)	TIME (SEC)	ALT (KM)	R-VEL (KM/S)	R-GAM (DEG)	DENSITY (KG/M**3)	PSTAG (ATM)	ACCEL (GE)	QDOT -RAD- ***(KW/CM**2)**	QDOT -CON-	QTOT -RAD- ****(KJOULE/CM**2)***	QTOT -CON-	QTOT
1	12.19	-20.00	17.350	51.7[illegible]	10.99	-19.72	8.312E-04	9.418E-01	-37.59	.69	1.71	2.95	15.55	18.51
2	12.19	-30.00	12.275	48.26	11.00	-30.44	1.298E-03	1.472E 00	-58.76	1.20	2.13	3.43	15.16	18.61
3	12.19	-40.00	9.825	45.74	10.99	-40.96	1.806E-03	2.046E 00	-81.66	1.73	2.51	3.87	13.45	17.32
4	12.19	-50.00	8.425	43.90	10.99	-51.37	2.313E-03	2.621E 00	-104.61	2.29	2.84	4.27	12.46	16.73
5	12.19	-60.00	7.575	42.54	11.00	-61.69	2.788E-03	3.165E 00	-126.32	2.86	3.13	4.72	11.89	16.61
6	12.19	-70.00	7.075	41.44	11.01	-71.93	3.244E-03	3.685E 00	-147.10	3.41	3.38	5.27	11.60	16.87
7	12.19	-80.00	6.825	40.58	11.00	-82.09	3.666E-03	4.158E 00	-165.98	3.88	3.59	5.54	11.55	17.09
8	12.19	-90.00	6.775	39.97	10.99	-87.81	3.996E-03	4.525E 00	-180.64	4.22	3.74	6.12	11.64	17.76
9	13.72	-20.00	16.375	48.18	11.89	-19.41	1.312E-03	1.740E 00	-69.45	2.65	2.75	10.50	24.04	34.54
10	13.72	-30.00	11.500	44.80	11.90	-30.18	2.049E-03	2.721E 00	-108.60	4.36	3.44	11.62	19.73	31.35
11	13.72	-40.00	9.100	42.92	11.97	-40.71	2.646E-03	3.553E 00	-141.81	6.12	3.98	1[illegible].64	17.48	30.13
12	13.72	-50.00	7.775	41.25	11.96	-51.11	3.333E-03	4.473E 00	-178.55	7.87	4.46	13.70	16.19	29.89
13	13.72	-60.00	6.975	40.00	11.96	-61.43	3.978E-03	5.333E 00	-212.89	9.54	4.86	14.72	15.43	30.15
14	13.72	-70.00	6.475	39.33	12.01	-71.67	4.377E-03	5.918E 00	-236.21	11.04	5.17	15.39	15.04	30.43
15	13.72	-80.00	6.225	38.71	12.02	-81.84	4.792E-03	6.487E 00	-258.94	12.25	5.42	15.96	14.91	30.87
16	13.72	-90.00	6.175	38.15	11.98	-88.06	5.196E-03	6.994E 00	-279.19	13.10	5.59	17.23	15.04	32.27
17	15.24	-20.00	15.525	45.06	12.51	-19.16	1.978E-03	2.904E 00	-115.92	5.99	3.96	24.01	30.47	54.48
18	15.24	-30.00	10.900	41.37	12.41	-29.96	3.277E-03	4.729E 00	-188.78	9.82	4.96	26.18	24.96	51.13
19	15.24	-40.00	8.650	39.14	12.36	-40.50	4.503E-03	6.454E 00	-257.64	13.64	5.75	27.76	22.11	49.87
20	15.24	-50.00	7.350	37.78	12.40	-50.90	5.489E-03	7.915E 00	-315.95	17.29	6.41	29.01	20.42	49.43
21	15.24	-60.00	6.550	36.96	12.48	-61.22	6.193E-03	9.042E 00	-360.92	20.52	6.94	31.04	19.47	50.51
22	15.24	-70.00	6.075	36.33	12.52	-71.46	6.803E-03	9.999E 00	-399.14	23.24	7.35	32.67	18.96	51.62
23	15.24	-80.00	5.850	35.57	12.44	-81.67	7.618E-03	1.105E 01	-441.20	25.44	7.62	32.16	18.72	50.87
24	15.24	-90.00	5.775	35.38	12.46	-88.25	7.847E-03	1.142E 01	-455.74	26.63	7.77	35.96	18.92	54.88
25	16.76	-20.00	14.000	45.75	13.98	-19.02	1.804E-03	3.306E 00	-131.95	11.76	5.36	43.61	37.73	81.34
26	16.76	-30.00	9.750	42.56	14.03	-29.83	2.780E-03	5.128E 00	-204.68	18.99	6.72	47.14	30.86	77.99
27	16.76	-40.00	7.725	40.43	14.03	-40.36	3.741E-03	6.907E 00	-275.70	26.11	7.81	50.58	27.31	77.89
28	16.76	-50.00	6.575	38.96	14.04	-50.75	4.618E-03	8.535E 00	-340.69	32.77	8.69	53.93	25.26	79.19
29	16.76	-60.00	5.850	38.27	14.16	-61.06	5.110E-03	9.611E 00	-383.63	38.84	9.39	57.52	24.02	81.54
30	16.76	-70.00	5.625	35.04	13.29	-71.29	8.258E-03	1.368E 01	-545.94	44.36	9.77	61.52	23.38	84.90
31	16.76	-80.00	5.375	34.84	13.38	-81.47	8.519E-03	1.431E 01	-571.05	48.89	10.15	57.91	35.91	93.83
32	16.76	-90.00	5.300	34.72	13.42	-88.41	8.669E-03	1.465E 01	-584.65	51.37	10.33	66.35	23.30	89.65
33	18.29	-20.00	13.150	44.34	14.79	-18.88	2.179E-03	4.469E 00	-178.38	20.73	7.03	70.69	45.81	116.49
34	18.29	-30.00	9.000	42.15	15.19	-29.71	2.941E-03	6.359E 00	-253.84	36.57	8.88	79.16	37.45	116.63
35	18.29	-40.00	6.950	41.79	15.73	-40.25	3.090E-03	7.167E 00	-286.08	51.14	10.16	86.50	33.15	119.65
36	18.29	-50.00	5.925	40.22	15.72	-50.63	3.857E-03	8.935E 00	-356.66	63.81 §	11.33	92.42	30.65	123.06
37	18.29	-60.00	5.275	39.49	15.83	-60.93	4.282E-03	1.007E 01	-401.79	75.29 §	12.22	103.17	29.13	132.30
38	18.29	-70.00	5.200	34.46	14.22	-71.15	9.015E-03	1.710E 01	-682.68	85.71 §	12.65	110.57	28.35	138.91
39	18.29	-80.00	5.000	33.82	14.16	-81.33	9.953E-03	1.870E 01	-746.52	98.35 §	13.09	105.20	27.88	133.08
40	18.29	-90.00	4.900	34.13	14.36	-88.54	9.490E-03	1.835E 01	-732.56	101.80 §	13.37	105.86	44.66	150.51
41	19.81	-20.00	12.250	43.87	15.84	-18.77	2.321E-03	5.462E 00	-218.04	36.52	9.01	111.07	54.75	165.82
42	19.81	-30.00	8.325	42.06	16.44	-29.62	2.978E-03	7.542E 00	-301.07	70.83 §	11.46	129.96	44.72	174.68
43	19.81	-40.00	6.400	41.99	17.11	-40.15	3.005E-03	8.251E 00	-329.37	101.74 §	13.07	146.32	39.60	185.93
44	19.81	-50.00	5.375	41.49	17.41	-50.54	3.222E-03	9.153E 00	-365.37	126.81 §	14.28	158.95	36.62	195.57
45	19.81	-60.00	4.800	40.55	17.47	-60.83	3.679E-03	1.052E 01	-420.05	148.84 §	15.42	183.62	34.82	218.44
46	19.81	-70.00	4.500	39.14	17.32	-71.05	4.498E-03	1.265E 01	-505.13	168.39 §	16.62	198.04	33.88	231.92
47	19.81	-80.00	4.600	34.06	15.45	-81.22	9.588E-03	2.146E 01	-856.62	195.81 §	16.92	190.26	33.38	223.65
48	19.81	-90.00	4.550	33.73	15.39	-88.65	1.010E-02	2.243E 01	-895.34	211.69 §	17.16	197.86	33.41	231.27

§ EXTRAPOLATED DATA

FIGURE 3-1

CONDITIONS AT PEAK CONVECTIVE HEAT FLUX FOR EARTH ENTRY OF A HIGH SPEED – LOW β(120 kg/m^2) VEHICLE

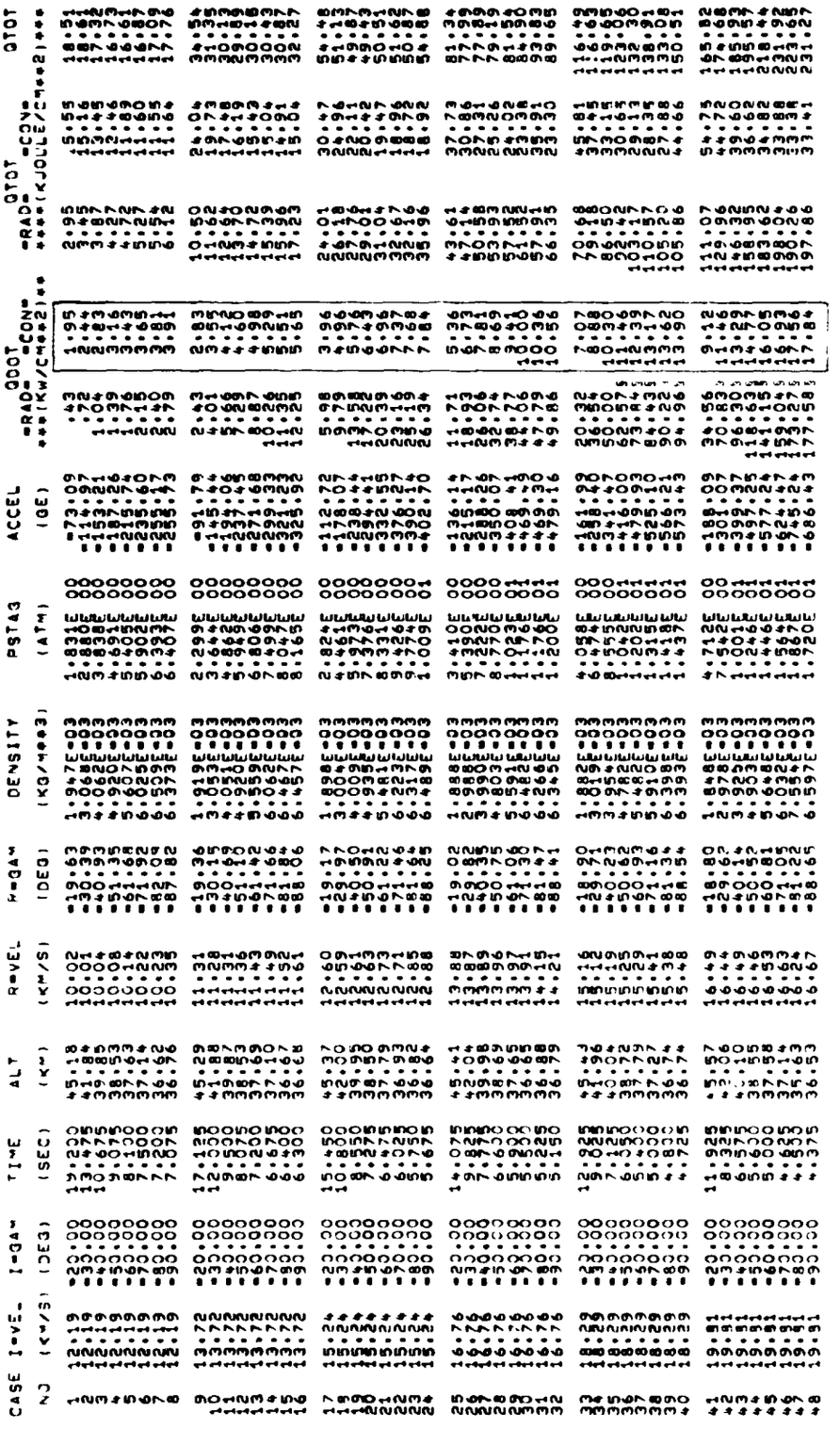

FIGURE 3-2

CONDITIONS AT PEAK DECELERATION AND STAGNATION PRESSURE
FOR EARTH ENTRY OF A HIGH SPEED-LOW β(120 kg/m^2) VEHICLE

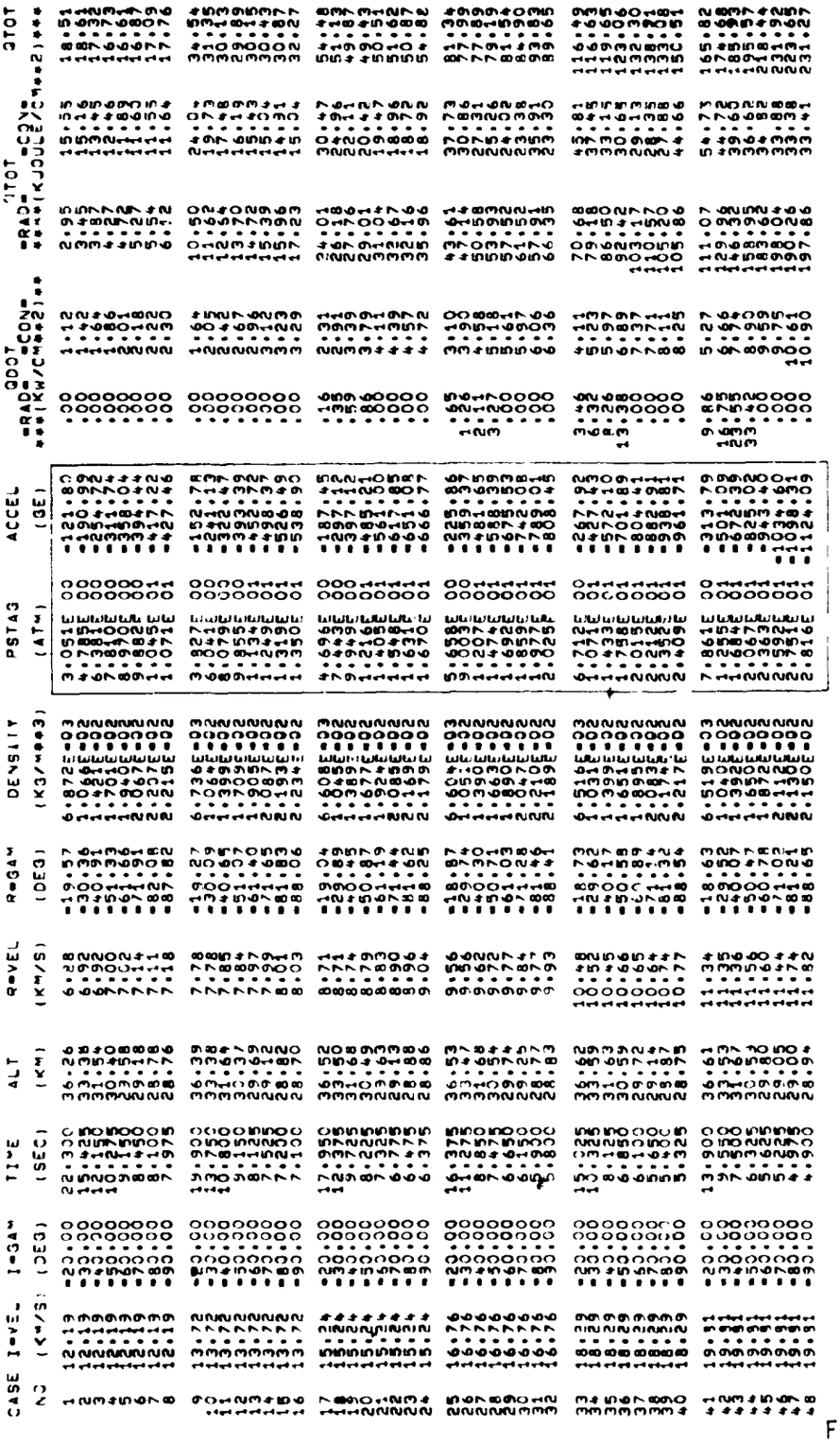

FIGURE 3-3

EARTH ENTRY HEATING RATES

- o STAGNATION POINT
- o NON-BLOWING
- o INERTIAL ENTRY CONDITIONS
- o β = 120 kg/m^2
- o R_N = .22 m

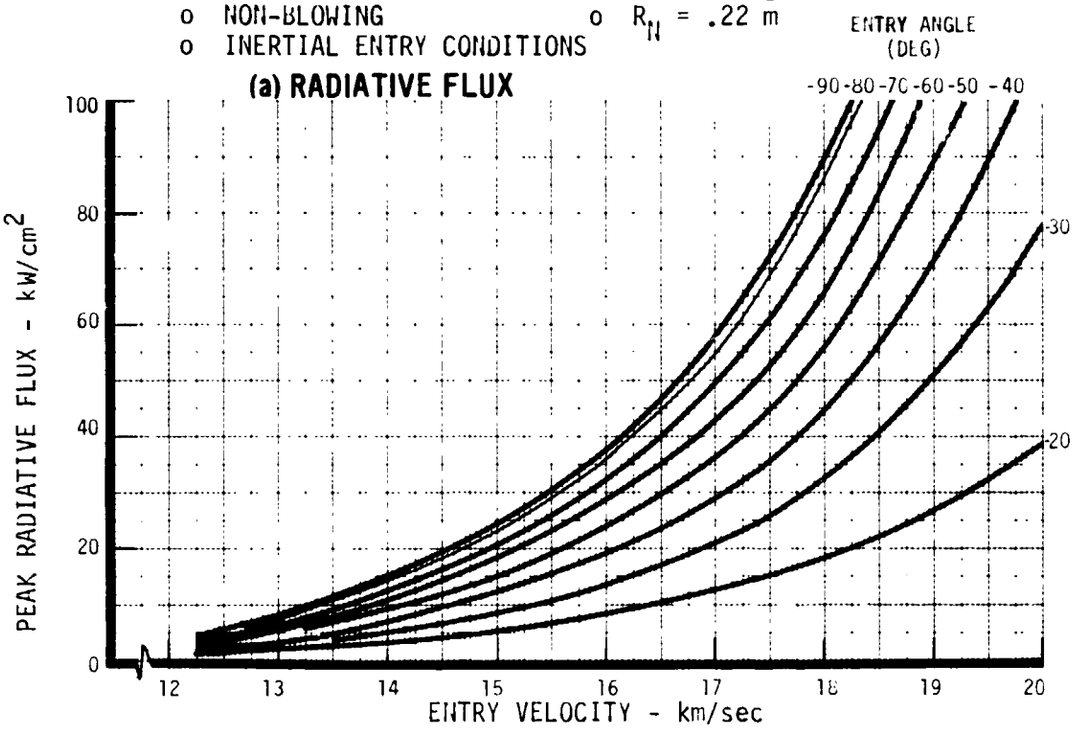

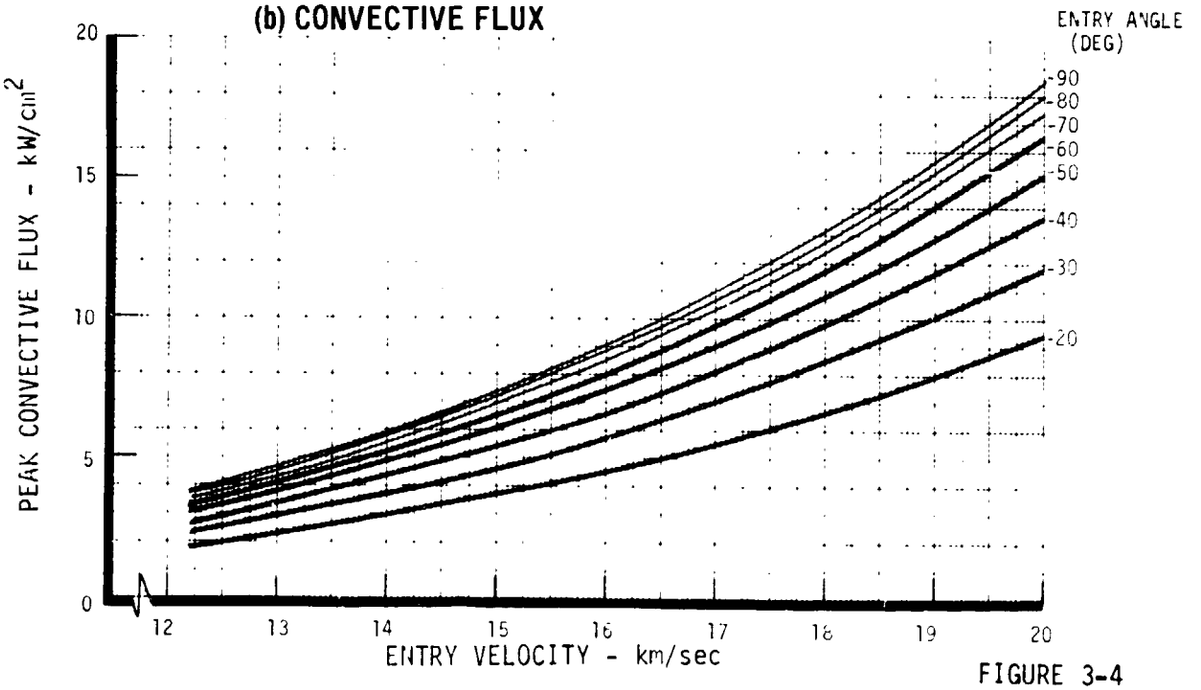

FIGURE 3-4

EARTH ENTRY PRESSURE

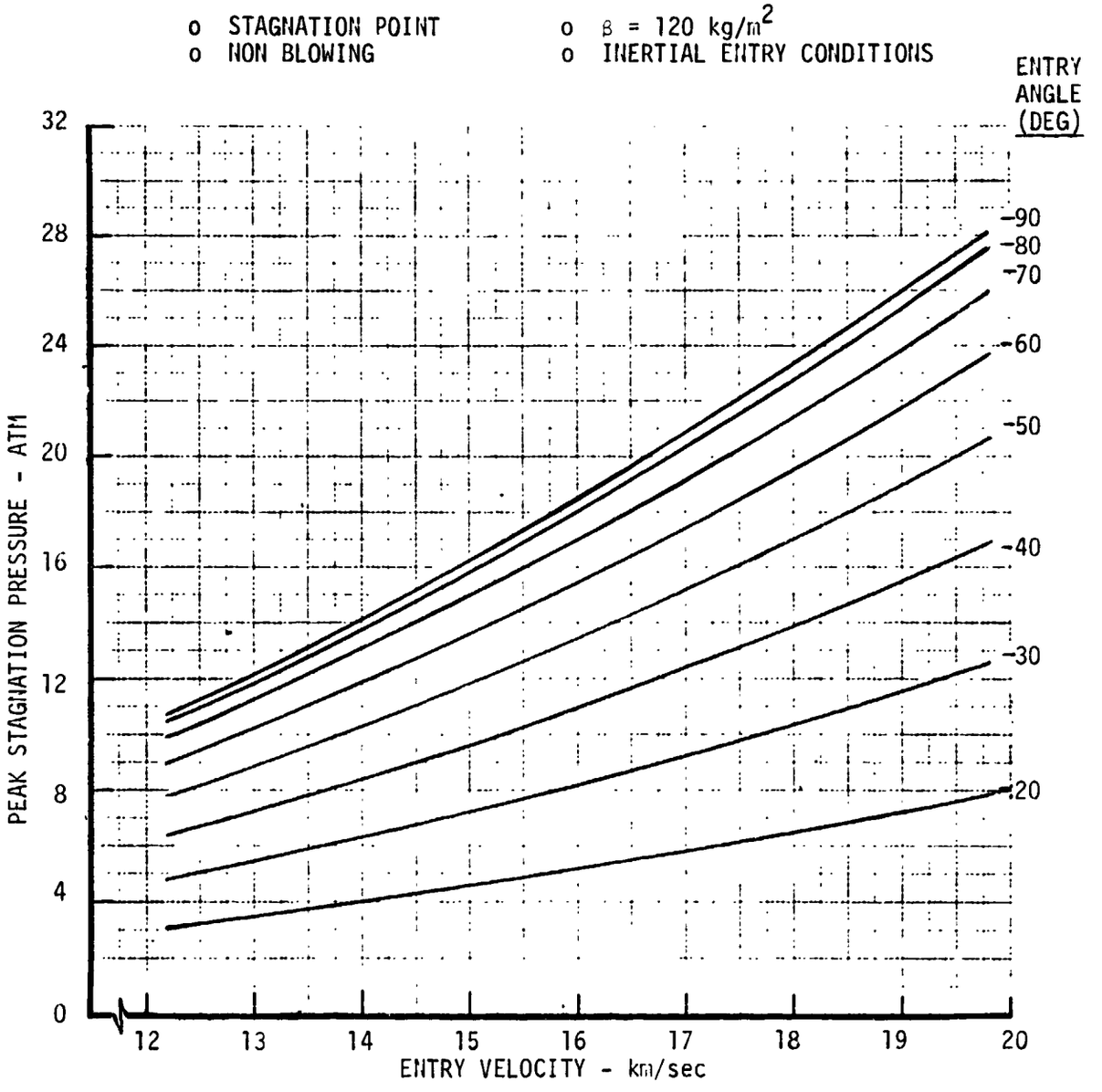

FIGURE 3-5

EARTH ENTRY DECELERATION LOADS

- o STAGNATION POINT
- o NON-BLOWING
- o β = 120 kg/m^2
- o INERTIAL ENTRY CONDITIONS

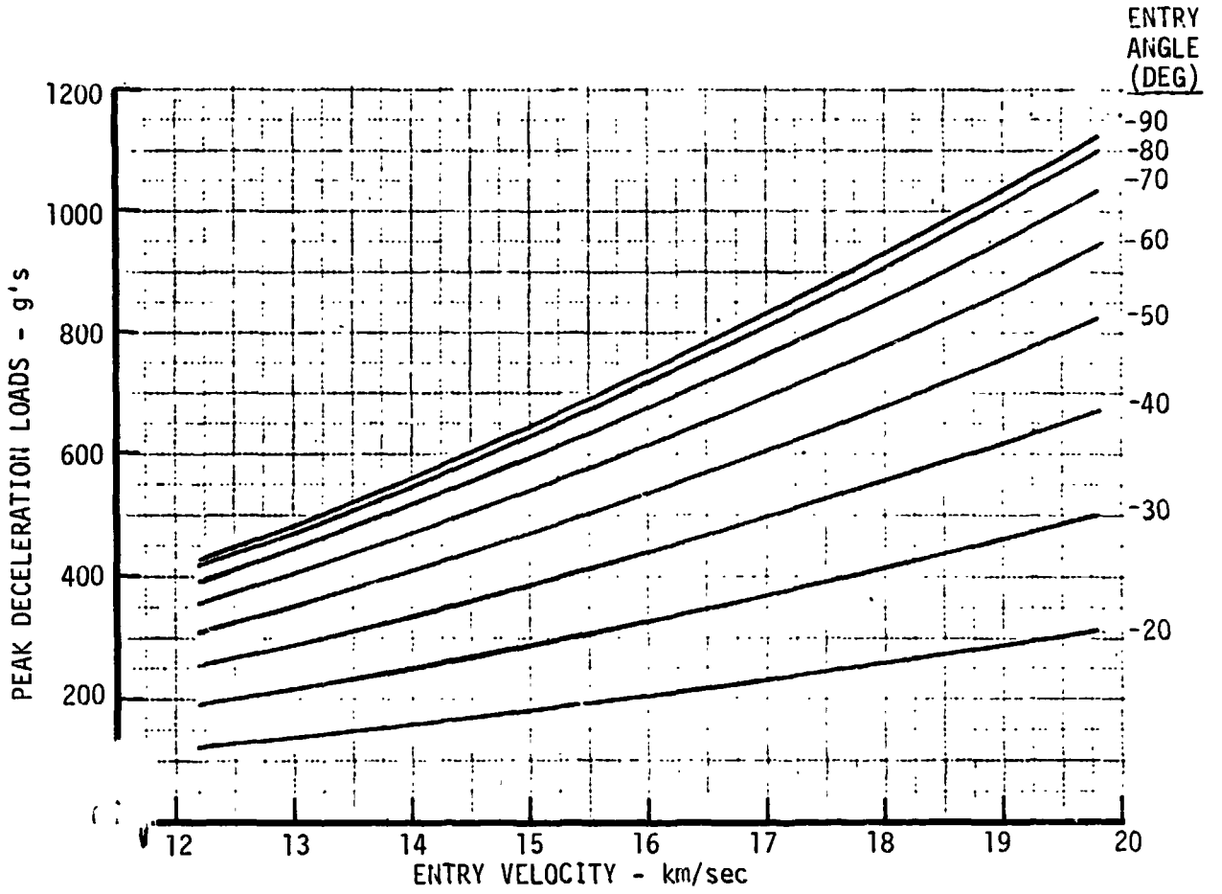

FIGURE 3-6

EARTH ENTRY RADIATIVE HEAT LOAD

- o STAGNATION POINT
- o NON-BLOWING
- o INERTIAL ENTRY CONDITIONS
- o β = 120 kg/m^2
- o R_N = .22 m

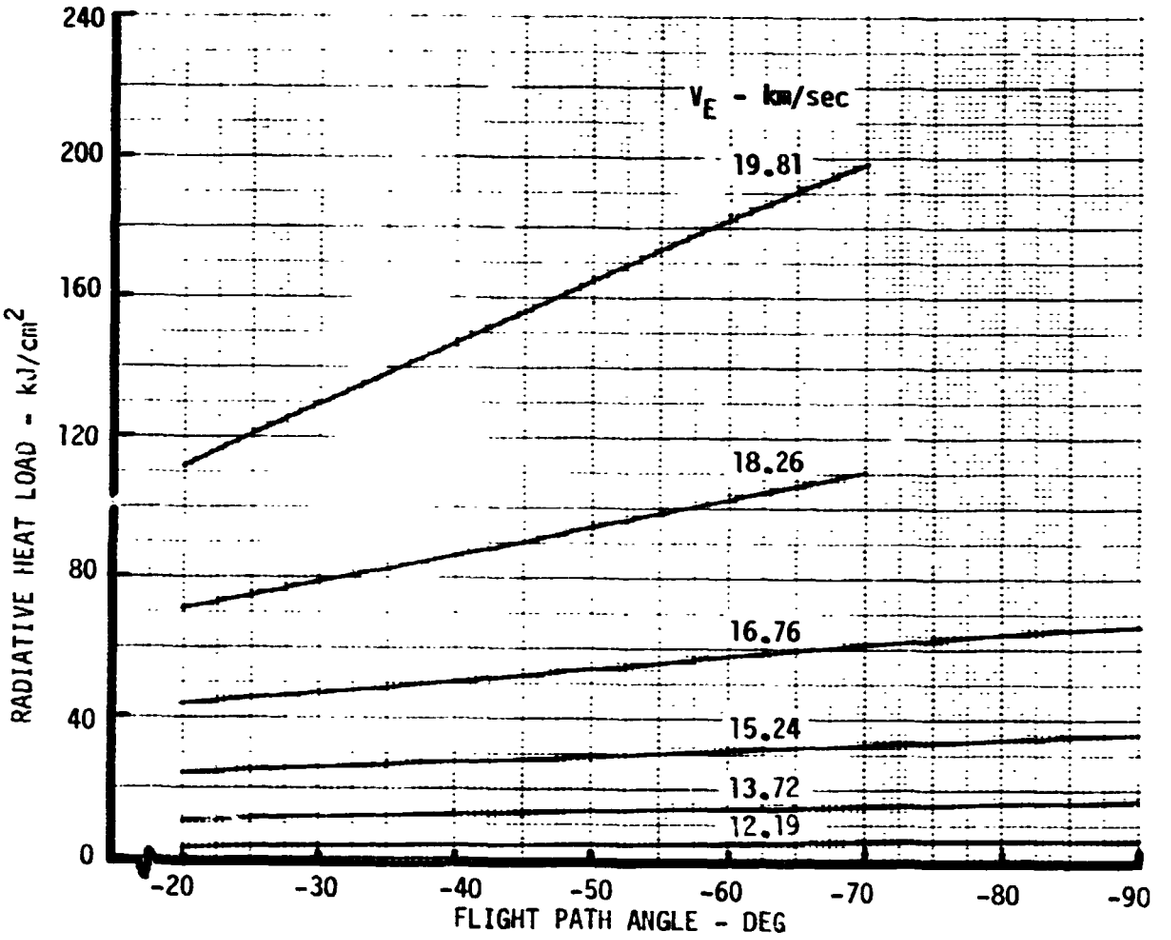

FIGURE 3-7

EARTH ENTRY CONVECTIVE HEAT LOAD

- o STAGNATION POINT
- o NON-BLOWING
- o INERTIAL ENTRY CONDITIONS
- o β = 120 kg/m^2
- o R_N = .22 m

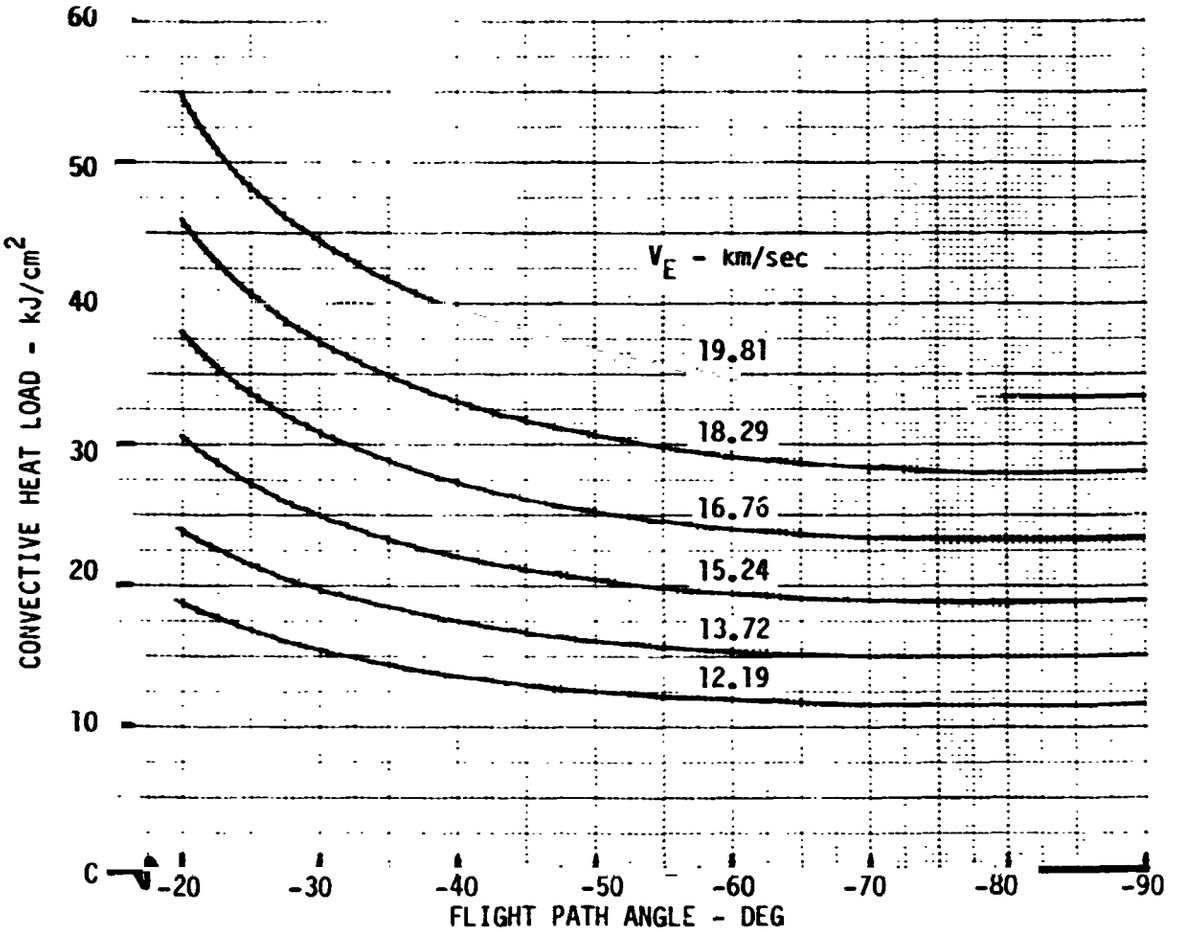

FIGURE 3-8

EARTH ENTRY TOTAL HEAT LOAD

- o STAGNATION POINT
- o NON-BLOWING
- o INERTIAL ENTRY CONDITIONS
- o β = 120 kg/m^2
- o R_N = .22 m

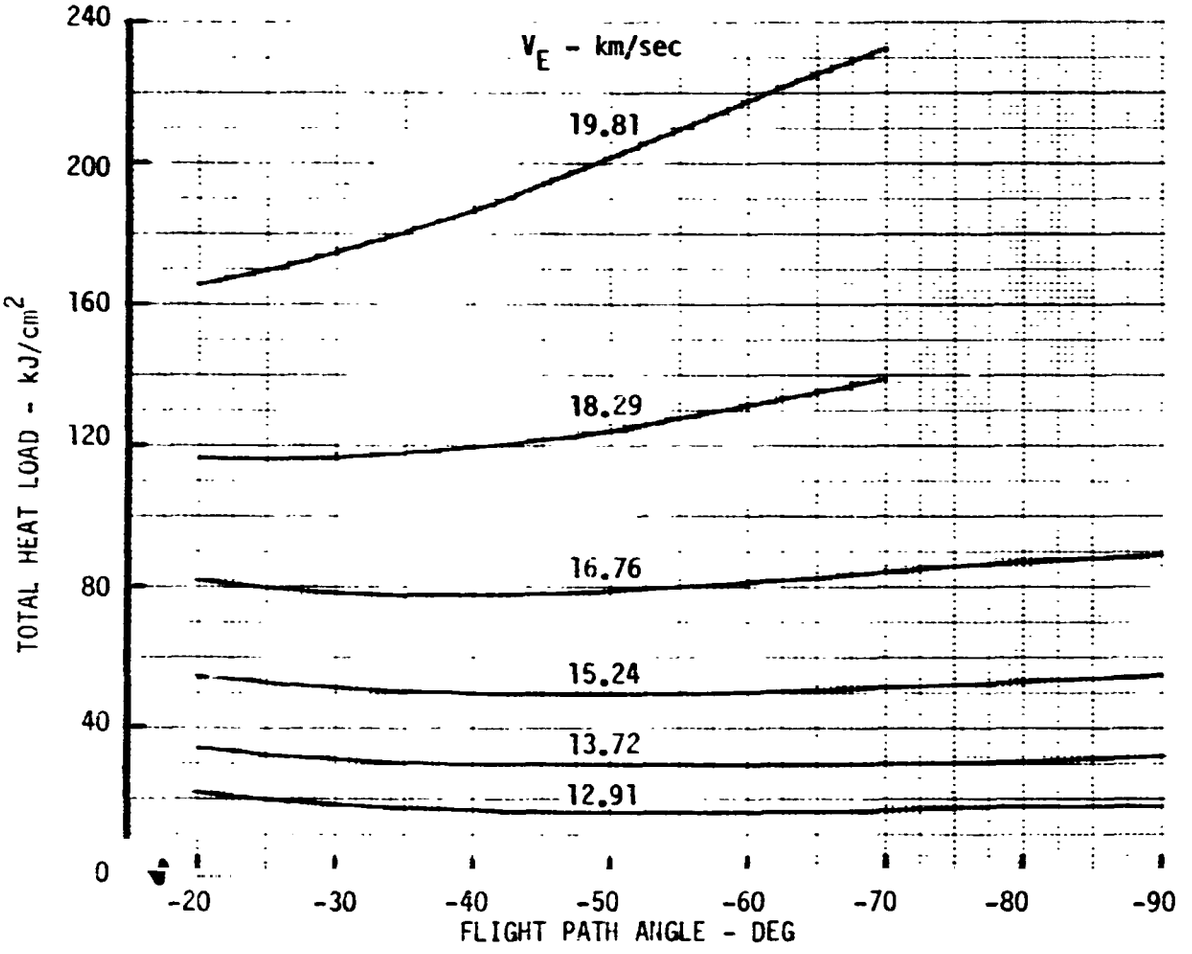

FIGURE 3-9

EARTH ENTRY HEAT PULSE DURATION

- o 0.5 kW/cm^2 THRESHOLD
- o β = 120 kg/m^2
- o R_N = .22 m

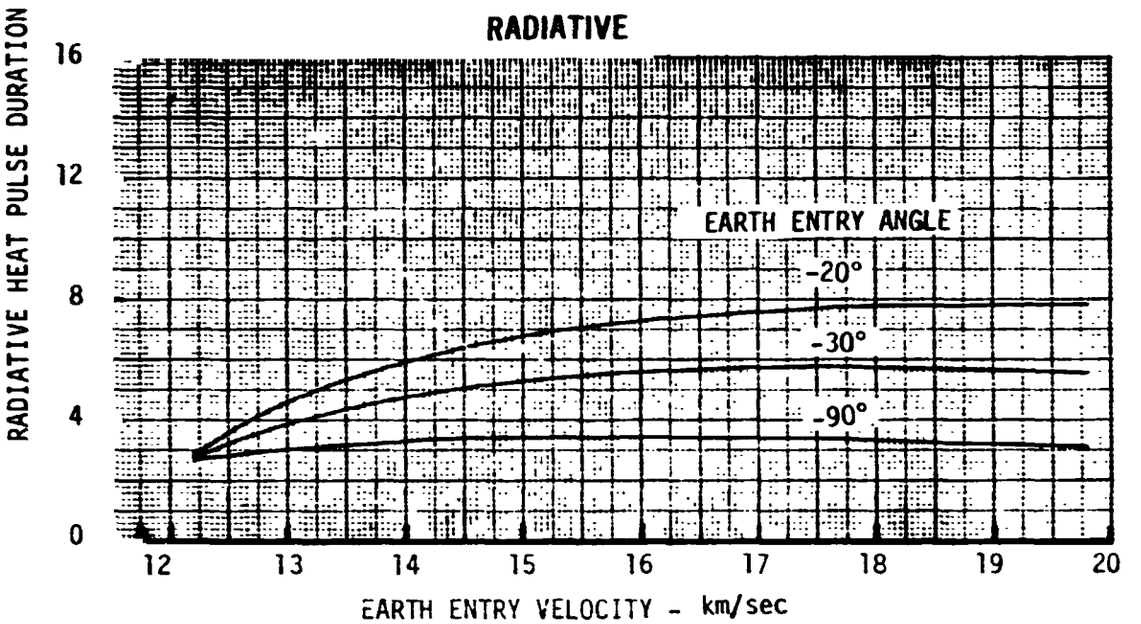

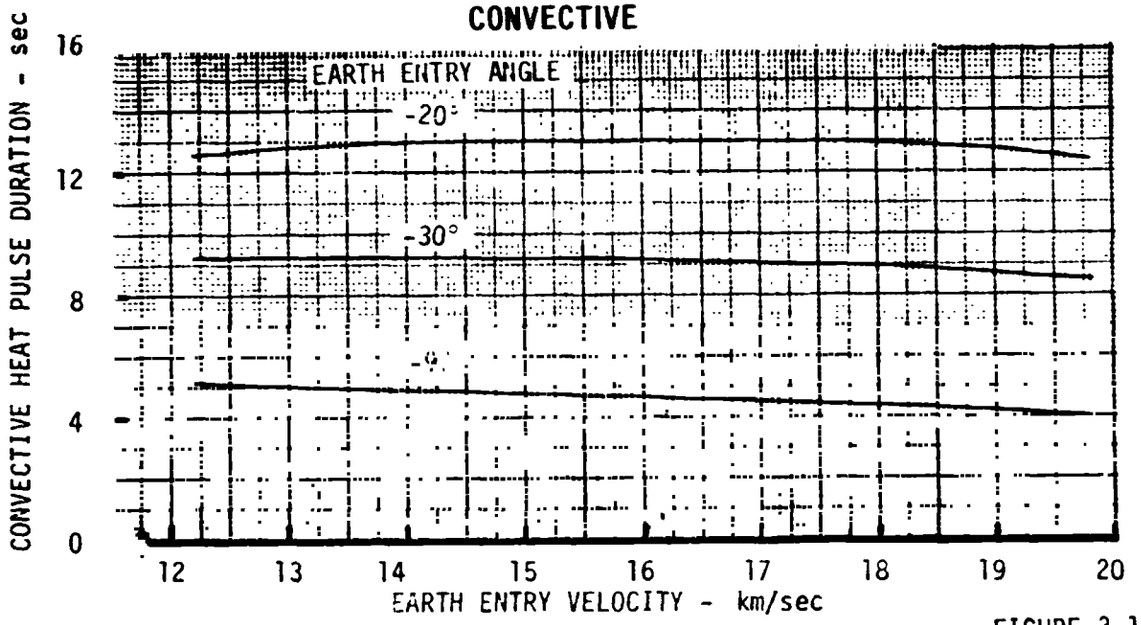

FIGURE 3-10

EARTH ENTRY CONDITIONS TO SIMULATE RADIATIVE HEAT FLUX

o β = 120 kg/m^2 o R_N = .22 m

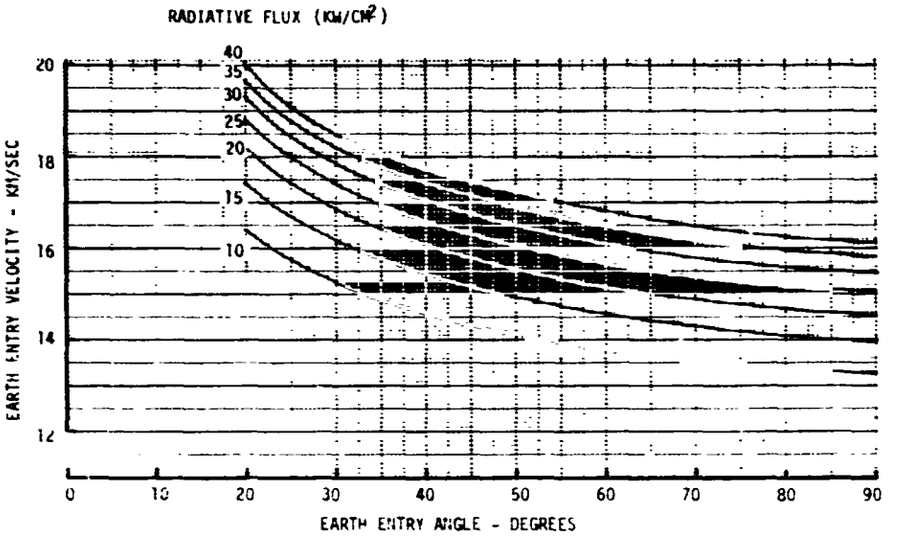

FIGURE 3-11

EARTH ENTRY CONDITIONS TO SIMULATE CONVECTIVE HEAT FLUX

o β = 120 kg/m^2 o R_N = .22 m

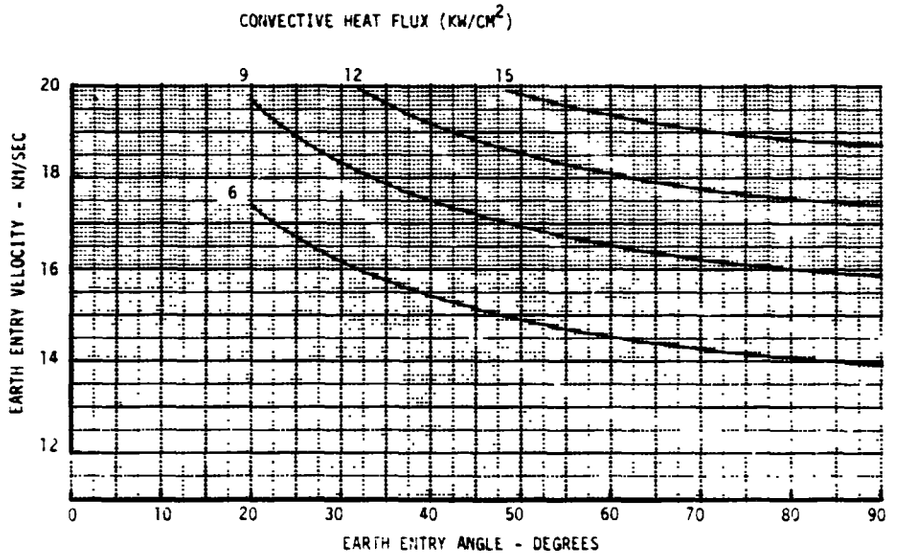

FIGURE 3-12

EARTH ENTRY CONDITIONS TO SIMULATE PEAK STAGNATION PRESSURE

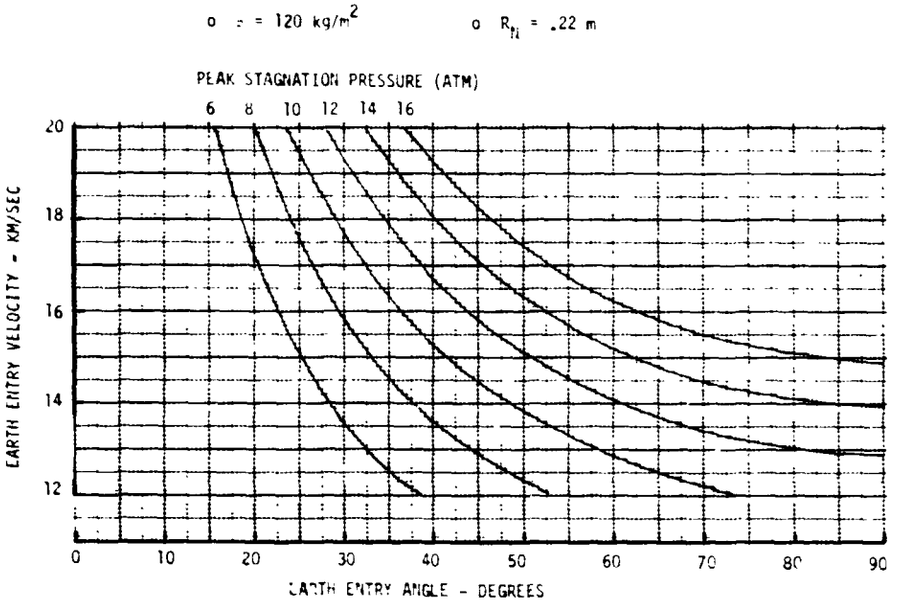

FIGURE 3-13

EARTH ENTRY CONDITIONS TO SIMULATE DECELERATION LOADS

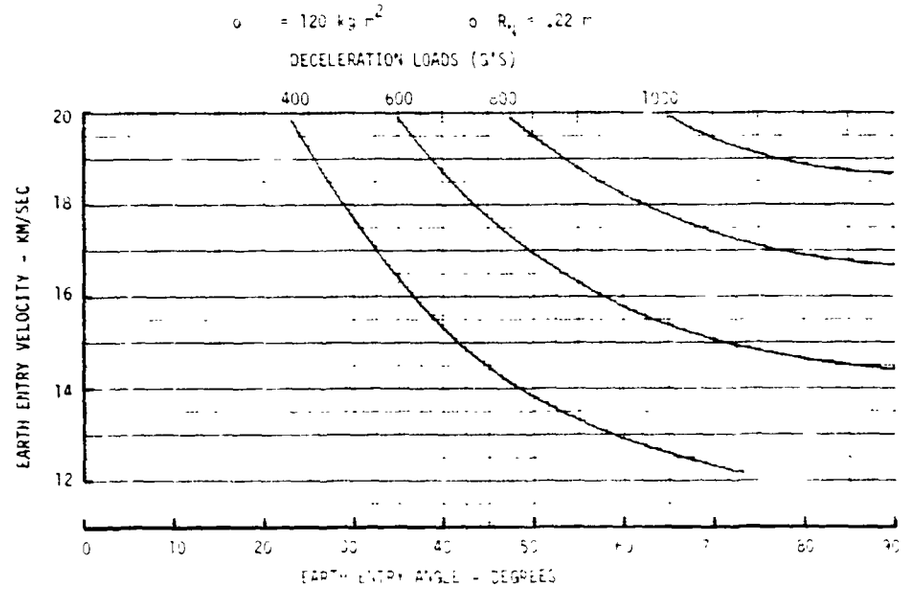

FIGURE 3-14

3.2 Environment Sensitivity to Configuration - The effect of variations in ballistic coefficient (β) and nose radius (R_N) are shown in terms of their effect on peak heating rates, pressure and "g" loads. Information is presented in the form of normalized sensitivity factors and also by illustrating the change in initial entry conditions required to achieve selected levels of radiative heat flux. These data are intended to provide a simplified scaling method that can be applied over a wide range of initial entry conditions. They reflect the combined results of many point design computer runs. However, a degree of environment approximation is incorporated to achieve the desired range of entry condition applicability with a simple presentation of data. Hence these predicted environment variations with vehicle configuration should be considered first order trend data as opposed to precise, point design solutions.

Normalized sensitivity factors are summarized in Figure 3-15 and presented graphically in Figures 3-16 through 3-19. Vehicle characteristics are referenced to the β and R_N values employed in Section 3.1. Similarly, the environment parameters are referenced to the values shown in Section 3.1 for any given entry angle and velocity combination. As indicated, both radiative and convective flux levels are influenced by both β and R_N. However, pressure level is strong function of β but independent of R_N while deceleration "g" loads are essentially independent of both vehicle parameters. These unequal dependences on vehicle configuration implies that various combinations of environment parameters can be produced by proper manipulation of vehicle design characteristics.

Vehicle configuration variations also influence entry condition requirements if the level of environment simulation is fixed. This influence is illustrated in Figures 3-20 through 3-25 for representative levels of radiative heat flux. Figures 3-20 through 3-22 show the effect of β changes only (R_N = reference) while Figures 3-23 through 3-25 indicate the β effect with a smaller R_N (higher convective flux). These data show that increasing β can substantially lower either the entry angle or the entry velocity requirement. This also implies that a reduction in required booster size may be possible. If β is increased by mass addition, the reduction in booster ΔV required (lower entry conditions) may be greater than the reduction in booster ΔV capability (payload mass increase).

EARTH ENTRY ENVIRONMENT SENSITIVITIES SUMMARY

- o STAGNATION POINT
- o NON BLOWING

- o $\beta_{REF} = 120\ kg/m^2$
- o $(R_N)_{REF} = .22\ m$

CONFIGURATION FACTORS					
β/β_{REF}	$R_N/(R_N)_{REF}$	$\frac{\dot{q}_R}{(\dot{q}_R)_{REF}}$	$\frac{\dot{q}_c}{(\dot{q}_c)_{REF}}$	$\frac{P_{STAG}}{(P_{STAG})_{REF}}$	$\frac{G's}{(G's)_{REF}}$
0.5	0.5	.346	.983	.474	.948
	1.0	.434	.696	.474	.948
	1.5	.480	.568	.474	.948
	2.0	.522	.492	.474	.948
1.0	0.5	.788	1.414	1.000	1.000
	1.0	1.000	1.000	1.000	1.000
	1.5	1.563	.816	1.000	1.000
	2.0	1.283	.707	1.000	1.000
1.5	0.5	1.268	1.731	1.540	1.027
	1.0	1.631	1.241	1.540	1.027
	1.5	1.893	1.007	1.540	1.027
	2.0	2.115	.872	1.540	1.027
2.0	0.5	1.756	2.033	2.094	1.047
	1.0	2.325	1.438	2.094	1.047
	1.5	2.725	1.174	2.094	1.047
	2.0	3.073	1.017	2.094	1.047

FIGURE 3-15

EARTH ENTRY ENVIRONMENT SENSITIVITY TO BALLISTIC COEFFICIENT

- o STAGNATION POINT
- o NON BLOWING
- o β_{REF} = 120 kg/m^2
- o $(R_N)_{REF}$ = .22 m

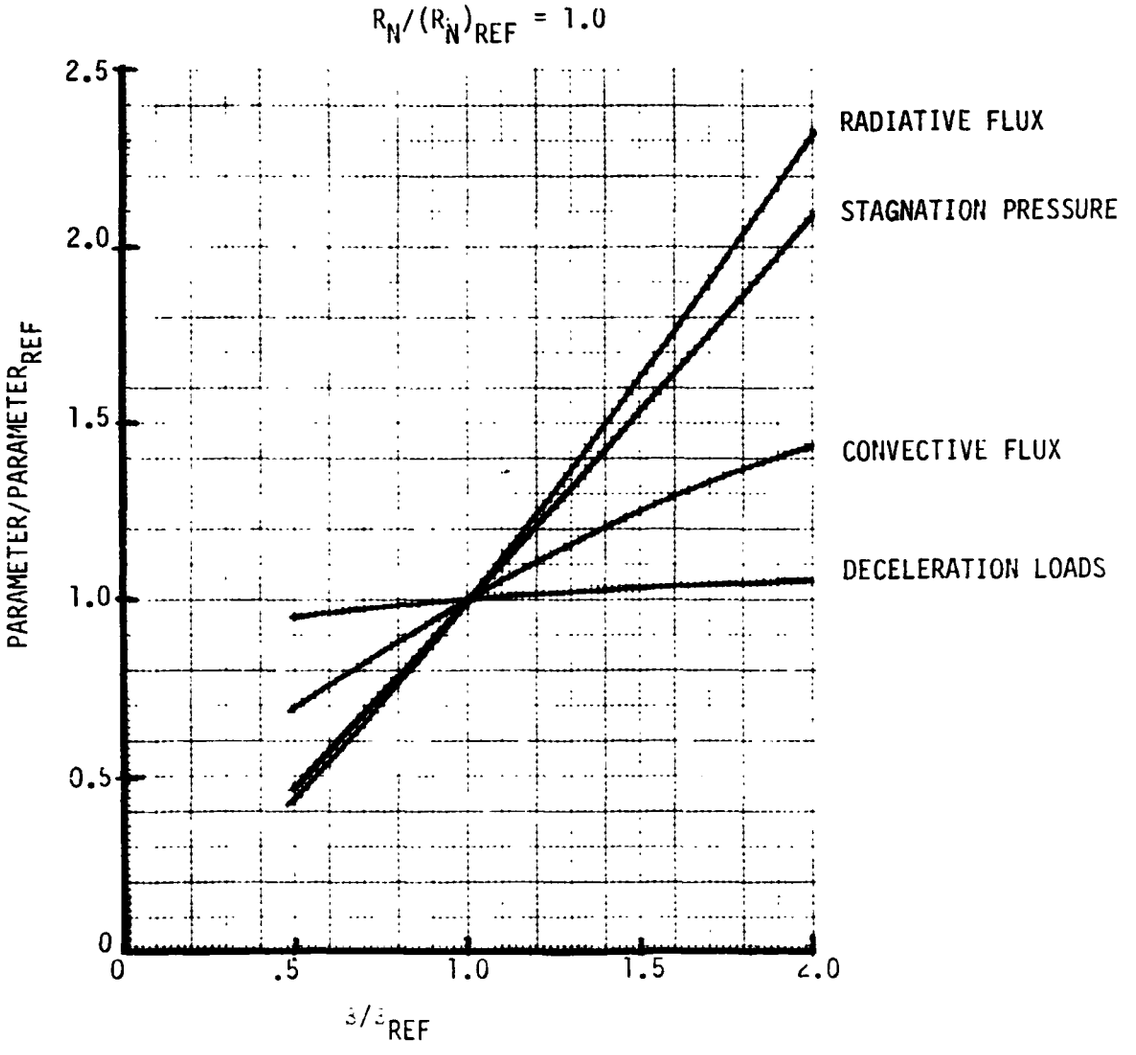

FIGURE 3-16

EARTH ENTRY ENVIRONMENT SENSITIVITY TO NOSE RADIUS

- o STAGNATION POINT
- o NON BLOWING

$\beta_{REF} = 120\ kg/m^2$

$(R_N)_{REF} = .22\ m$

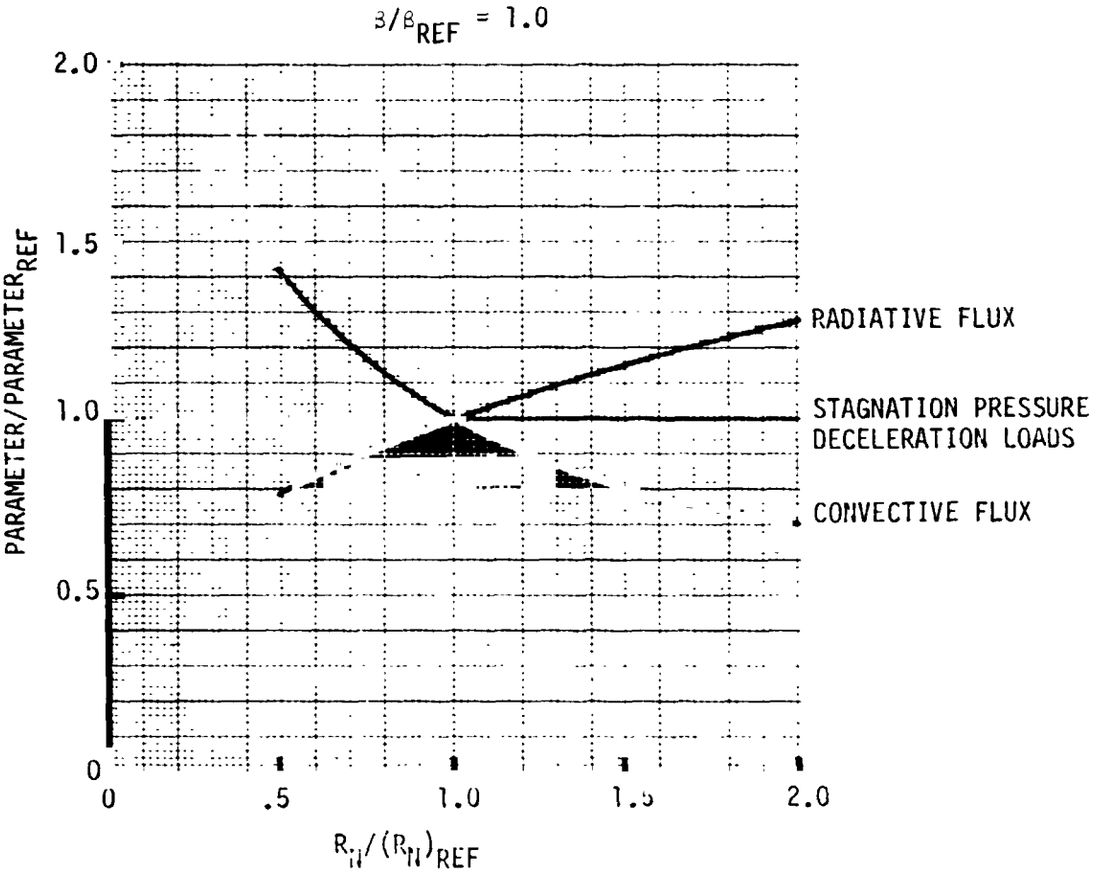

FIGURE 3-17

RADIATIVE FLUX SENSITIVITY TO VEHICLE CONFIGURATION

- o EARTH ENTRY
- o STAGNATION POINT
- o NON-BLOWING
- o $\beta_{REF} = 120\ kg/m^2$
- o $(R_N)_{REF} = .22\ m$

(a) BALLISTIC COEFFICIENT

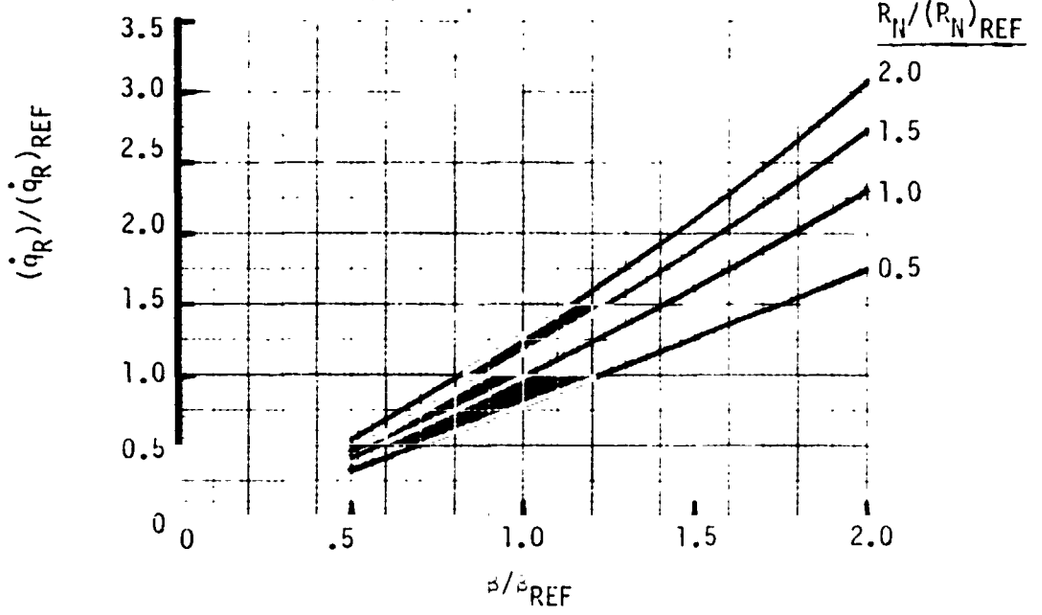

(b) NOSE RADIUS

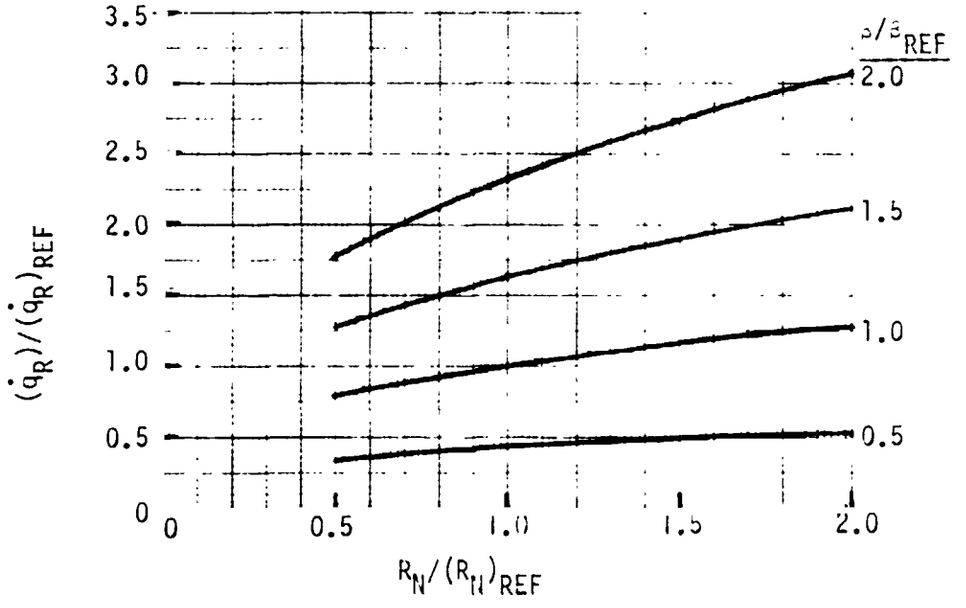

FIGURE 3-18

CONVECTIVE FLUX SENSITIVITY TO VEHICLE CONFIGURATION

- o EARTH ENTRY
- o STAGNATION POINT
- o NON BLOWING
- o $\beta_{REF} = 120\ kg/m^2$
- o $(R_N)_{REF} = .22\ m$

(a) BALLISTIC COEFFICIENT

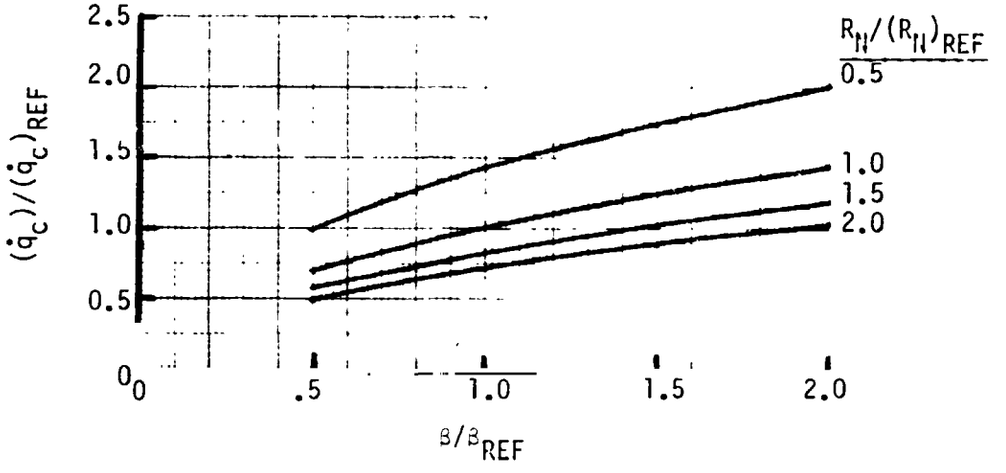

(b) NOSE RADIUS

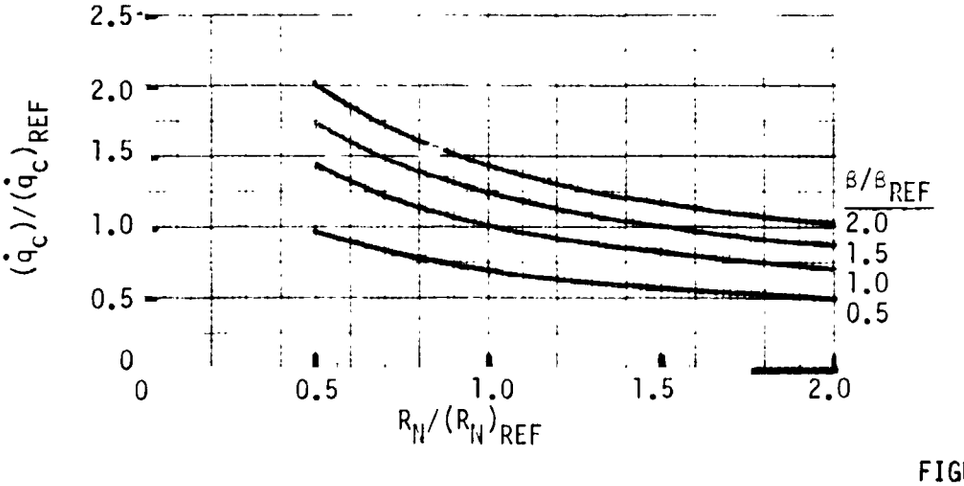

FIGURE 3-19

ENTRY CONDITION SENSITIVITY TO BALLISTIC COEFFICIENT FOR RADIATIVE FLUX SIMULATION

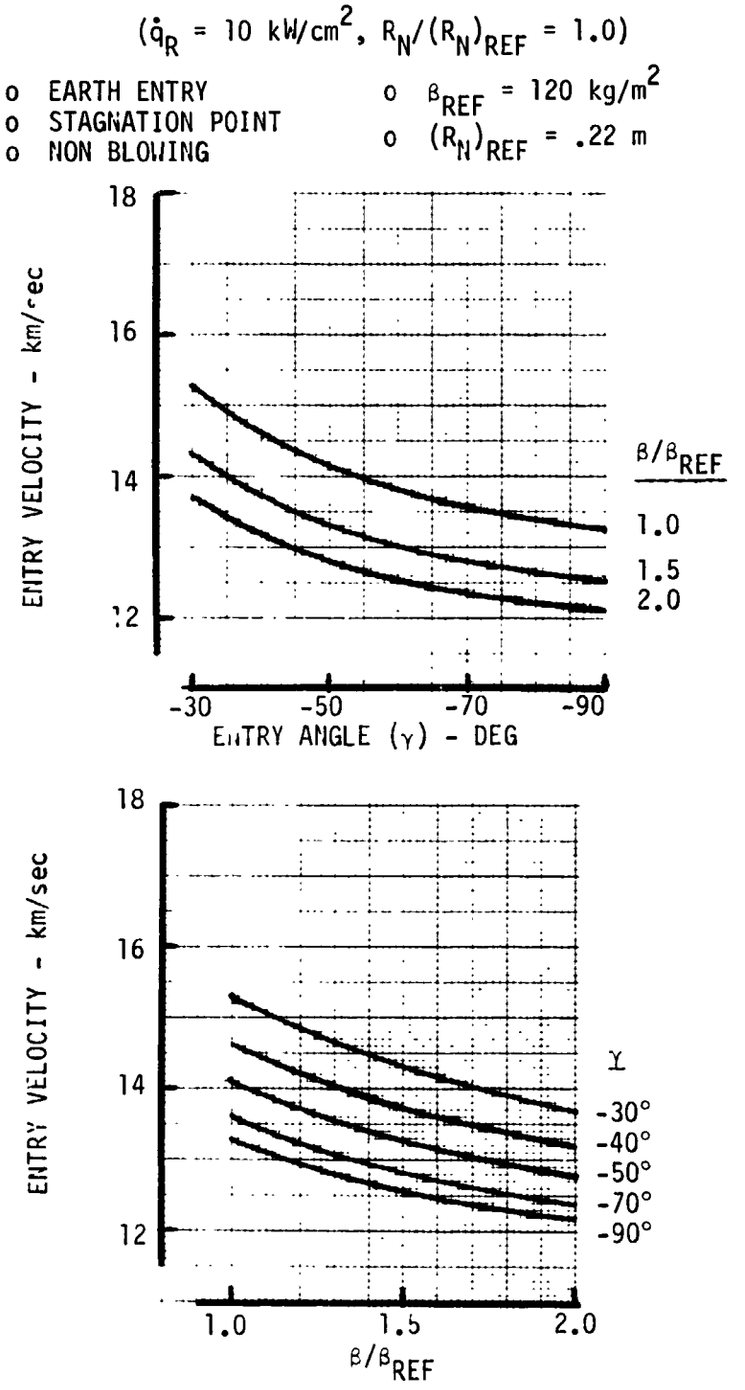

FIGURE 3-20

ENTRY CONDITION SENSITIVITY TO BALLISTIC COEFFICIENT FOR RADIATIVE FLUX SIMULATION

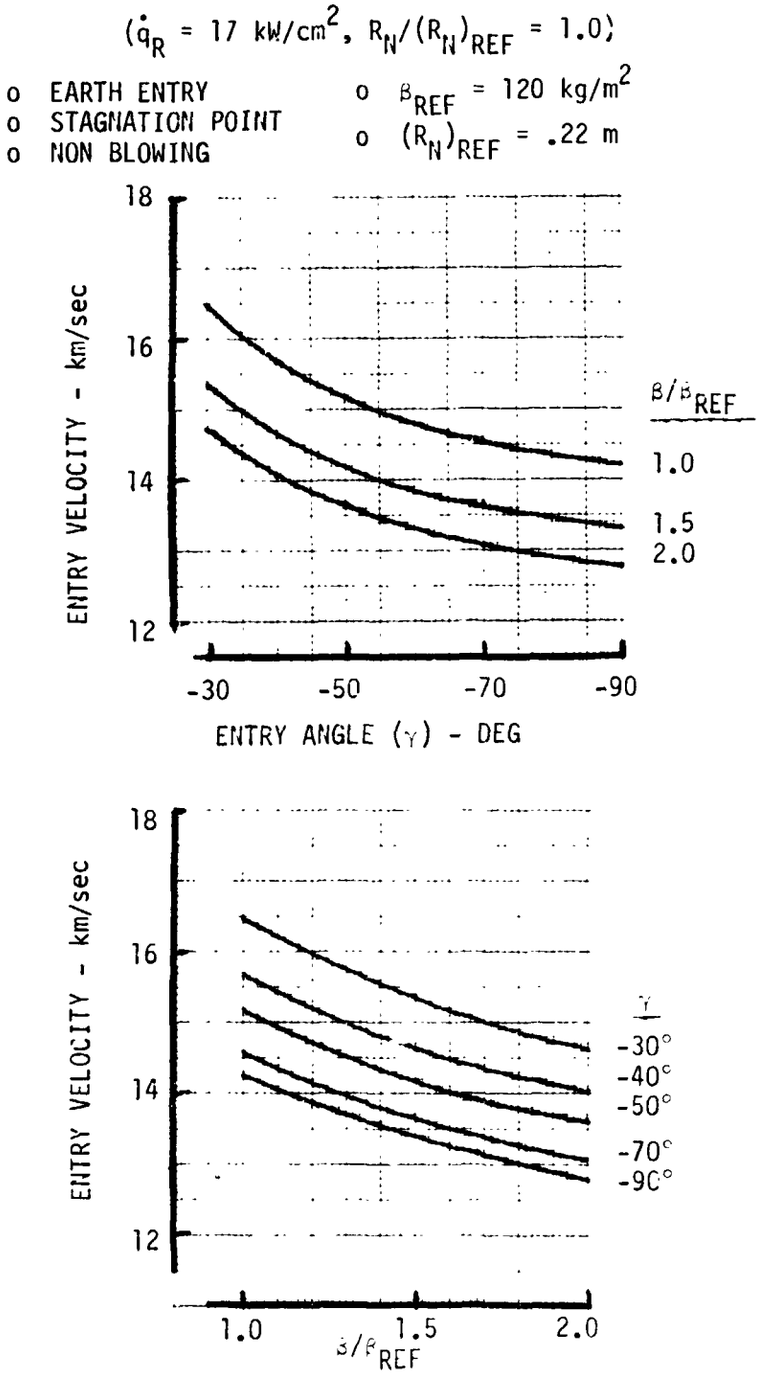

FIGURE 3-21

ENTRY CONDITION SENSITIVITY TO BALLISTIC COEFFICIENT FOR RADIATIVE FLUX SIMULATION

($\dot{q}_R$ = 40 kW/cm^2, $R_N/(R_N)_{REF}$ = 1.0)

- o EARTH ENTRY
- o STAGNATION POINT
- o NON BLOWING
- o β_{REF} = 120 kg/m^2
- o $(R_N)_{REF}$ = .22 m

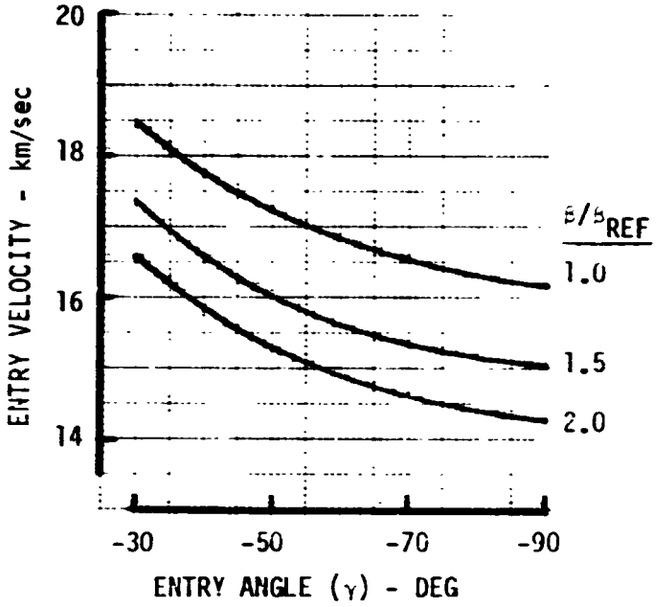

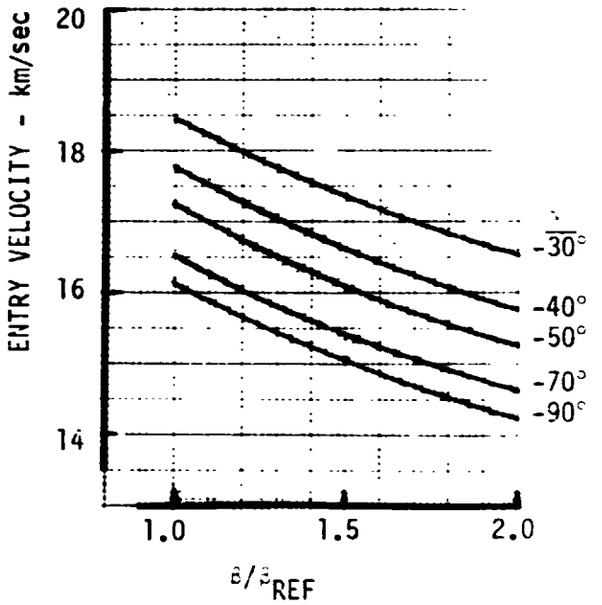

FIGURE 3-22

ENTRY CONDITION SENSITIVITY TO BALLISTIC COEFFICIENT FOR RADIATIVE FLUX SIMULATION

($\dot{q}_R$ = 10 kW/cm^2, $R_N/(R_N)_{REF}$ = 0.5)

- o EARTH ENTRY
- o STAGNATION POINT
- o NON BLOWING
- o β_{REF} = 120 kg/m^2
- o $(R_N)_{REF}$ = .22 m

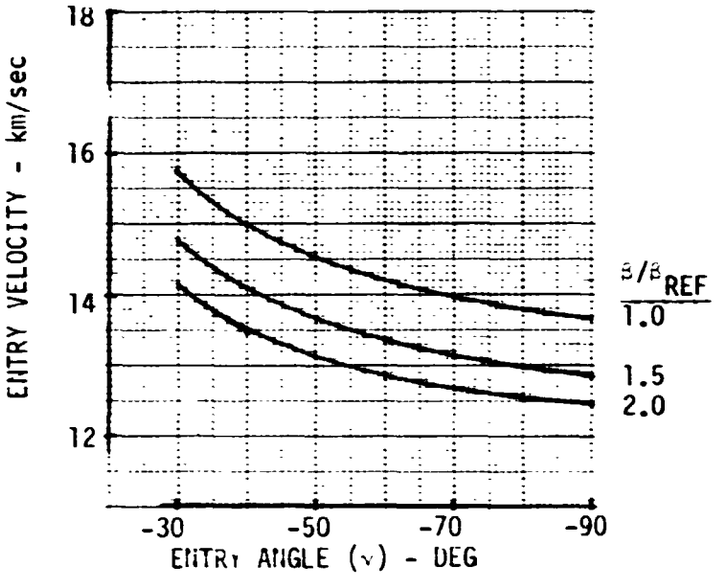

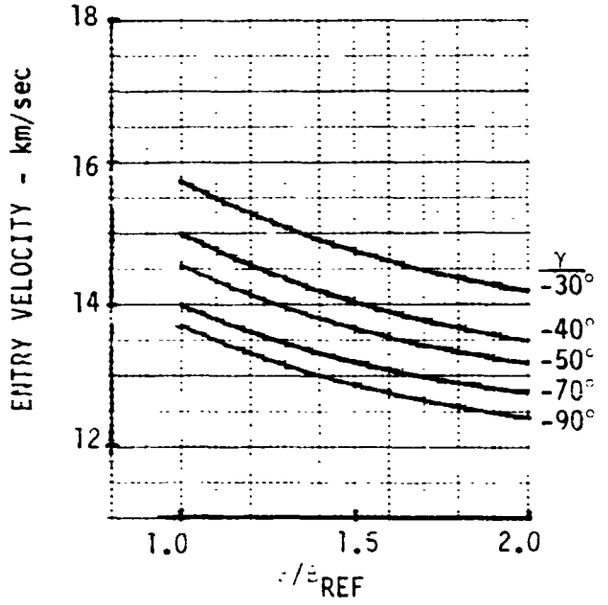

FIGURE 3-23

ENTRY CONDITION SENSITIVITY TO BALLISTIC COEFFICIENT FOR RADIATIVE FLUX SIMULATION

(q_R = 17 kW/cm^2, $R_N/(R_N)_{REF}$ = 0.5)

- o EARTH ENTRY
- o STAGNATION POINT
- o NON BLOWING
- o β_{REF} = 120 kg/m^2
- o $(R_N)_{REF}$ = .22 m

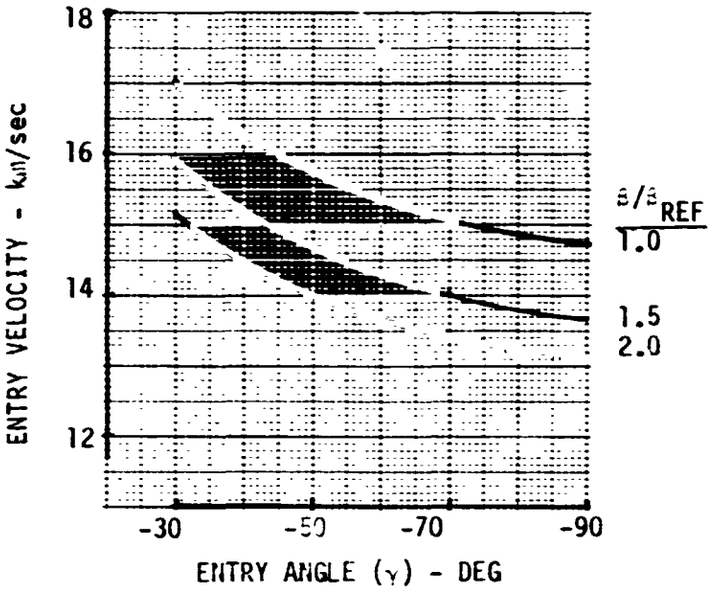

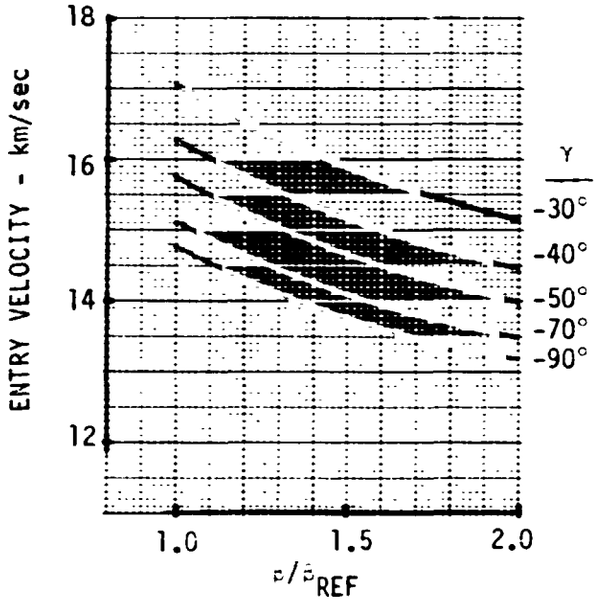

FIGURE 3-24

ENTRY CONDITION SENSITIVITY TO BALLISTIC COEFFICIENT FOR RADIATIVE FLUX SIMULATION

($\dot{q}_R$ = 40 kW/cm^2, $R_N/(R_N)_{REF}$ = 0.5)

- o EARTH ENTRY
- o STAGNATION POINT
- o NON BLOWING
- o β_{REF} = 120 kg/m^2
- o $(R_N)_{REF}$ = .22 m

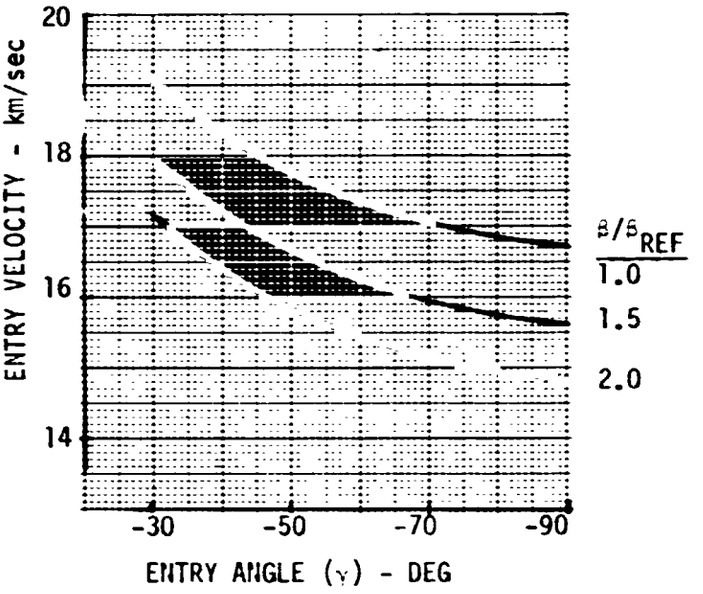

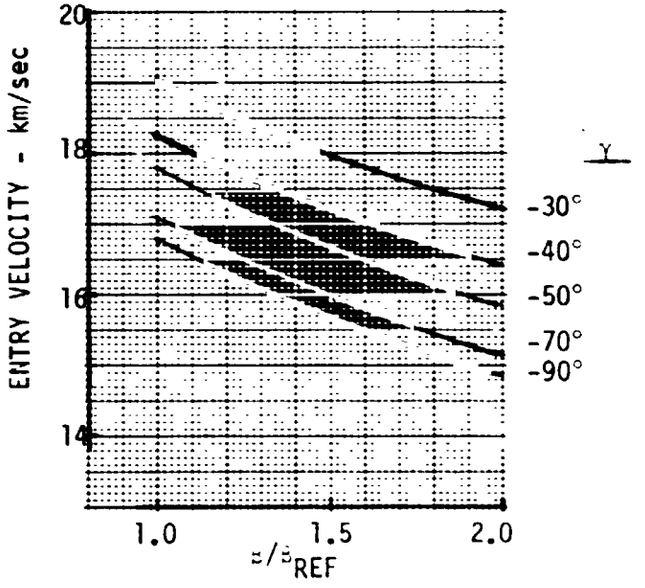

FIGURE 3-25

4.0 EARTH ORBIT MANEUVERS

A description of the maneuver requirements necessary to achieve a range of steep, fast entry conditions are presented in this section. This information is intended to give experiment planners an initial insight into the scope and nature of the orbital mission phase. Additionally, these data provide a means of comparing the initial entry conditions required for environment simulation (Section 3) with the performance capability of typical Shuttle launched boosters (Section 5).

This presentation of earth orbit maneuver requirements is organized in four parts. The first describes the basic, high apoapsis deorbit maneuver necessary to produce the extreme entry conditions of interest. The second part defines the required velocity increments for each maneuver burn as a function of entry conditions. The third part shows representative mission profiles in terms of ascent and descent ground tracks. The fourth part illustrates the correlation of environment simulation with velocity increment requirements using radiative heat flux as the example.

4.1 Deorbit Maneuver Description - The selected deorbit maneuver strategy is pictorially described in Figure 4-1. This highly elliptical trajectory technique, suggested by NASA-Ames, allows high speed and angle entries to be efficiently achieved from a low, circular initial orbit. Compared with a direct deorbit from low altitude, this maneuver strategy reduces thrust level requirements to those normally attainable with typical Shuttle upper stages and minimizes the velocity increment (ΔV) needed for steep entries.

As shown in Figure 4-1, three maneuver burns are used to accomplish deorbit beginning in a 185 km circular orbit. This initial orbit is selected as typical of Shuttle insertion conditions. The first maneuver is a tangential, posigrade burn that initiates hohmann transfer to a preselected apoapsis altitude (R_a). The value of R_a is treated as a basic mission variable and ranges from 2 to 40 earth radii above the earth's center. The second maneuver is a tangetial, retrograde burn applied at apoapsis to achieve the desired entry angle. This maneuver also adjusts the trajectory so that entry occurs at a proper location relative to the desired impact point. Any plane change corrections required to attain such an entry location would be included in the second burn by vector summing. The third maneuver burn is applied along the flight path just before entry to increase velocity up to the desired entry value.

DEORBIT MANEUVER STRATEGY

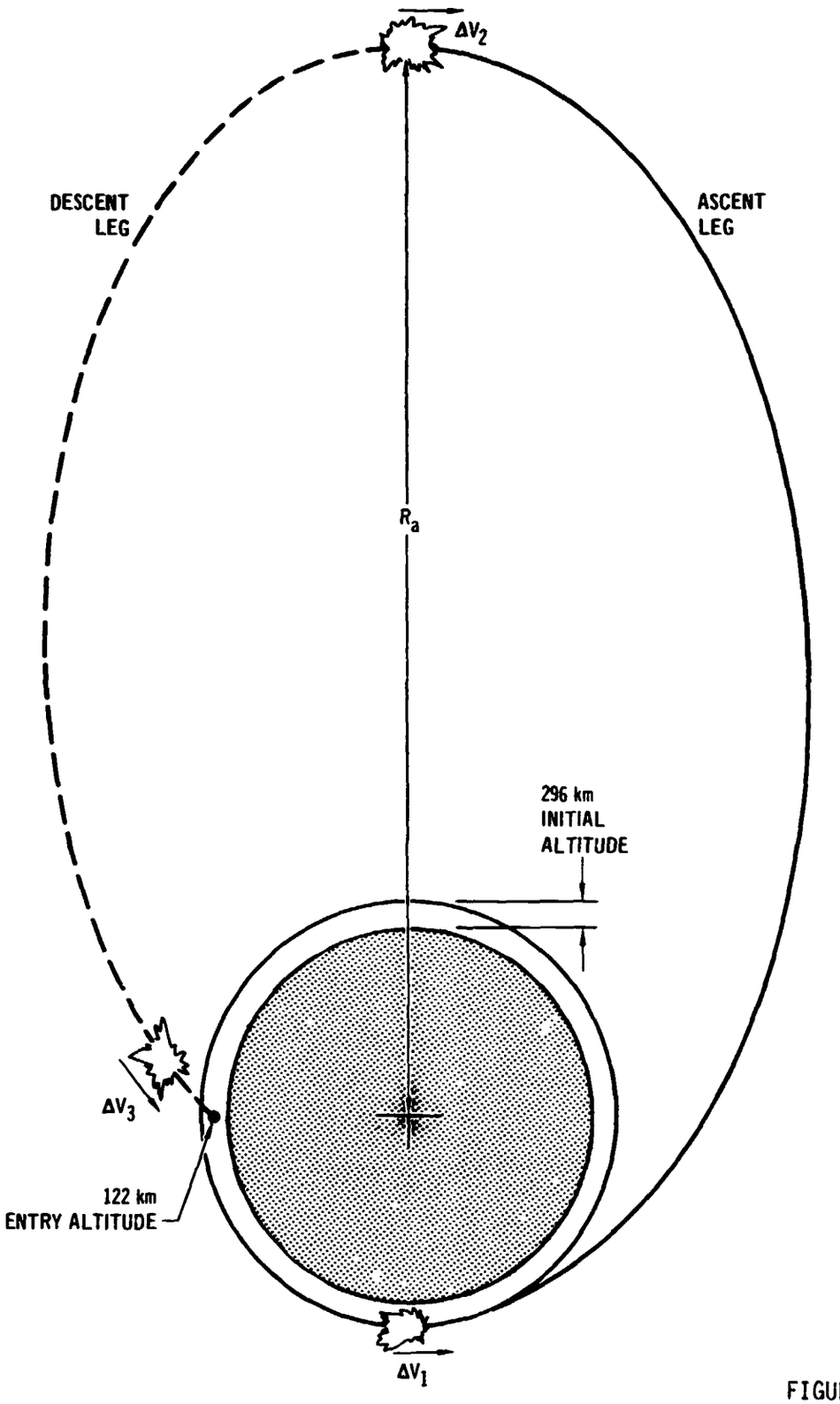

FIGURE 4-1

Figure 4-2 shows the entry velocity that would result if only the first two maneuver burns were accomplished. As indicated, each combination of entry angle and apoapsis distance produce a unique value of entry velocity that decreases with steeper angles and increases with high apoapsis distances. As apoapsis increases, the effect of entry angle diminishes to essentially zero and entry velocity approaches an upper limit of about 11 km/sec. This is well below the 13 to 20 km/sec range of required entry velocity (reference Section 3.0). Hence a third burn is always required, the magnitude of which is the difference between the required entry velocity and that achieved by a two burn maneuver.

Figure 4-3 shows the mission time interval required to accomplish the deorbit maneuver. This is the elapsed time between the first maneuver burn and the beginning of atmospheric entry at 122 km (400,000 ft). As shown, the time interval required is a strong function of apoapsis altitude but essentially independent of entry angle.

TWO BURN MANEUVER ENTRY VELOCITY (V*)

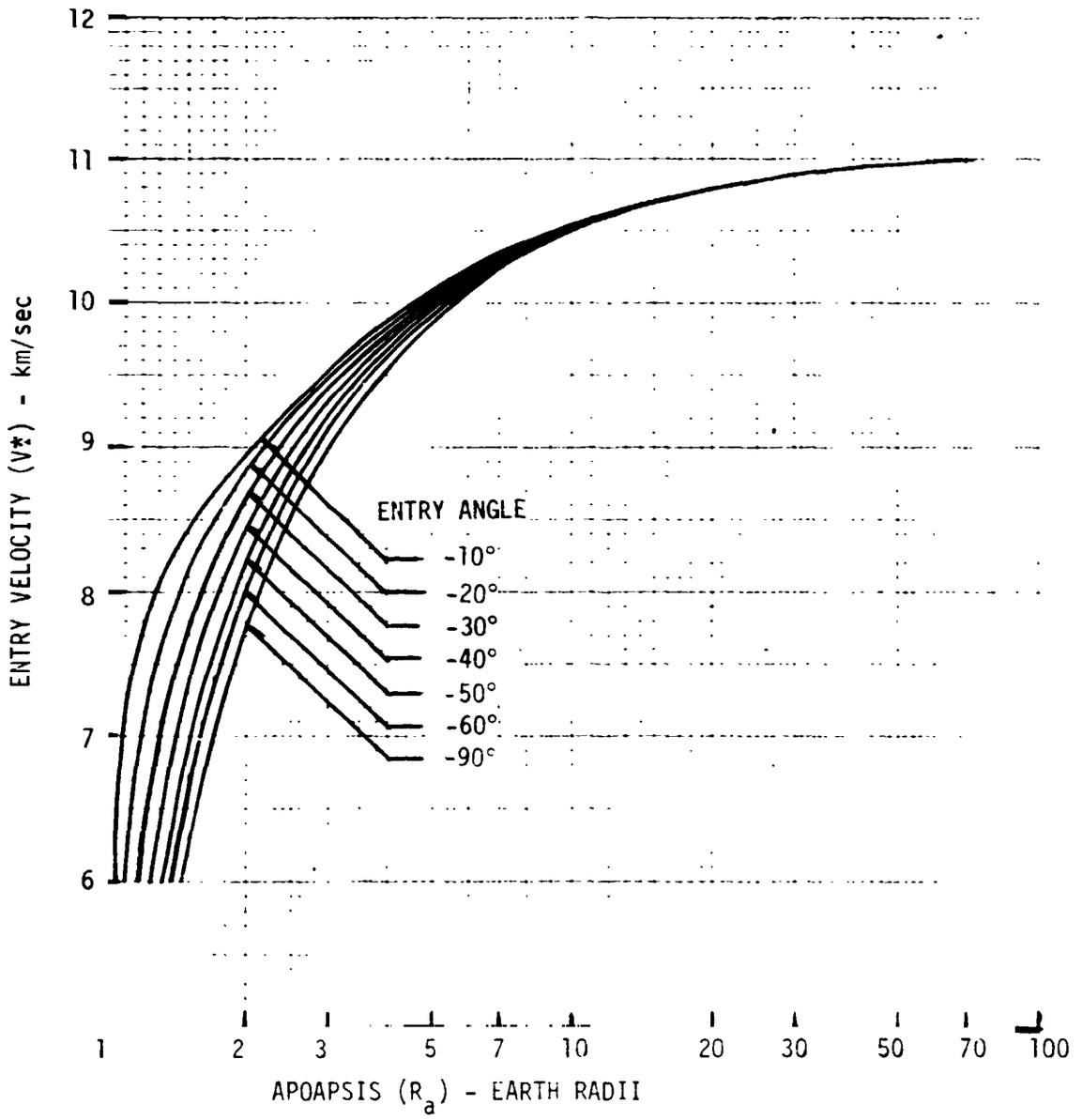

FIGURE 4-2

DEORBIT MANEUVER TIMES

o TIME FROM FIRST MANEUVER BURN TO ENTRY

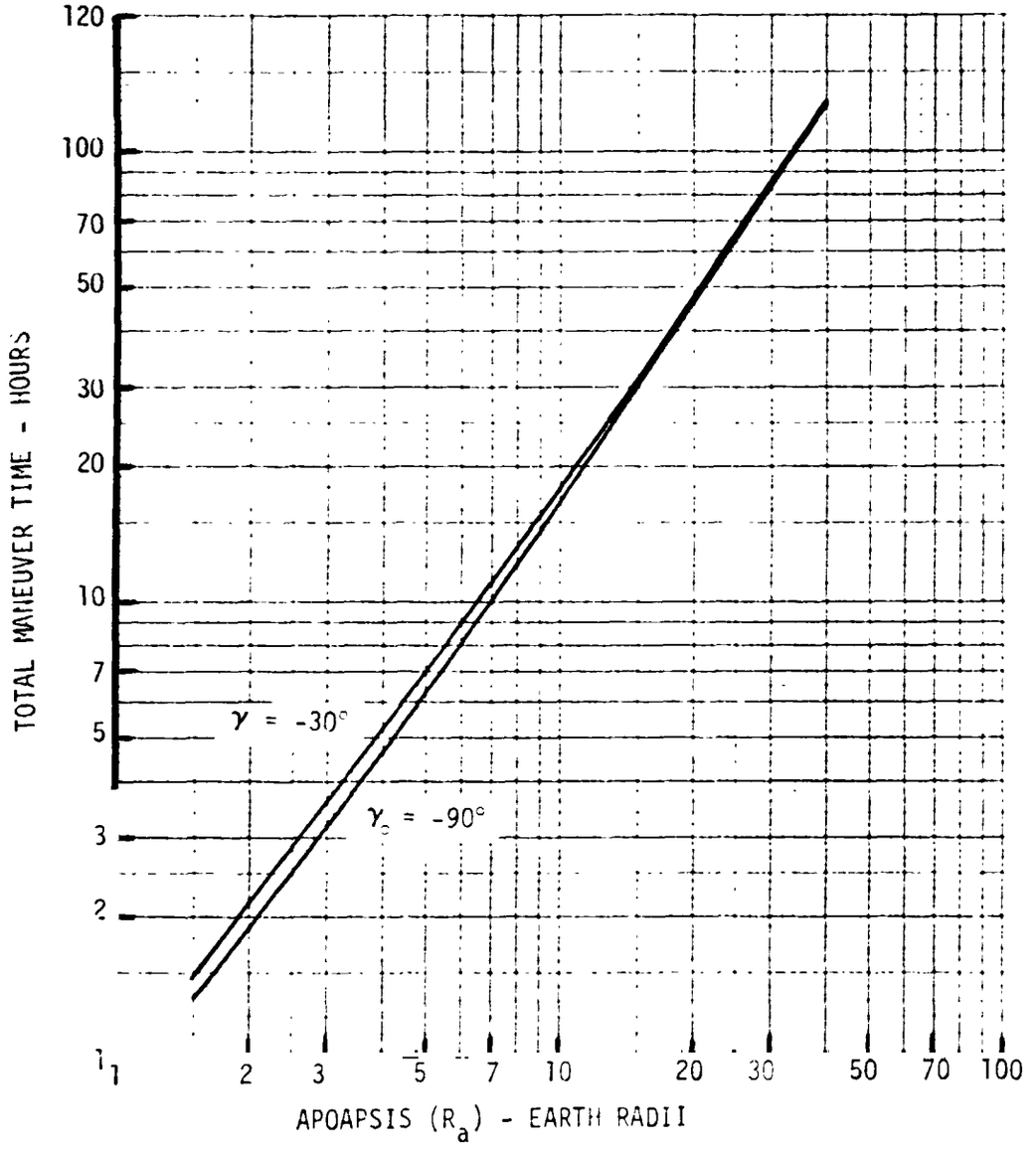

FIGURE 4-3

4.2 Velocity Increment Requirements - The inplane velocity increment (ΔV) required to accomplish the deorbit maneuvers are summarized in Figures 4-4 through 4-8. These data illustrate that the ΔV requirements are large but that they can be minimized by increasing apoapsis altitude, particularly for steep entry angles.

The ΔV required for the first or Hohmann transfer burn (Figure 4-4) increases with apoapsis but is independent of entry angle. However, the second or apoapsis burn ΔV requirements (Figure 4-5) reduce with increasing apoapsis and increase as entry angle becomes steeper. The net effect is illustrated by the Figure 4-6 summation of ΔV_1 and ΔV_2. At entry angles steeper than about -50 degrees, increasing apoapsis reduces the total two burn ΔV requirements. This trend becomes very pronounced as entry angle approaches -90 degrees. However, for shallow entries, a moderate ΔV penalty results from increasing apoapsis.

The ΔV required for the third or velocity adjustment burn is presented in Figure 4-7 as a function of desired entry velocity. As noted in the previous subsection, this ΔV_3 is the difference between the desired entry velocity and the entry velocity resulting from a two burn velocity only (reference Figure 4-2). Hence the ΔV_3 requirement decreases as apoapsis altitude increases. The trend is similar with entry angle although at high apoapsis, the ΔV dependency on entry angle diminishes to essentially zero.

The total deorbit maneuver ΔV requirements, summarized in Figure 4-8, increase linearly with entry velocity for a given apoapsis altitude and entry angle. Lowering entry angle reduces the total ΔV required as does increasing apoapsis altitude, particularly for steep entries.

An example of the ΔV penalty associated with out-of-plane maneuvers is illustrated in Figures 4-9 and 4-10. These values represent ΔV increments that must be added to the second burn, in plane requirements to achieve a preselected impact point location. The example shown assumes impact near Ascension Island and a due east launch of Shuttle from ETR. The Shuttle orbit numbers shown correspond to deorbit maneuver initiation (ΔV_1) sometime during the second, third or fourth Shuttle orbits following initial insertion. This is discussed further in the following subsection.

These data show that plane change ΔV penalties reduce with increasing apoapsis altitude and can be minimized by selecting a relatively steep entry angle. However, for apoapsis above 3 earth radii, this ΔV penalty is small to negligible compared to the total inplane ΔV requirements of Figure 4-8.

FIRST BURN VELOCITY INCREMENT (ΔV_1) REQUIREMENTS

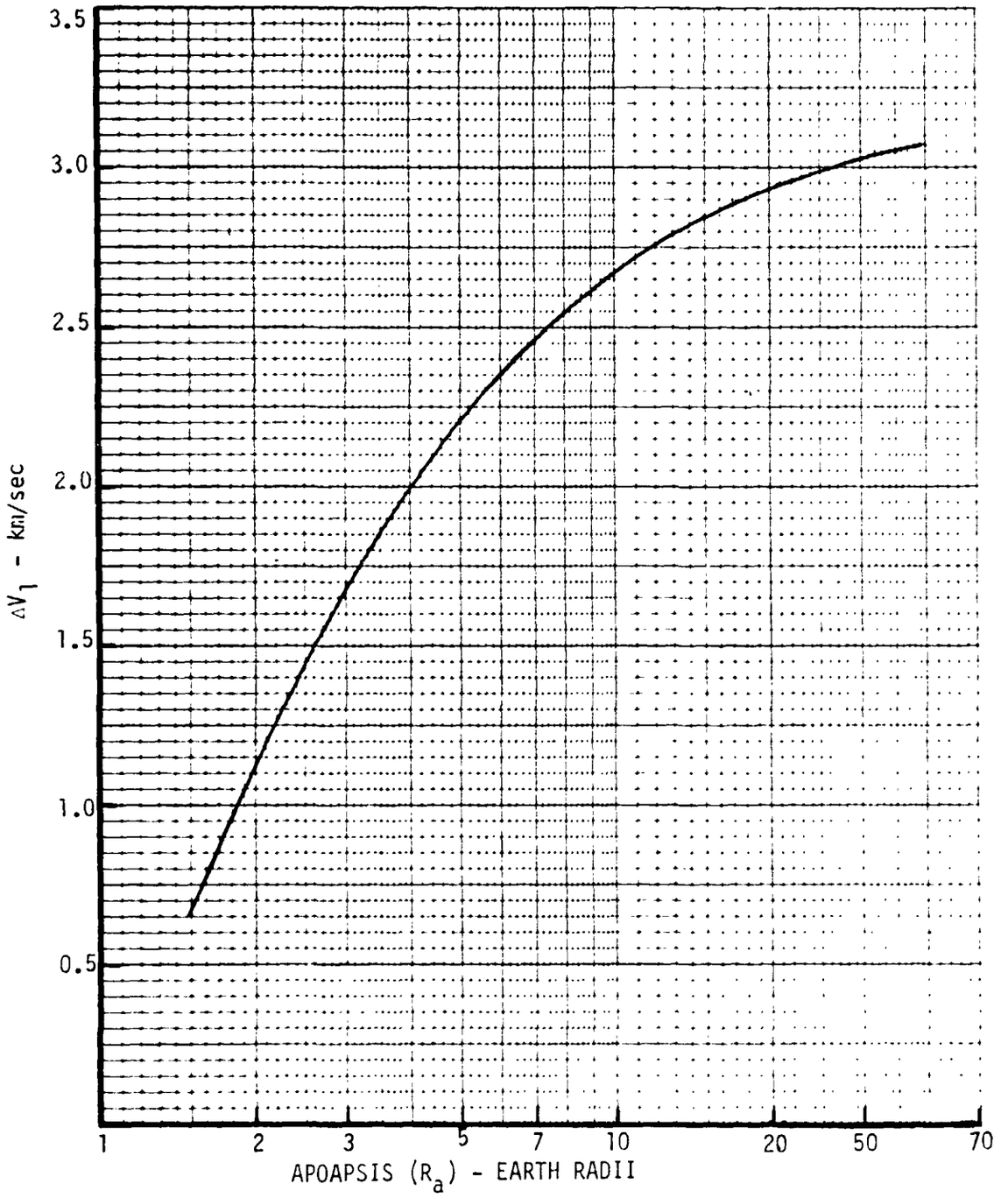

FIGURE 4-4

SECOND BURN VELOCITY INCREMENT (ΔV_2) REQUIREMENTS

o IN PLANE MANEUVER

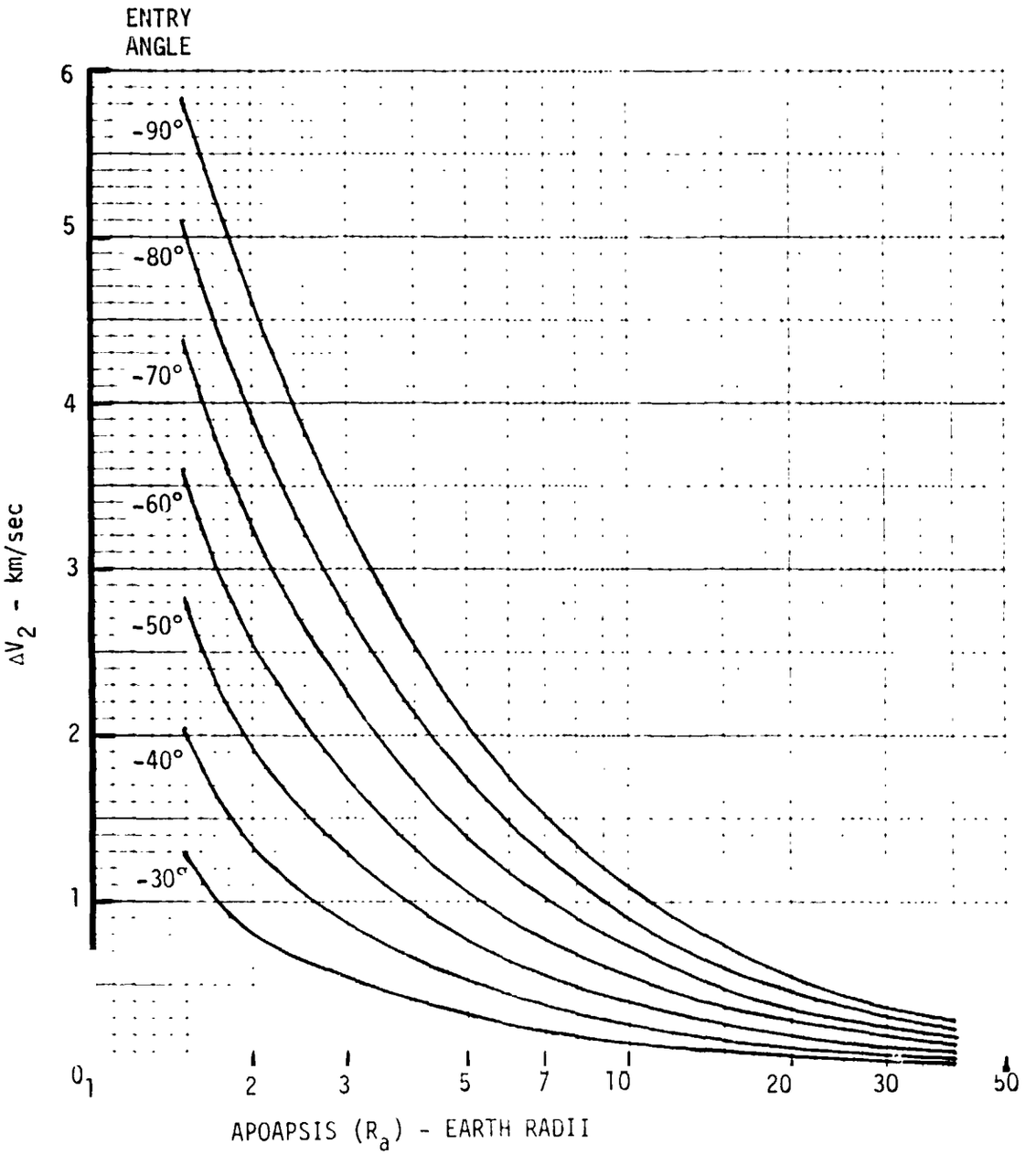

FIGURE 4-5

ASCENT PLUS ENTRY ANGLE VELOCITY INCREMENT ($\Delta V_1 + \Delta V_2$) REQUIREMENTS

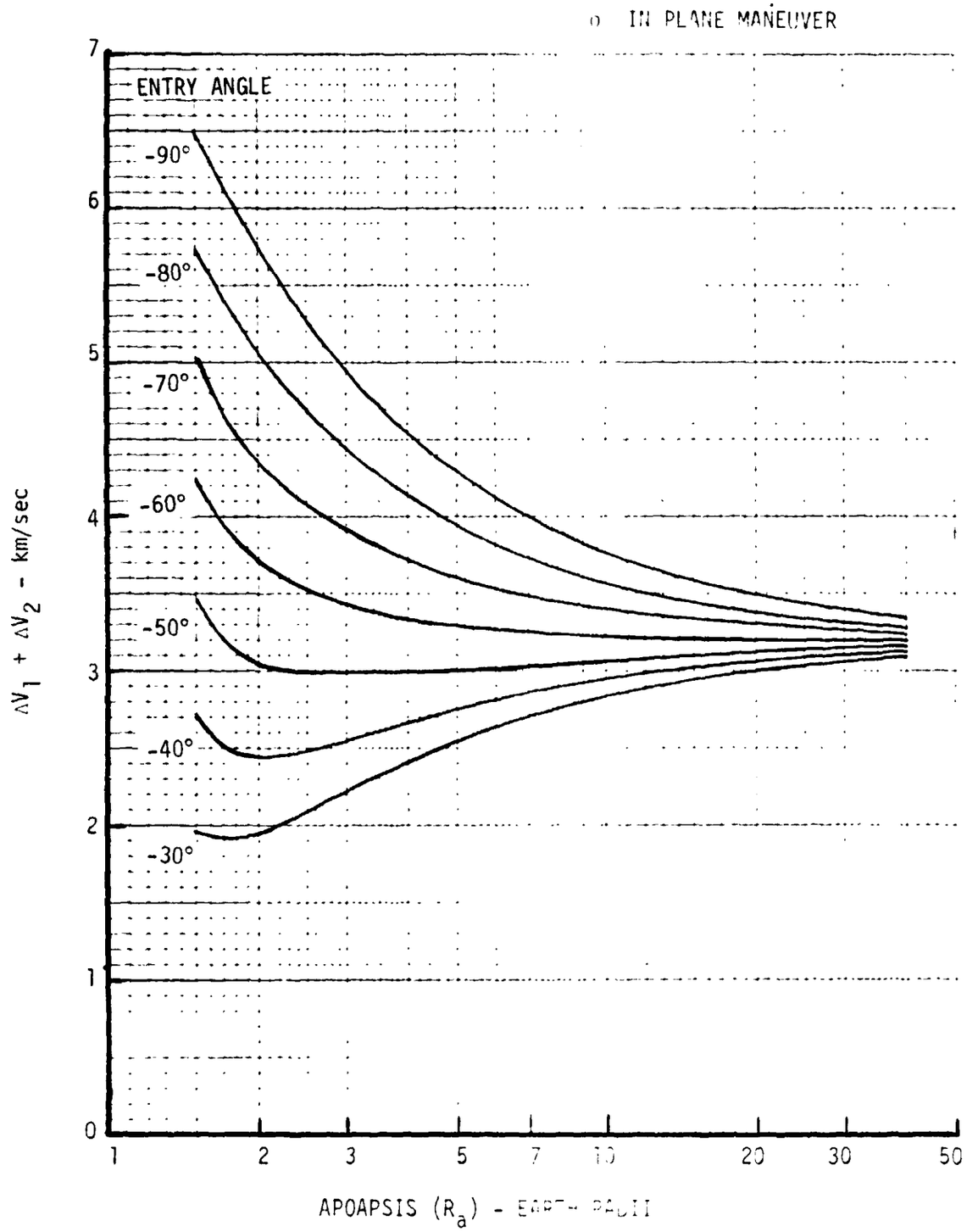

FIGURE 4-6

THIRD BURN VELOCITY INCREMENTS (ΔV_3) REQUIREMENT

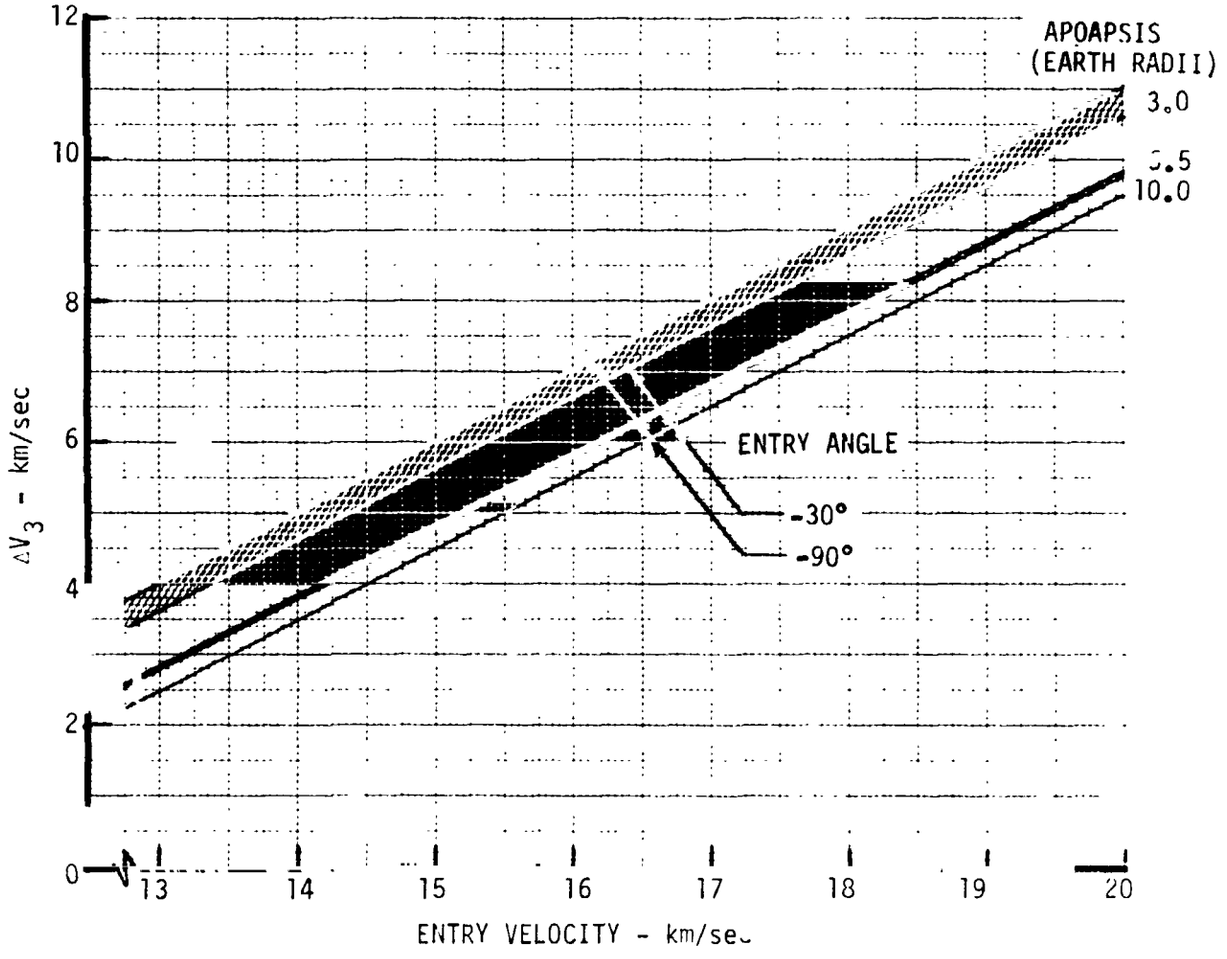

FIGURE 4-7

TOTAL VELOCITY INCREMENT (ΔV_{TOT}) REQUIREMENT

o IN PLANE MANEUVERS

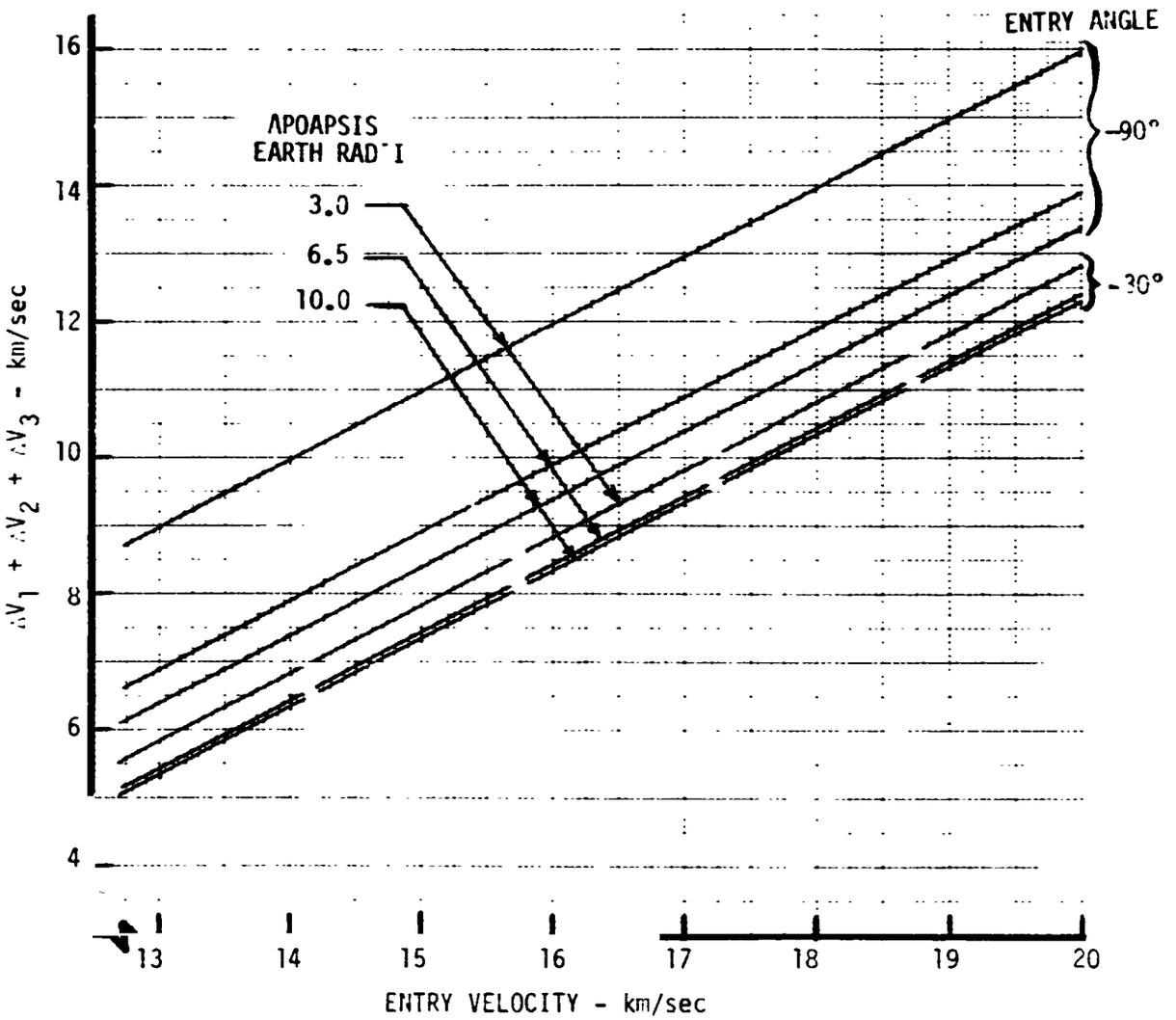

FIGURE 4-8

PLANE CHANGE ΔV PENALTY – R_a = 3.0

- o TOTAL ΔV_2 = ΔV_2 (IN PLANE) + $\Delta(\Delta V_2)$
- o DUE EAST LAUNCH FROM ETR TO 296 KM CIRCULAR ORBIT
- o ASCENSION ISLAND RECOVERY ZONE

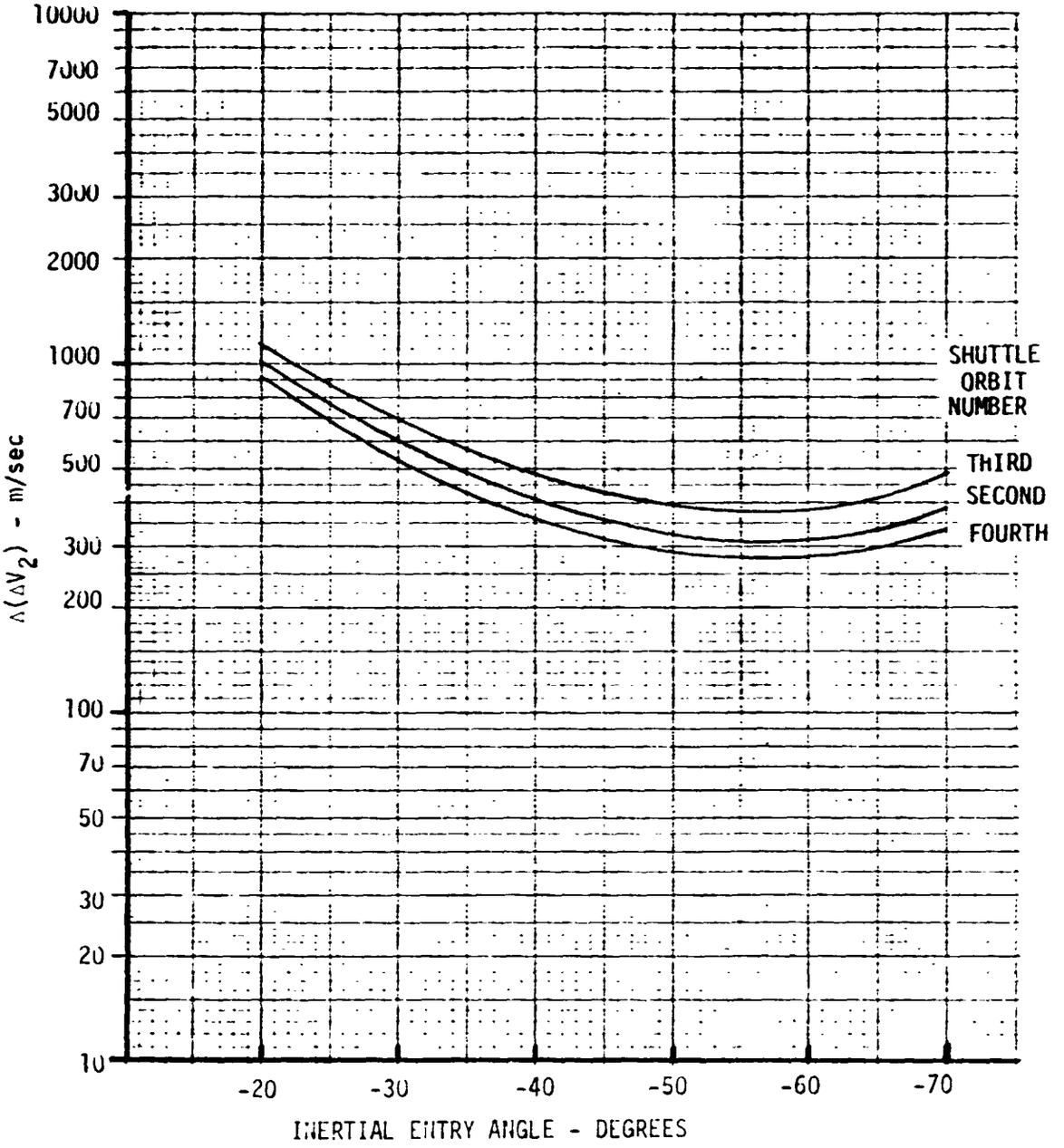

FIGURE 4-9

PLANE CHANGE ΔV PENALTY – R_a = 6.5

- o TOTAL ΔV_2 = ΔV_2 (IN PLANE) + $\Delta(\Delta V_2)$
- o DUE EAST LAUNCH FROM ETR TO 296 KM CIRCULAR ORBIT
- o ASCENSION ISLAND RECOVERY ZONE

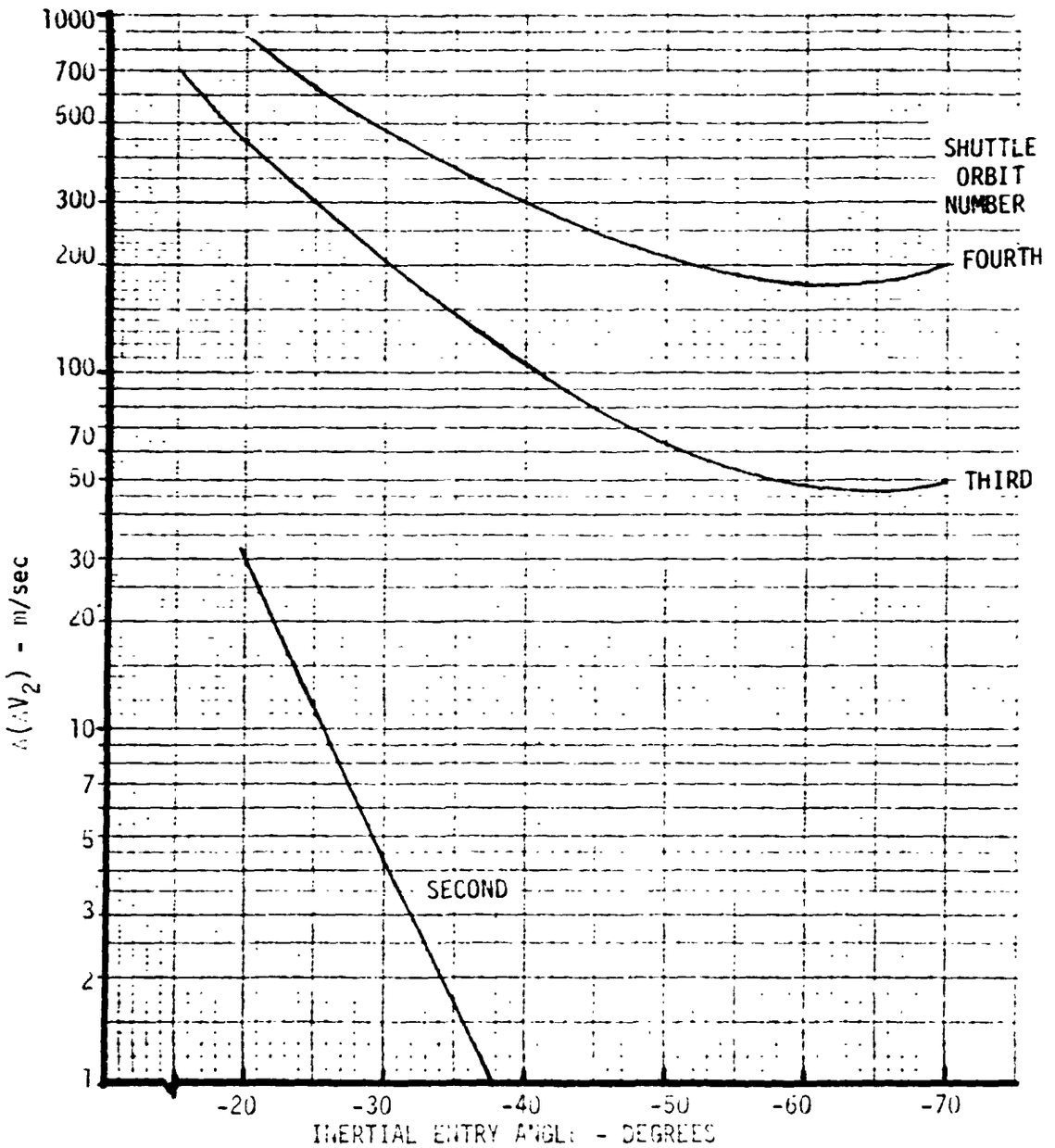

FIGURE 4-10

4.3 Ground Tracks - In the previous sections the booster ΔV requirements for each burn and the resultant inertial entry conditions have been defined. This section identifies the latitude and longitude of the first and second booster burns, the resultant entry conditions for impact at Ascension Island, the Shuttle orbits from which these can be achieved, and two representative ground tracks.

To establish these parameters, the following deorbit strategy was used. The first burn of the Hohmann transfer was assumed to be made from a point on the Shuttle orbit and at the same heading as the Shuttle, i.e., no plane change was associated with the first burn. The location of apogee on the Hohmann transfer orbit is then at a latitude equal in magnitude but opposite in sign to the first burn latitude. The apogee longitude will be the first burn longitude plus 180 degree minus the earth's angular velocity, Ω , multiplied by the Hohmann transfer time, T, from the first burn to apogee, i.e.,

$$\theta_{apogee} = \theta_{perigee} + 180 - \Omega T$$

Once the apogee location was determined, the trajectory from apogee to impact at Ascension was computed as follows. First the impact point latitude and longitude at Ascension was selected as -7.95 deg (7.95 deg south),345.667 deg (14.333 deg west), respectively. Then the deorbit trajectory required to hit the impact point from apogee was computed along with the inertial entry conditions at the pierce point. The deorbit trajectory velocity, flight path angle, and azimuth at apogee is established by the second burn of the booster. The vectorial difference between pre-burn and post-burn conditions at apogee establish the ΔV requirements for the booster. This analysis identifies a latitude and longitude for the first and second burns on specified Shuttle orbits and the resultant velocity, flight path angle, and azimuth that can be achieved at Ascension Island. The trajectory from entry to impact neglects atmospheric effects. This does not affect the results significantly.

The first question to be resolved was: what Shuttle launch azimuth should be used from KSC? Fortunately, a due east launch from KSC to a 296 km circular orbit provides impact at Ascension with essentially no plane change requirements at apogee and entry velocities (prior to the third burn) of more than 10 km/sec over a wide range of flight path angles. Figure 4-11 is a summary table defining potential first burn locations and resultant entry conditions for a 6.5 earth radii deorbit trajectory. The Shuttle longitude and latitude correspond to 10 deg increments along the orbital path. The particular values selected provide inertial entry conditions in

the 10 km/sec velocity range and flight path angles between -20 and -79 deg. The azimuth on the Shuttle orbit is the inertial value and corresponds to the payload azimuth during the first burn. The entry azimuth is an inertial azimuth at the entry altitude of 121.92 km. The inplane ΔV requirement, ΔV_2, and the ΔV penalty, $\Delta\Delta V$, for plane change at apogee are also provided. Finally, the time between the end of the first orbit and the first Hohmann transfer burn is given. For the first window on orbit 2 and 3 almost no plane change penalty is incurred. During later Shuttle orbits, the plane change ΔV penalty is minimum for the intermediate values of flight path angles. Deorbit opportunities are available on three consecutive Shuttle orbits with at least a 25 minute launch window on each orbit (at the sacrifice of entry flight path angle). This allows for very flexible mission planning.

Figure 4-12 presents the same type of data as Figure 4-11 but for a deorbit trajectory with a 3.0 earth radii apogee. The first Hohmann transfer burn must occur further east than for the higher apogee deorbit discussed previously. This is due to the shorter flight time of the low apogee mission. The entry velocities are between 9 and 9.5 km/sec and the approach azimuth is more from the west than the previous case. The most significant difference is the higher plane change ΔV penalty which on the first opportunity exceeds 300 km/sec for all cases.

To provide mission planning information, the times given in the last column of Figures 4-11 and 4-12 are plotted as a function of the inertial entry angle in Figure 4-13. For a given entry angle this time can be added to the total deorbit times given in Figure 4-3 to give the total time from end of first orbit to impact at Ascension. The end of the first orbit is used as the initial time because Shuttle orbit insertion requires most of the first orbit. Depending upon the procedure for circularizing the Shuttle orbit, the time for the first orbit can vary significantly.

The data provided in Figures 4-11, 4-12 and 4-13 can be used for mission planning and to define ground tracks. Figures 4-14 and 4-15 provides typical ground tracks for the 6.5 and 3.0 earth radii missions, respectively. The deorbit maneuvers are made from the second Shuttle orbit and the entry conditions are noted on the figures. For the high apogee case of Figure 4-14, the first burn occurs near Hawaii and could be tracked from there. The Hohmann transfer ground track goes over Mexico and the northern coast of South America. As the payload approaches apoapsis the relative ground speed is faster than the payload velocity and the ground track reverses. The second burn occurs at apoapsis just off the east coast of South America. After the apoapsis burn, the ground track continues westward until the

SUMMARY OF DEORBIT CONDITIONS FOR R_a = 6.5

SHUTTLE ORBIT ALTITUDE = 160 NMI

SHUTTLE ORBIT #	FIRST BURN CONDITIONS LONG. (DEG)	LAT. (DEG)	AZIMUTH (DEG)	ENTRY INERTIAL CONDITIONS V_E (KM/SEC)	γ_E (DEG)	AZIMUTH (DEG)	BOOSTER ΔV AT APOGEE ΔV_2 (KM/SEC)	$\Delta\Delta V$ (KM/SEC)	TIME SINCE FIRST ORBIT TIME (MIN)
2	174.04	13.80	64.82	10.29	-19.60	39.90	113.81	32.310	75.26
	182.90	17.86	67.42	10.28	-23.97	60.83	160.27	13.59	77.77
	192.17	21.44	70.76	10.27	-28.57	61.51	218.40	5.595	80.28
	201.90	24.41	74.81	10.26	-33.37	62.00	288.73	2.248	82.79
↓	212.07	26.64	79.48	10.25	-38.36	62.35	371.64	.845	85.30
2	222.58	28.03	84.61	10.24	-43.51	62.56	467.20	.275	87.80
3 & 2	233.28	28.50	90.00	10.23	-48.82	62.66	575.24	.062	90.31
3	254.49	26.64	100.52	10.21	-59.81	62.57	825.39	.005	95.33
	264.66	24.41	105.19	10.20	-65.44	62.42	965.00	.021	97.84
3	274.39	21.44	109.24	10.19	-71.10	62.23	1111.69	.033	100.34
3	169.06	21.44	70.76	10.29	-19.76	46.65	115.38	454.28	170.59
	178.79	24.41	74.81	10.28	-23.87	51.29	159 07	327.97	173.10
	188.96	26.64	79.48	10.27	-28.26	54.81	214.08	234.90	175.61
↓	199.47	28.03	84.61	10.26	-32.87	57.67	280.90	167.34	178.11
3 & 4	210.17	28.50	90.00	10.25	-37.69	60.13	359.91	120.27	180.62
4	220.88	28.03	95.39	10.24	-42.68	62.37	451.24	88.92	183.13
	231.39	26.64	100.52	10.23	-47.84	64.56	554.68	68.74	185.64
	241.55	24.41	105.19	10.22	-53.13	66.85	669.37	56.33	188.15
	251.28	21.44	109.24	10.21	-58.50	69.47	794.09	49.37	190.65
	260.56	17.86	112.58	10.20	-63.92	72.78	926.83	46.76	193.16
	269.42	13.80	115.18	10.19	-69.31	77.45	1064 63	48.63	195.67
↓	277.94	9.39	117.03	10.18	-74.52	84.93	1202 55	56.93	198.18
4	286.23	4.753	118.13	10.18	-79.27	98.95	1330.94	78.59	200.69
4	165.85	26.64	79.48	10.29	-20.40	38.36	121.62	863.33	265.92
4	176.36	28.03	84.61	10.28	-23.99	46.00	160.43	634 69	268.42
4 & 5	187.06	28.50	90.00	10.39	-27.05	51.80	209.65	546.27	270.93
5	197.77	28.03	95.39	10.27	-32.14	57.09	269.80	437.12	273.44
	208.28	26.64	100.52	10.26	-36.59	61.52	341.14	351.69	275.95
	218.44	24 41	105.19	10.25	-41.23	65.64	423.67	286.61	278.46
	228.17	21.44	109.24	10.24	-46.01	69.74	516.97	239.04	280.96
	237.45	17.86	112.58	10.23	-50.90	73.95	620.13	206.30	283.47
	246.31	13.80	115.18	10.22	-55.84	78.70	731.28	186.41	285.98
	254.83	9.39	117.03	10.21	-60.73	84.39	847.82	177.97	288.49
	271.29	0.0	118.50	10.19	-69.83	101.62	1078.21	199.15	293.51
	279.45	-4.75	118.13	10.19	-73.49	115.77	1174.98	238.79	296.02
↓	287.74	-9.39	117.03	10.18	-75.90	135.46	1239.54	313.63	298.53
5	296.26	-13.80	115.18	10.18	-76.43	159.02	1253.79	438.86	301.03

FIGURE 4-11

SUMMARY OF DEORBIT CONDITIONS FOR R_a = 3.0

SHUTTLE ORBIT ALTITUDE = 160 NMI

SHUTTLE ORBIT #	FIRST BURN CONDITIONS LONG. (DEG)	LAT. (DEG)	AZIMUTH (DEG)	ENTRY INERTIAL CONDITIONS V_E (DEG)	γ_E (DEG)	AZIMUTH (DEG)	BOOSTER ΔV AT APOGEE ΔV_2 (KM/SEC)	ΔV (KM/SEC)	TIME SINCE FIRST ORBIT TIME (MIN)
2	96.214	-24.408	74.81	9.50	-19.83	114.80	247.75	1047.64	52.68
	105.944	-21.440	70.76	9.47	-23.30	110.36	327.41	847.89	55.19
	115.221	-17.861	67.42	9.44	-27.05	106.62	426.21	692.03	57.70
	124.082	-13.803	64.82	9.41	-31.09	103.27	546.31	569.59	60.21
	132.605	- 9.393	62.97	9.37	-35.42	100.09	689 92	474.99	62.72
	140.892	- 4.753	61.87	9.32	-40.05	96.86	859.02	404.58	65.23
	149.059	0	61.50	9 27	-44.98	93.38	1054.90	355.21	67.74
	157.225	4.753	61.87	9.22	-50.19	89.40	1277.56	324.49	70.24
	165.512	9.393	62.97	9 17	-55.64	84.52	1524.79	311.38	72.75
	174.035	13.803	64.82	9.12	-61.20	78.11	1790.13	317.59	75.26
	182.897	17.861	67.42	9 08	-66.67	69.03	2061.11	349.53	77.77
	192.17	21.44	70.76	9.05	-71.61	55.19	2312.95	424.15	80.28
	201.90	24.41	74.81	9.04	-75.18	33.69	2498.16	579.76	82.79
2	212.07	26.64	79.48	9.03	-76.14	5.23	2548.30	874.81	85.30
3	92.111	-17.861	67.42	9.51	-18.10	107.20	212.38	1312.40	148.01
	100.972	-13.803	64.82	9.49	-21.35	101.73	281.24	1067.79	150.52
	109.496	- 9.393	62.97	9.46	-24.89	97.27	367.69	879.84	153.03
	117.783	- 4.753	61.87	9.43	-28.71	93.40	473.90	731.88	155.54
	125.949	0	61.50	9.39	-32.81	89.81	601.84	615.28	158.05
	134.116	4.753	61.87	9.35	-37.20	86.29	753.46	525.36	160.55
	142.403	9.393	62.97	9.30	-41.88	82.63	930.29	458.87	163.06
	150.926	13.803	64.82	9.25	-46.84	78.59	1132.88	413.43	165.57
	159.787	17.861	67.42	9.20	-52.05	73.86	1360.19	387.45	168.08
	169.064	21.440	70.76	9.16	-57.41	67.98	1607.85	381.29	170.59
	178.794	24.408	74.812	9.11	-62.78	60.18	1867.26	398.54	173.10
	188.958	26.640	79.480	9 06	-67.87	49.14	2121 60	449.29	175.61
3	199.47	28.03	84.61	9.05	-72.13	32.78	2339.75	556.47	178.11
3 & 4	210.17	28.50	90.00	9.04	-74.64	9.61	2469.74	762.47	180.62
4	94.673	- 4.753	61.866	9 50	-19.13	90.13	233.04	983.70	245.85
	102.804	0	61.500	9.48	-22.60	86.08	310.27	790.90	248.36
	111.006	4.753	61.866	9.45	-26.34	82.56	406.44	642.56	250.86
	119.294	9.393	62.969	9.41	-30.36	79.42	523.67	527.08	253.37
	127.817	13.803	64.816	9.37	-34.67	76.43	664.21	483.44	255.88
	136.676	17.861	67.416	9.33	-39.28	73.41	830.12	372.47	258.39
	145.955	21.440	70.761	9 28	-44.20	70.16	1022.97	325.82	260.90
	155.685	24.408	74.812	9.23	-49.41	66.46	1243.34	295.87	263.41
	165.849	26.640	79.480	9 18	-54.85	61.98	1489.45	281.19	265.92
4	176.359	28.028	84.614	9.13	-60.32	56.18	1756 79	282.53	268.42
4 & 5	187.063	28.500	90.00	9.09	-65.10	48.34	2035.26	304.59	270.93
5	197.766	28.028	95 386	9.05	-71.45	35.61	2304 60	360.66	273.44
	208.276	26.640	100.52	9. 3	-75.65	15.44	2522.65	483.85	275.95
5	218.44	24.41	105.19	9.03	-77 41	165.72	2614.84	739.84	278.46

FIGURE 4-12

TIME IN INITIAL ORBIT

o TIME MEASURED FROM END OF 1ST ORBIT TO FIRST MISSION BURN

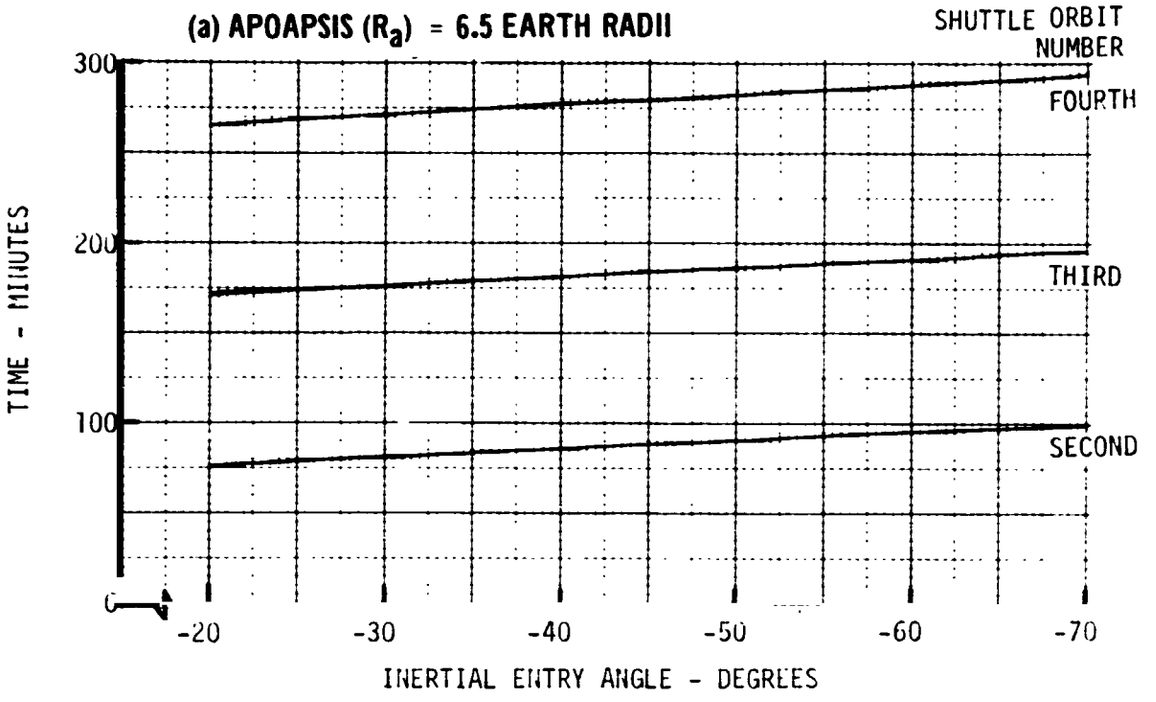

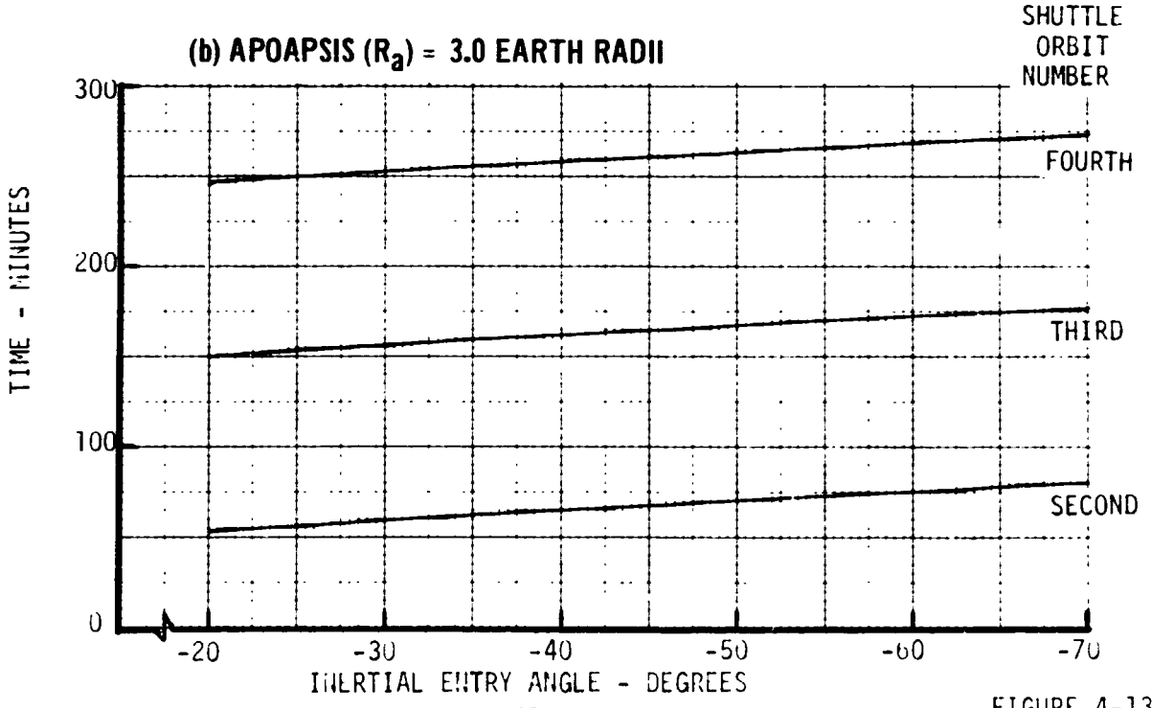

FIGURE 4-13

SUMMARY OF DEORBIT CONDITIONS FOR R_a = 6.5

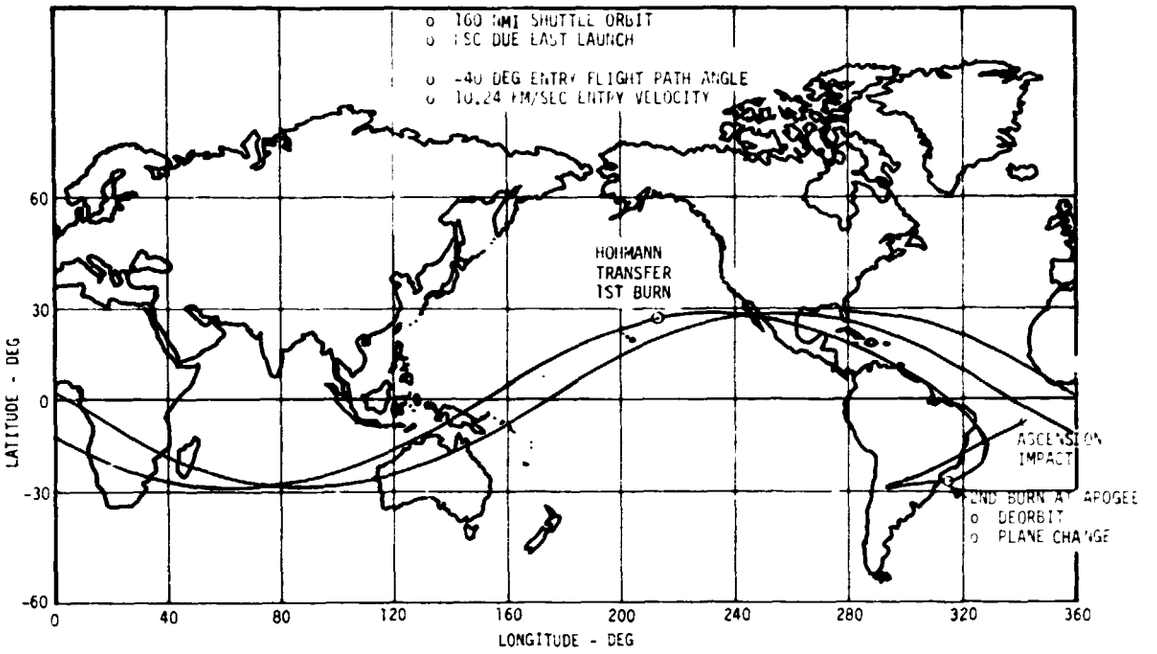

FIGURE 4-14

SUMMARY OF DEORBIT CONDITIONS FOR R_a = 3.0

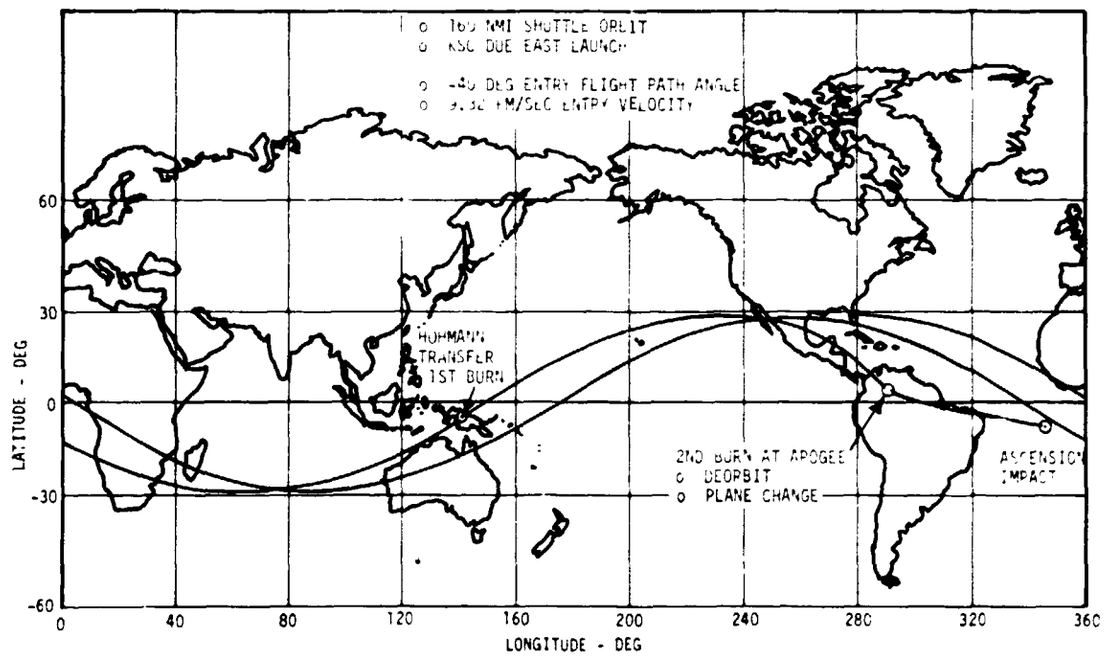

FIGURE 4-15

PLANETARY ENTRY MISSION EVENT SEQUENCE

TIME (HR: MIN)		EVENT
Ra = 6.5	RA = 3.0	
00:00	00:00	LIFTOFF
01:27	01:27	OMS SHUTDOWN- 296 km CIRCULAR ORBIT
02:25	02:02	DEPLOY IUS
02:55	02:32	IGNITE IUS FOR FIRST BURN OF HOHMANN TRANSFER
08:06	04:34	IGNITE IUS FOR SECOND BURN AT APOGEE
12:32	05:55	IGNITE IUS FOR THIRD BURN TO INCREASE ENTRY VELOCITY
12:37	06:00	ENTRY AT 121.92 KM
12:41	06:04	IMPACT

FIGURE 4-16

velocity again exceeds earth rotational speed near the west coast of South America. The ground track then proceeds northeast until impact at Ascension. Because of the apogee altitude of 6.5 earth radii, the second burn is observable from Ascension.

The ground track for the low apogee deorbit is quite different as shown in Figure 4-15. The first Hohmann transfer burn occurs over Indonesia and north of Australia - considerably west of the previous case. The Hohmann transfer orbit track is only slightly different from a typical Shuttle track until it passes over the coast of Mexico. Apogee is achieved over northern South America. At this altitude the second burn will be observable from Ascension. The ground track from apogee to impact then approaches Ascension from the west as compared to the south-west approach for the higher apogee.

The time line for the R_a = 3.0 and 6.5 missions are summarized in Figure 4-16. The R_a = 3.0 mission takes about six hours and the R_a = 6.5 mission takes just under 13 hours.

In conclusion, a due east launch from KSC provides multiple opportunities for payload targeting at Ascension. Opportunities exist during the second, third, or fourth orbits. The plane change penalty at apogee can be minimized by selecting appropria. launch points on the Shuttle orbit. Coverage of the second burn is excellent from Ascension; coverage of the first burn may be possible from Hawaii, KMR, or Guam for specific entry conditions.

OPTIMUM ENTRY ANGLE FOR RADIATIVE FLUX SIMULATION

o MINIMUM ΔV REQUIREMENTS o IN PLANE MANEUVERS ONLY

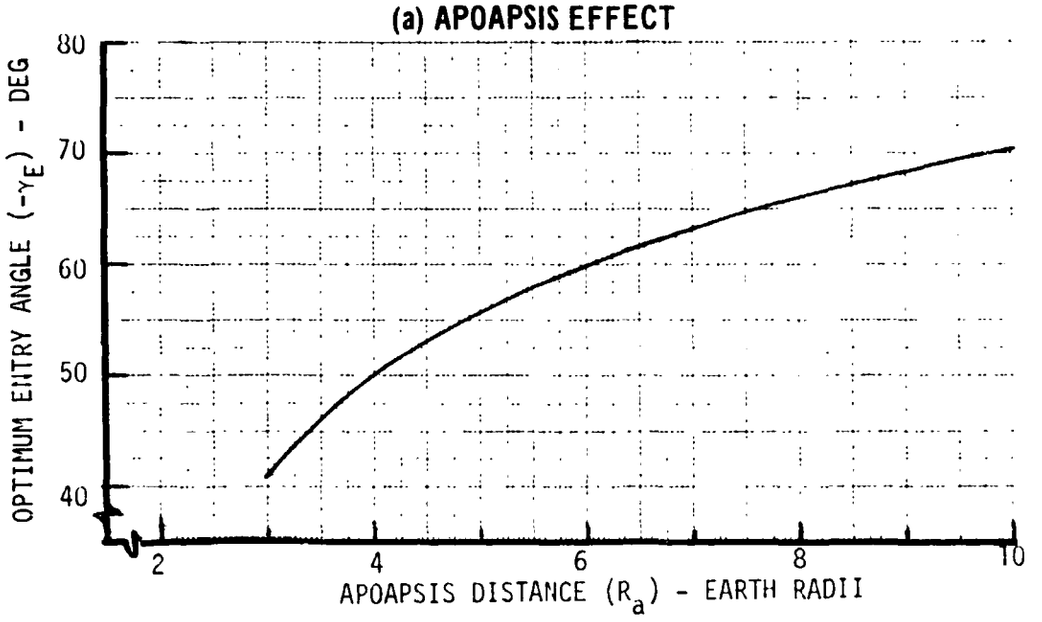

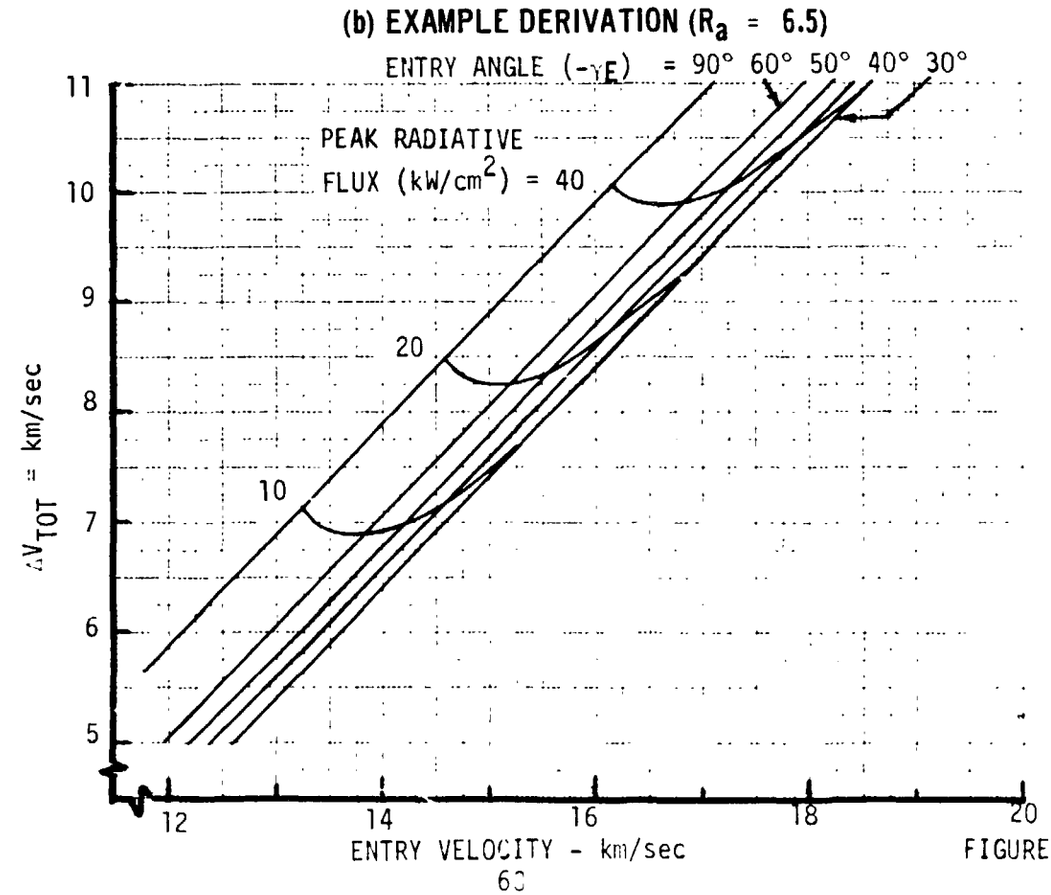

FIGURE 4-17

4.4 Typical Environment Simulation - The previous subsections have addressed the deorbit maneuver requirements in the general terms of initial entry conditions. However, these requirements can also be expressed more directly in terms of environment parameter simulation. For example, the deorbit maneuver ΔV requirements are presented in Figures 4-17 and 4-18 using peak radiative flux as the specific environment parameter.

The optimum entry angle (γ) is shown in Figure 4-17(a) as a function of apoapsis distance (R_a). This is the γ that minimizes the total inplane ΔV needed to simulate a given level of radiative flux. Figure 4-17(b) graphically illustrates the procedure for identifying the optimum value of γ. Note that the optimum is rather flat; variations of ± 5 degrees around the optimum γ do not significantly effect ΔV requirements.

Figure 4-18 presents the total ΔV required as a function of apoapsis distance and radiative flux level. The beneficial effect of increasing R_a is quite pronounced at low altitudes but diminishes rapidly above an R_a of about 4 earth The effect of radiative flux level or ΔV is nearly linear above about 20

RADIATIVE FLUX SIMULATION ΔV REQUIREMENTS

- o STAGNATION POINT
- o NON BLOWING
- o β = 120 kg/m^2
- o R_N = .22 m
- o OPTIMUM γ_E
- o IN PLANE MANEUVER

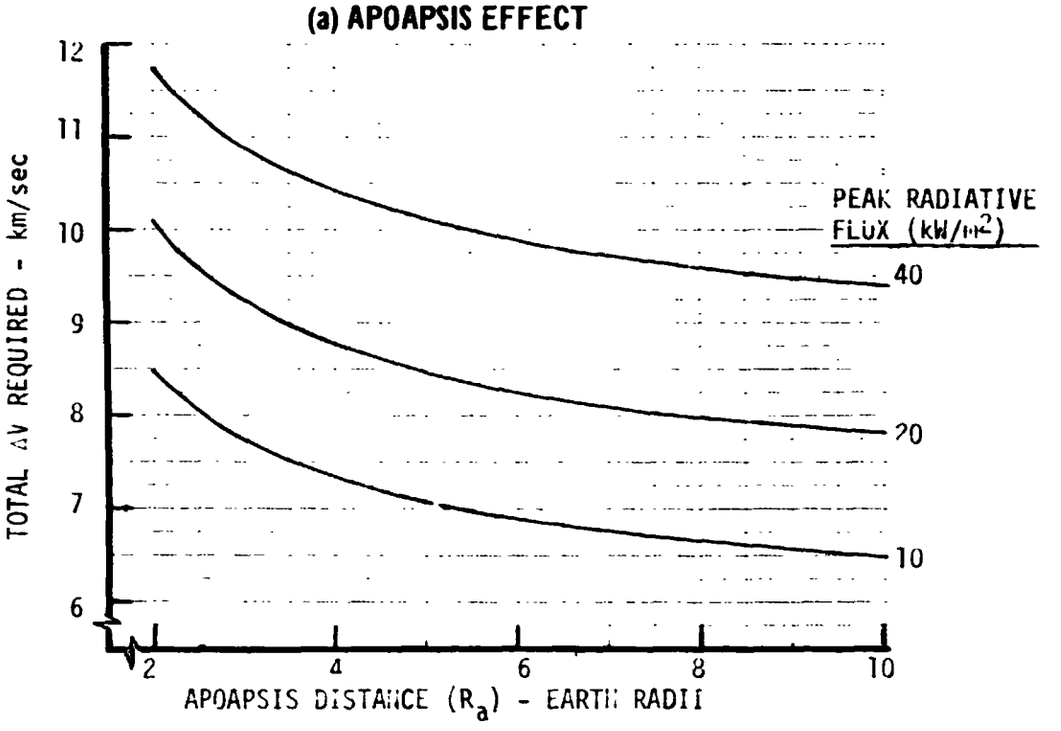

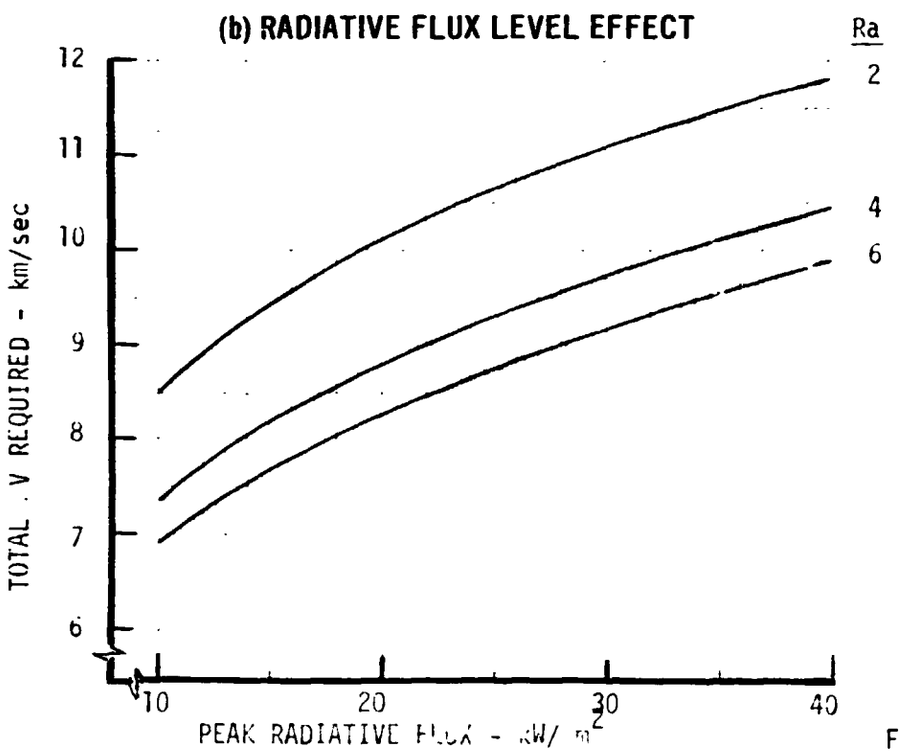

FIGURE 4-18

5.0 SHUTTLE LAUNCHED BOOSTERS

The physical characteristics and performance capabilities of typical Shuttle launched boosters are summarized in this section. The purpose of these data is to provide the experiment planner with an understanding of the payload mass versus earth entry condition constraints imposed by current technology, Shuttle upper stages. This information is intended for use with the maneuver requirements of Section 4 to determine the environment simulation capability of earth entry flight tests.

Four classes of boosters are shown which cover the existing technology range of upper stage performance and physical size. Each class is illustrated by a representative design. First, an existing cryogenic propellant class of booster is shown using the Centaur as the example. This class represents the highest available performance but also the largest physical size design. Next, an existing storable propellant stage, illustrated by the Trarstage, is presented as an example of intermediate size and performance. Another class of storable propellant designs is shown based on existing components from the Shuttle auxiliary propulsion system. This multi-stage velocity package is an example of a very compact configuration that allows maximum opportunity for shared payload launches of the Shuttle. Finally, the solid propellant class of boosters is shown using the best available definition of the recently selected Interim Upper Stage (IUS) concept.

Each booster class is described by a summary of dimensional and mass characteristics and by parametric performance curves. The performance capability is shown in terms of payload mass versus velocity increment (ΔV) and also by the entry angle versus velocity attainable for selected values of apopasis distance and payload mass.

5.1 Existing Cryogenic Booster - The Centaur, which is the only cryogenic (O_2/H_2) stage currently in use, is shown as the example design for this class of booster. Figure 5-1 presents the mass, dimensional and propulsion characteristics of the Centaur plus a spin stabilized, TE364-4 solid motor second stage. Although the Centaur alone performance is within the entry simulation range of interest, it is less than other candidate multi-stage vehicles. Addition of a small second stage increases its performarce to the extent that it is the highest of any booster considered. Hence, this two stage configuration is presented as an example of the maximum performance capability available.

Figure 5-2 illustrates performance capability in terms of payload mass versus velocity increment (ΔV). Figure 5-3 describes the entry conditions that can be

TYPICAL CRYOGENIC PROPELLANT BOOSTER DESCRIPTION (CENTAUR/TE364-4)

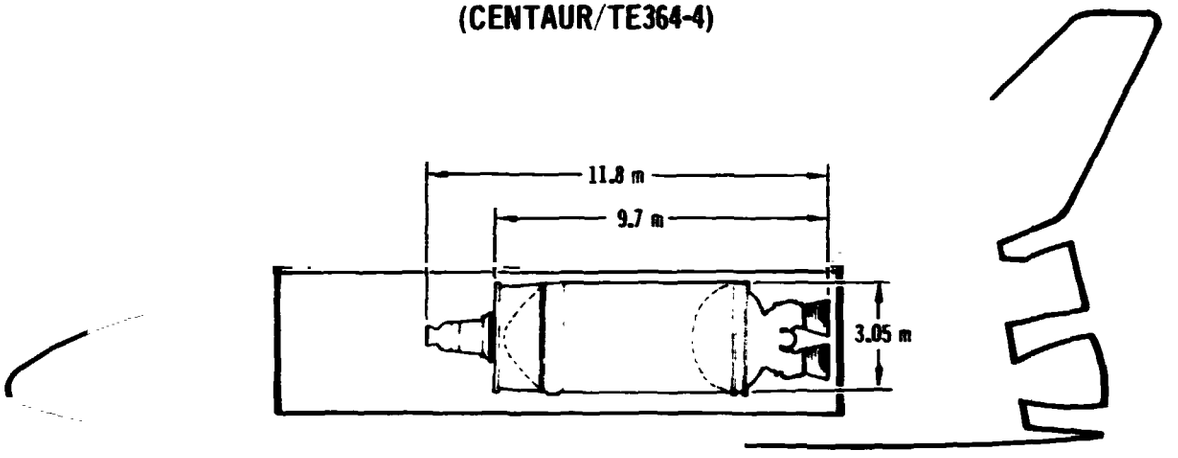

STAGE	MASS kg (lb)		THRUST N (lb)	I_{SP} m/sec (sec)
SECOND STAGE	ADAPTER	0 0	68,500 (15400)	2782 (283.8)
	INERT	75.8 (167.0)		
	BURNOUT	75.8 (167.0)		
	EXPENDED	1045.5 (2305.0)		
	IGNITION	1121.3 (2472.0)		
FIRST STAGE	INTERSTAGE *	86.7 (191.2)	129,900 (29200)	4311 (439.6)
	INERT **	2495.0 (5501.0)		
	BURNOUT	3703.0 (8164.2)		
	EXPENDED	13532.0 (29833.0)		
	IGNITION	17235.0 (37997.2)		

* INCLUDES 2ND STAGE SPIN TABLE
** INCLUDES AVIONICS

FIGURE 5-1

CENTAUR/TE364-4 PAYLOAD MASS CAPABILITY

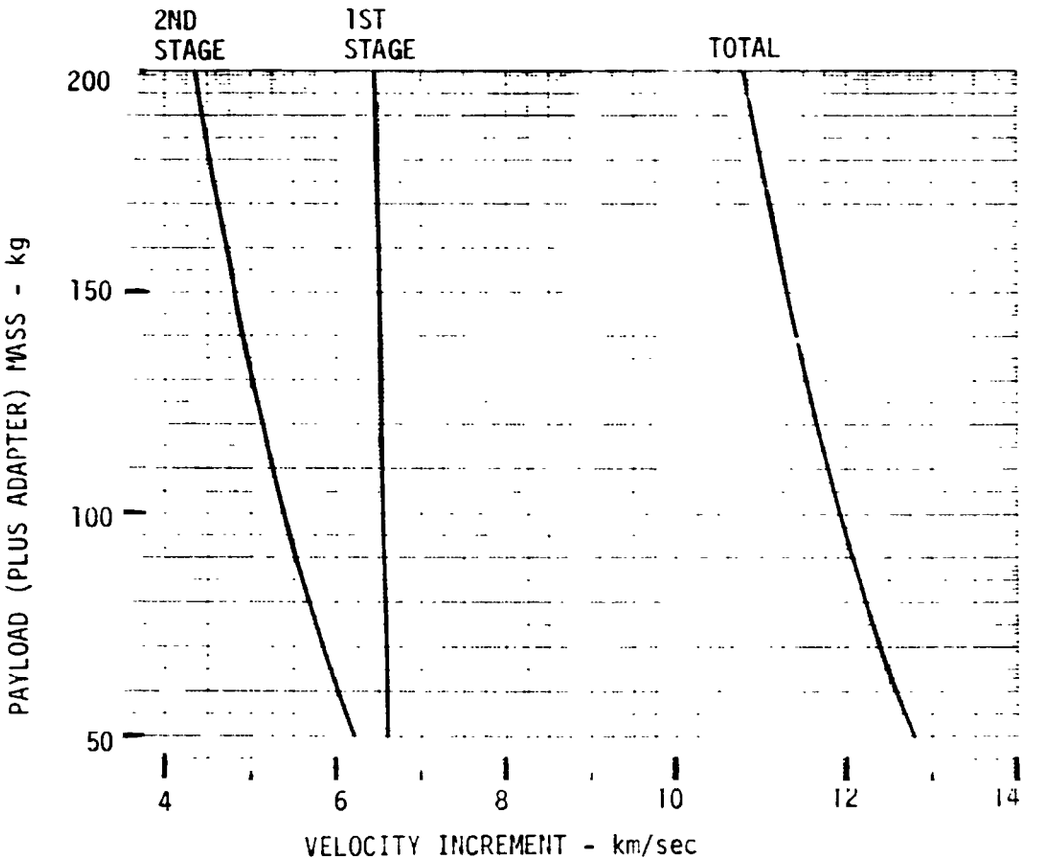

FIGURE 5-2

CENTAUR/TE364-4 ENTRY CONDITIONS CAPABILITY

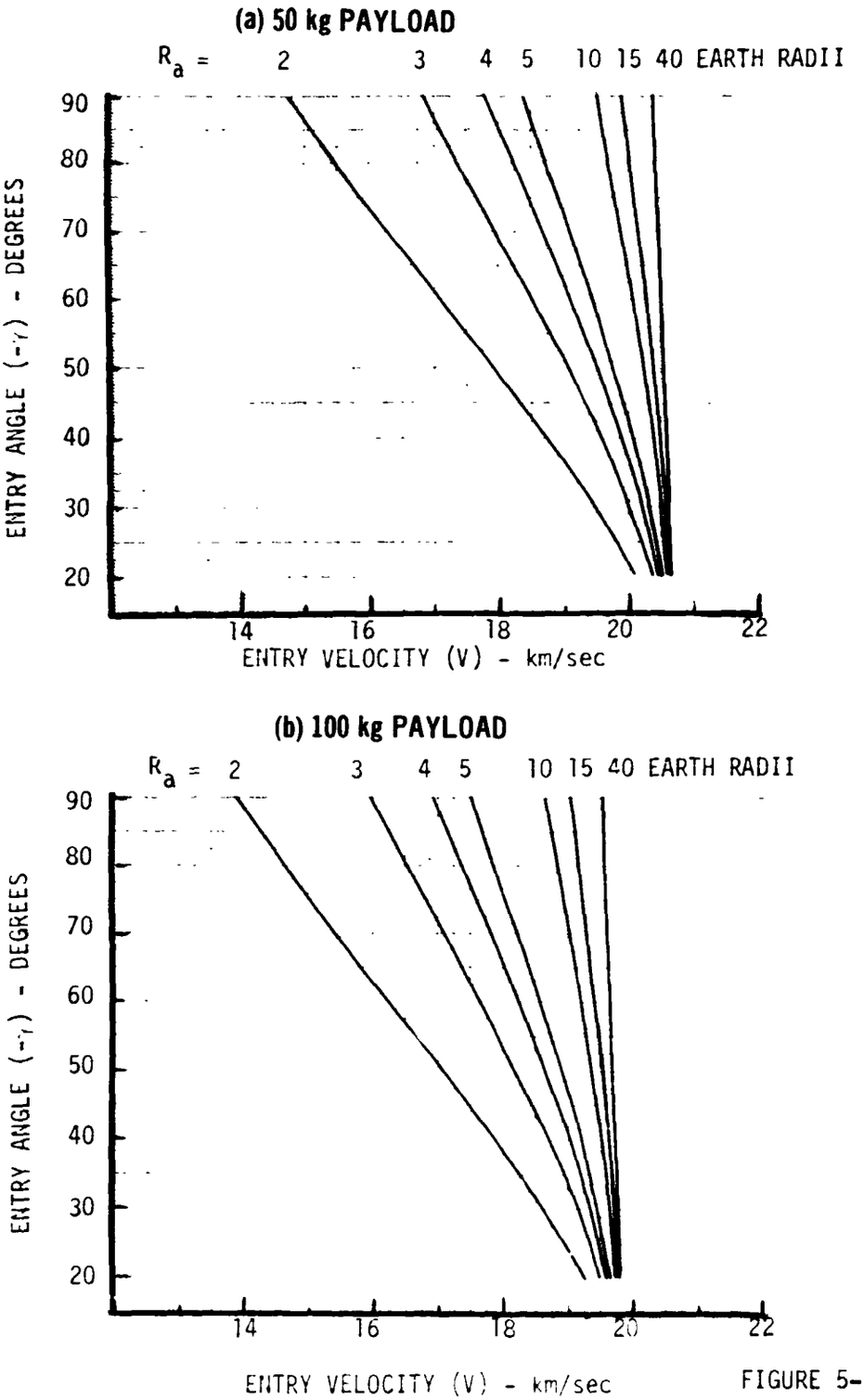

FIGURE 5-3

CENTAUR/TE364-4 ENTRY CONDITIONS CAPABILITY (Continued)

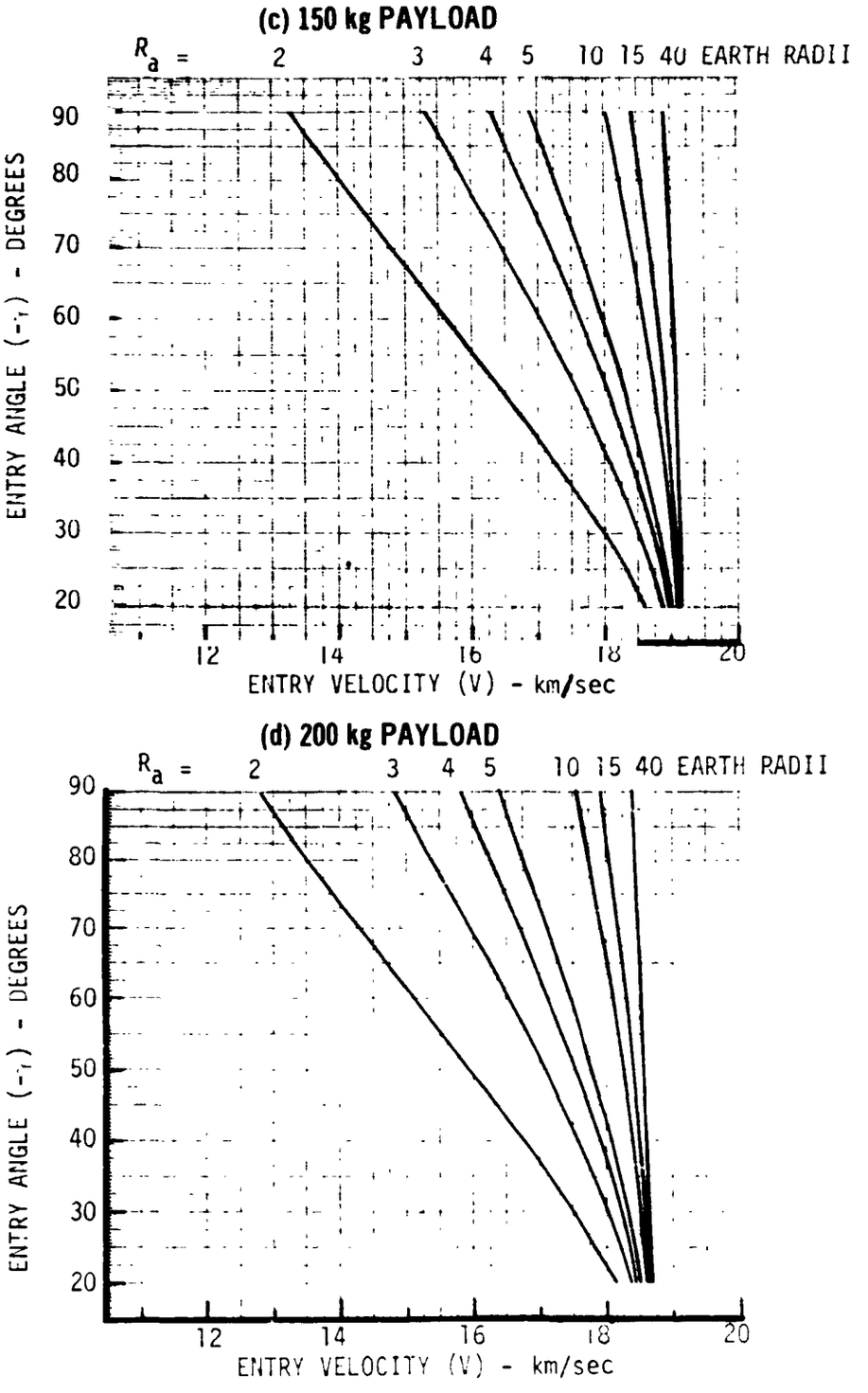

FIGURE 5-3

achieved for selected values of apoapsis distance and payload mass. Note that as apoapsis is increased, higher entry velocities can be attained at steeper entry angles. In all cases, the Centaur stage accomplishes the first and second maneuver burn and a portion of the third or final burn while the solid motor is used to complete the final burn.

5.2 Existing Storable Booster - The Transtage is selected as the example design for this booster class on the basis that it provides maximum performance capability with minimum modification. Of the designs considered were the Delta and Agena stages. Physical and propulsion characteristics of the Transtage plus a TE364-4 solid motor upper stage are described in Figure 5-4. An auxiliary stage is necessary to achieve performance levels high enough to be of interest for environment simulation missions.

Figures 5-5 and 5-6 present the Transtage/TE364-4 performance capability in terms of payload mass and entry conditions respectively. The second stage restart line of Figure 5-6 reflects the limited ΔV capability of the Transtage plus the single start limitation of current solid motors. To achieve steep entries at lower apoapsis altitudes, the first two maneuver burns require more ΔV than is available from the Transtage alone. Hence the second stage must be used to complete the second or apoapsis burn. It must then be shut down during the coast to low altitude and restarted to accomplish the third or velocity adjustment burn.

5.3 Short Length Existing Component Storable Booster - A multi-stage velocity package composed of Shuttle Auxiliary Propulsion System Components is shown to illustrate a short length high ΔV class of storable (N_2O_4/MMH) boosters. The compact velocity package is an example of how existing components can be configured to best utilize the wide but length limited shape of the Shuttle payload bay. This maximizes opportunity for shared payload launches of the Shuttle. In contrast, the other booster classes represent relatively long, narrow upper stages that were originally designed for ground launched, expendable boosters.

Figure 5-7 describes the physical and propulsion characteristics of the three stage velocity package. The first two stages are identical and composed of tank, engine and flow control components being developed for the Reaction Control System (RCS) of Shuttle. The third stage is a spin stabilized, TE364-4 solid motor.

Figure 5-8 shows the basic payload mass versus ΔV performance capability of each stage while Figure 5-9 presents the entry condition capability for representative apoapsis distances and payload masses. The third stage restart limit of

TYPICAL EARTH STORABLE PROPELLANT BOOSTER DESCRIPTION (TRANSTAGE/TE364-4)

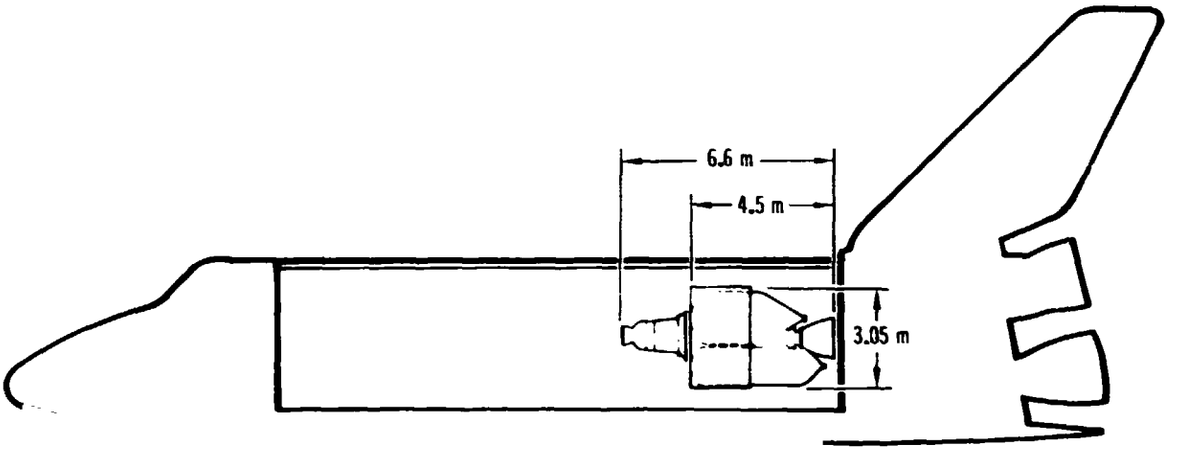

STAGE	MASS	kg	(lb)	THRUST N (lb)	I_{SP} m/sec (sec)
SECOND STAGE	ADAPTER	0	0	68500 (15400)	2782 (283.8)
	INERT	75.8	(167.0)		
	BURNOUT	75.8	(167.0)		
	EXPENDED	1045.5	(2305.0)		
	IGNITION	1121.3	(2472.0)		
FIRST STAGE	INTERSTAGE *	86.7	(191.2)	69980 (15733)	2955 (301.3)
	INERT **	1701.0	(3750.7)		
	BURNOUT	2909.0	(6413.9)		
	EXPENDED	10447.0	(23032.0)		
	IGNITION	13356.0	(29445.9)		

* INCLUDES 2ND STAGE SPIN TABLE
** INCLUDES AVIONICS

FIGURE 5-4

TRANSTAGE/TE364-4 PAYLOAD MASS CAPABILITY

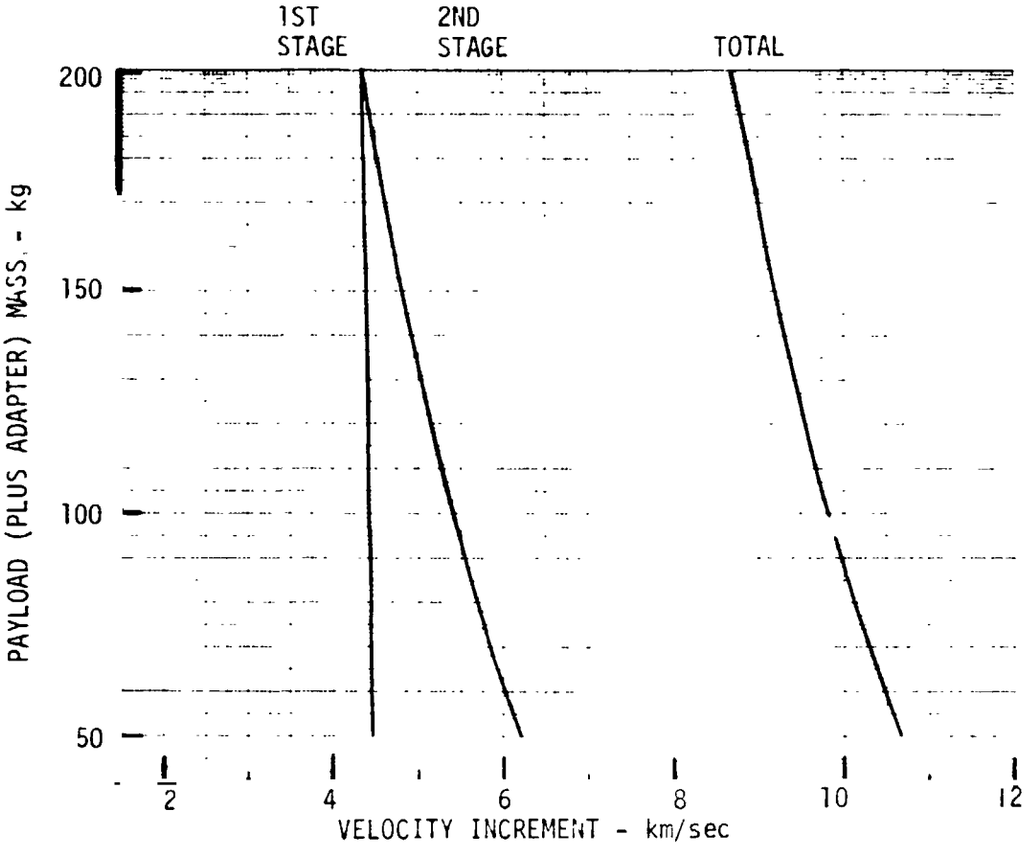

FIGURE 5-5

TRANSTAGE/TE364-4 ENTRY CONDITION CAPABILITY

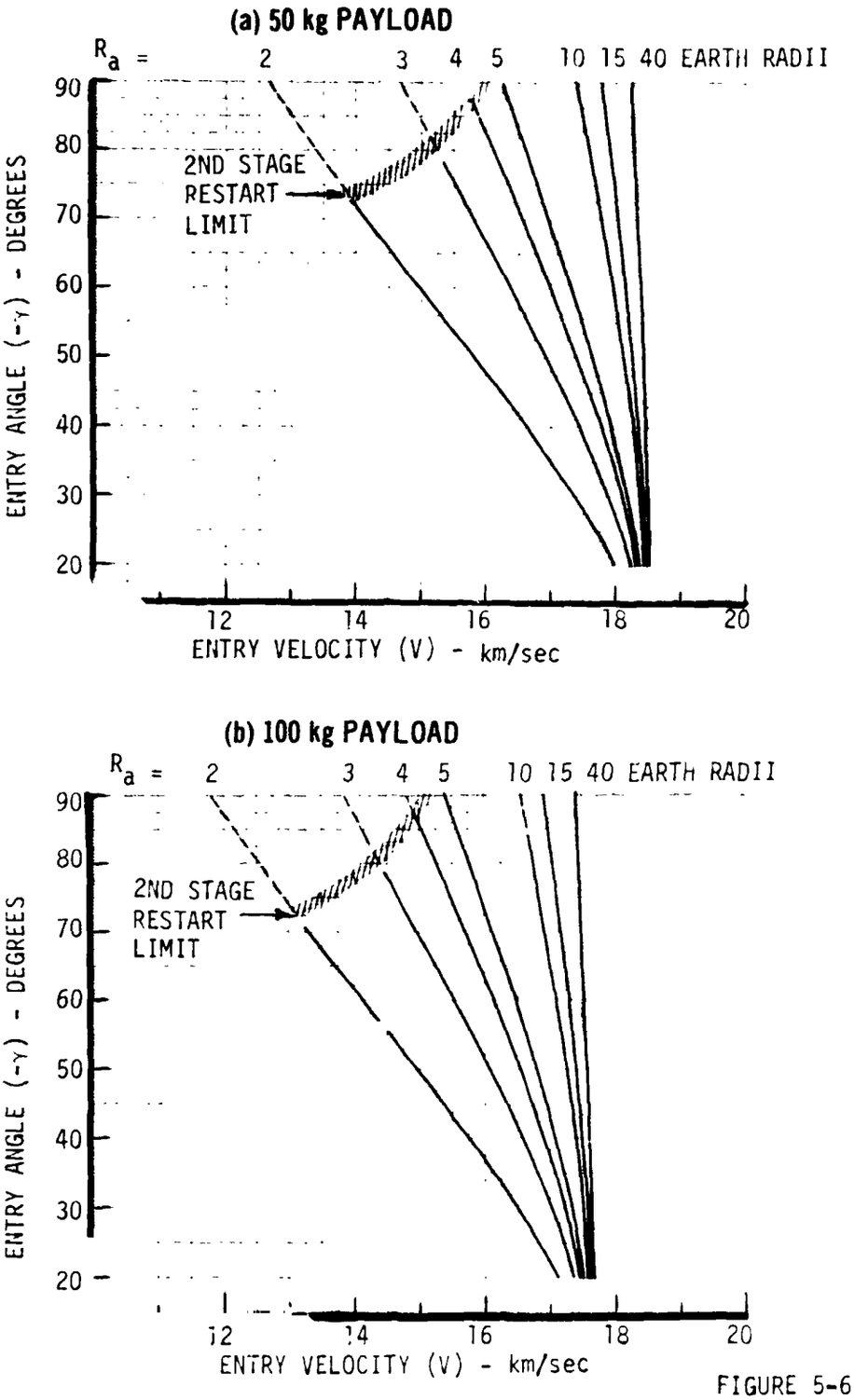

FIGURE 5-6

TRANSTAGE/TE364-4 ENTRY CONDITION CAPABILITY (Continued)

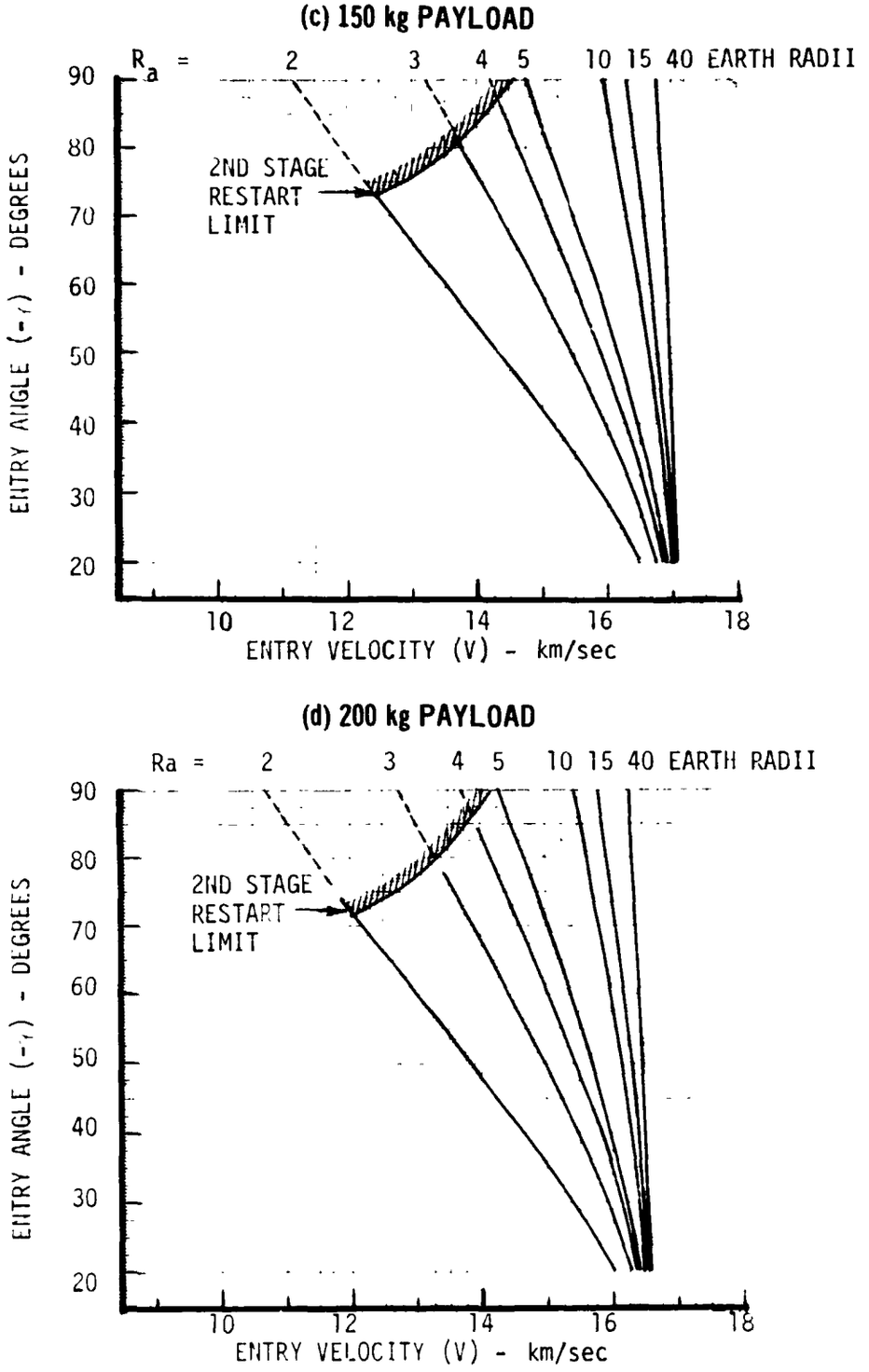

FIGURE 5-6

TYPICAL "SHORT LENGTH" BOOSTER DESCRIPTION (SHUTTLE COMPONENT VELOCITY PACKAGE)

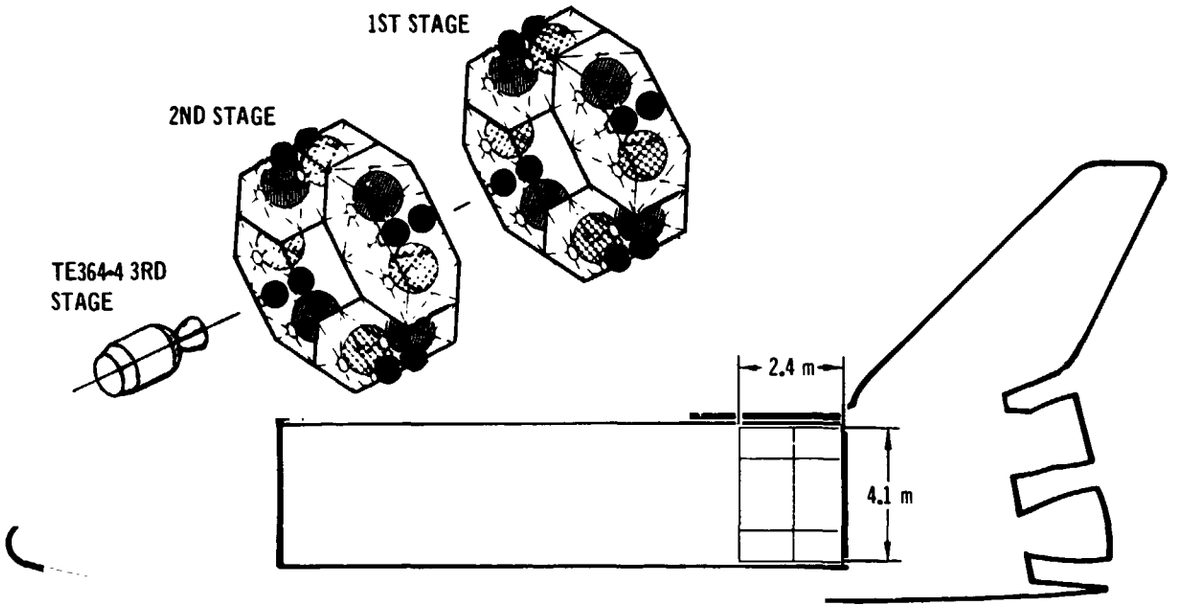

STAGE		MASS kg (lb)		THRUST N (lb)	I_{SP} m/sec (sec)
THIRD STAGE	ADAPTER	0	0		
	INERT	75.8	(167.0)	68,500 (15400)	2782 (283.8)
	BURNOUT	75.8	(167.0)		
	EXPENDED	1045.5	(2305.0)		
	IGNITION	1121.3	(2472.0)		
SECOND STAGE	INTERSTAGE *	349.0	(770.0)		
	INERT	1316.0	(2902.0)	15984 (3600)	2834 (289)
	BURNOUT	2786.3	(6144.0)		
	EXPENDED	3931.0	(8667.0)		
	IGNITION	6717.3	(14811.0)		
FIRST STAGE	INTERSTAGE	45.0	(100.0)		
	INERT	1316.0	(2902.0)	15984 (3600)	2834 (289)
	BURNOUT	8076.3	(17813.0)		
	EXPENDED	3931.0	(8667.0)		
	IGNITION	12009.3	(26480.0)		

* INCLUDES AVIONICS AND 3RD STAGE SPIN TABLE

FIGURE 5-7

VELOCITY PACKAGE PAYLOAD MASS CAPABILITY

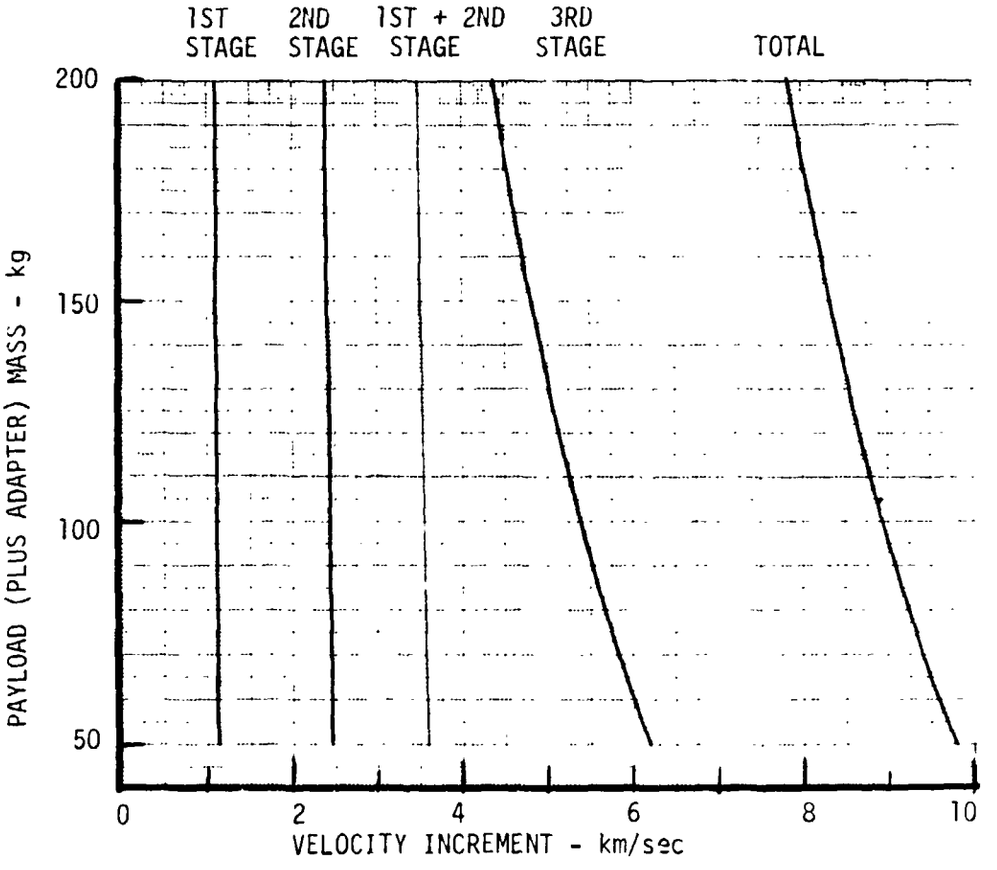

FIGURE 5-8

VELOCITY PACKAGE ENTRY CONDITION CAPABILITY

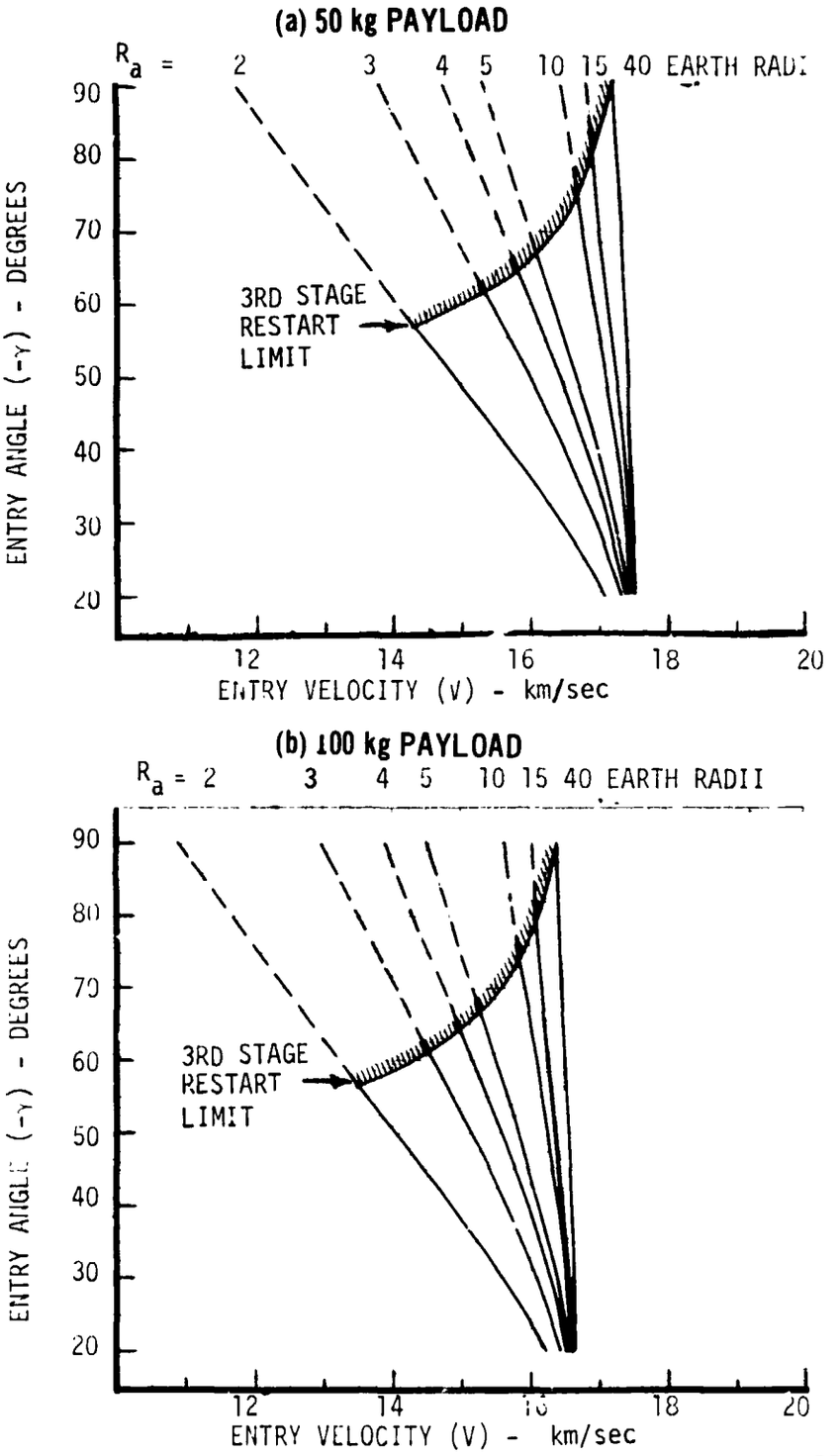

FIGURE 5-9

VELOCITY PACKAGE ENTRY CONDITION CAPABILITY (Continued)

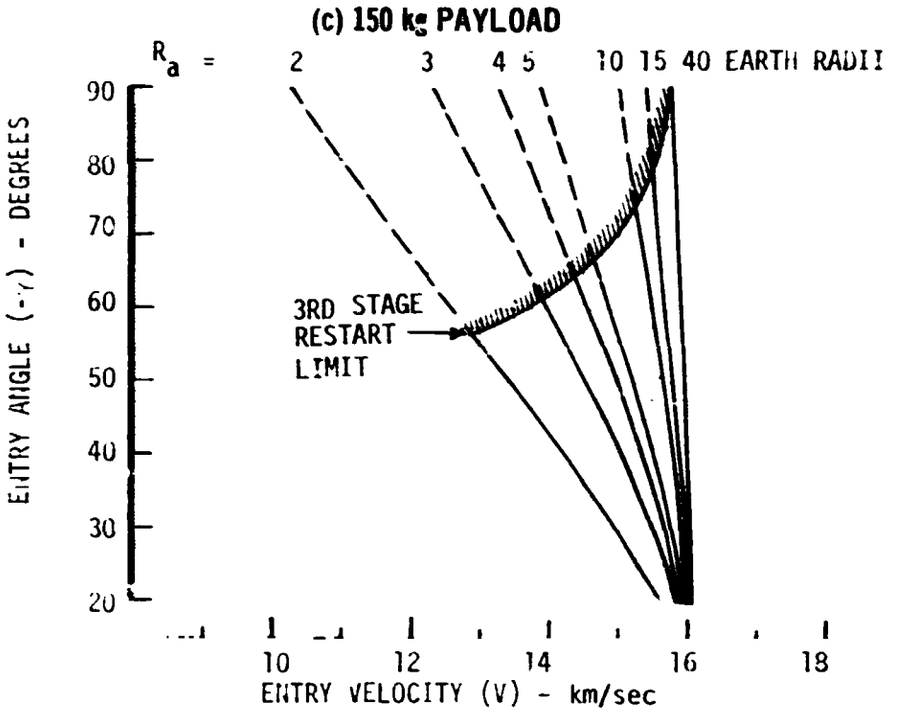

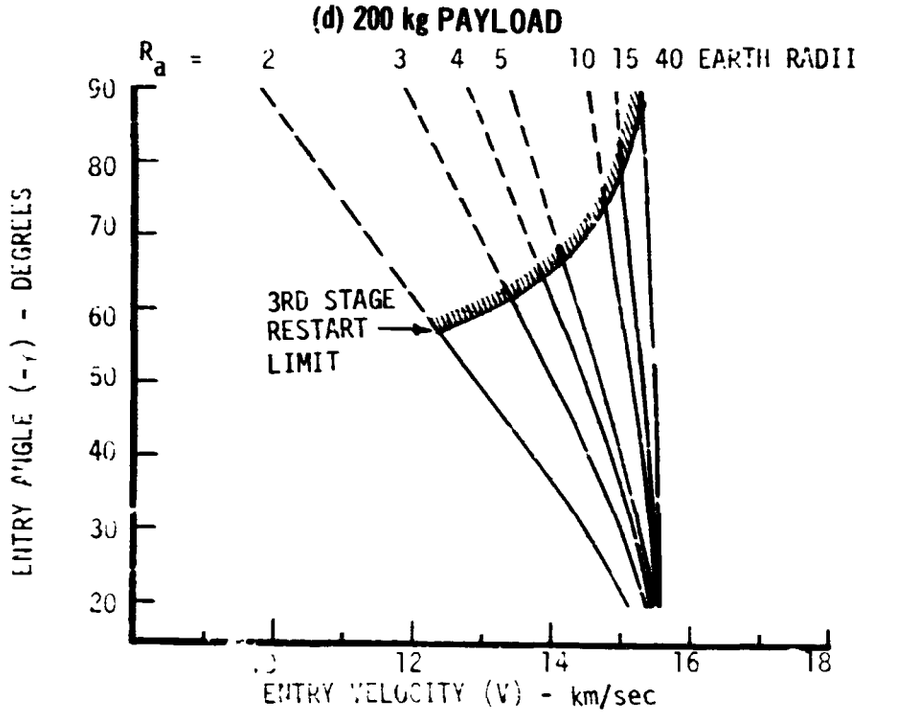

FIGURE 5-9

Figure 5-9 represents the same operational constraint as discussed in the preceeding subsection.

5.4 Existing Solid Motor Booster - A preliminary version of the Interim Upper Stage (IUS) is presented as an example of the solid propellant class of booster. The configuration shown is necessarily preliminary since the Air Force is in the process of awarding a contract to define the final IUS characteristics. Figure 5-10 summarizes the characteristics of a two stage IUS plus a spin stabilized, TE364-4 solid motor used as an auxiliary third stage. A third stage is required because of the three burn nature of the deorbit maneuver and the single start limitation of current solid motors.

The performance capability of the IUS/TE364-4 is shown in Figures 5-11 and 5-12. The third stage restart limit of Figure 5-12 is imposed for the same reasons as discussed in previous subsections. The first stage ΔV limit is a similar constraint arising from the single start nature of the second stage. It should be noted that the Figure 5-12 entry condition capability is conservative in that it was assumed that any excess ΔV from either the first or second stage was dissipated by non-optimum trajectory usage. In particular, the second stage apoapsis burn can probably be applied in a manner that utilizes this excess energy to increase entry velocity. This should be the subject of detailed trajectory analysis for a given mission application.

TYPICAL SOLID PROPELLANT BOOSTER DESCRIPTION
(2 STAGE IUS/TE364-4)

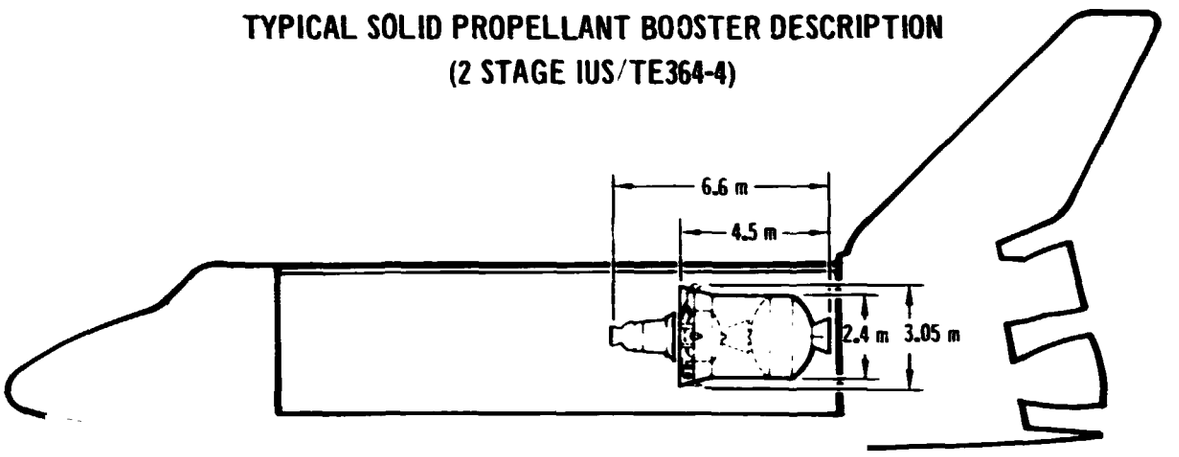

STAGE	MASS	kg	(lb)	THRUST N (lb)	I_{SP} m/sec (sec)
THIRD STAGE	ADAPTER	0	0	68,500 (15400)	2782 (283.8)
	INERT	75.8	(167.0)		
	BURNOUT	75.8	(167.0)		
	EXPENDED	1045.5	(2305.0)		
	IGNITION	1121.3	(2472.0)		
SECOND STAGE	INTERSTAGE *	86.7	(191.2)	62,720 (14100)	2909 (296.6)
	INERT **	648.5	(1430.0)		
	BURNOUT	1856.3	(4093.2)		
	EXPENDED	2161.9	(4767.0)		
	IGNITION	4018.2	(8860.2)		
FIRST STAGE	INTERSTAGE	–	–	186800 (32000)	2838 (289.4)
	INERT	932.9	(2057.0)		
	BURNOUT	4951.1	(10917.2)		
	EXPENDED	3144.7	(20164.0)		
	IGNITION	14095.8	(31081.2)		

* INCLUDES 3RD STAGE SPIN TABLE
** INCLUDES AVIONICS

FIGURE 5-10

SOLID IUS/TE364-4 PAYLOAD MASS CAPABILITY

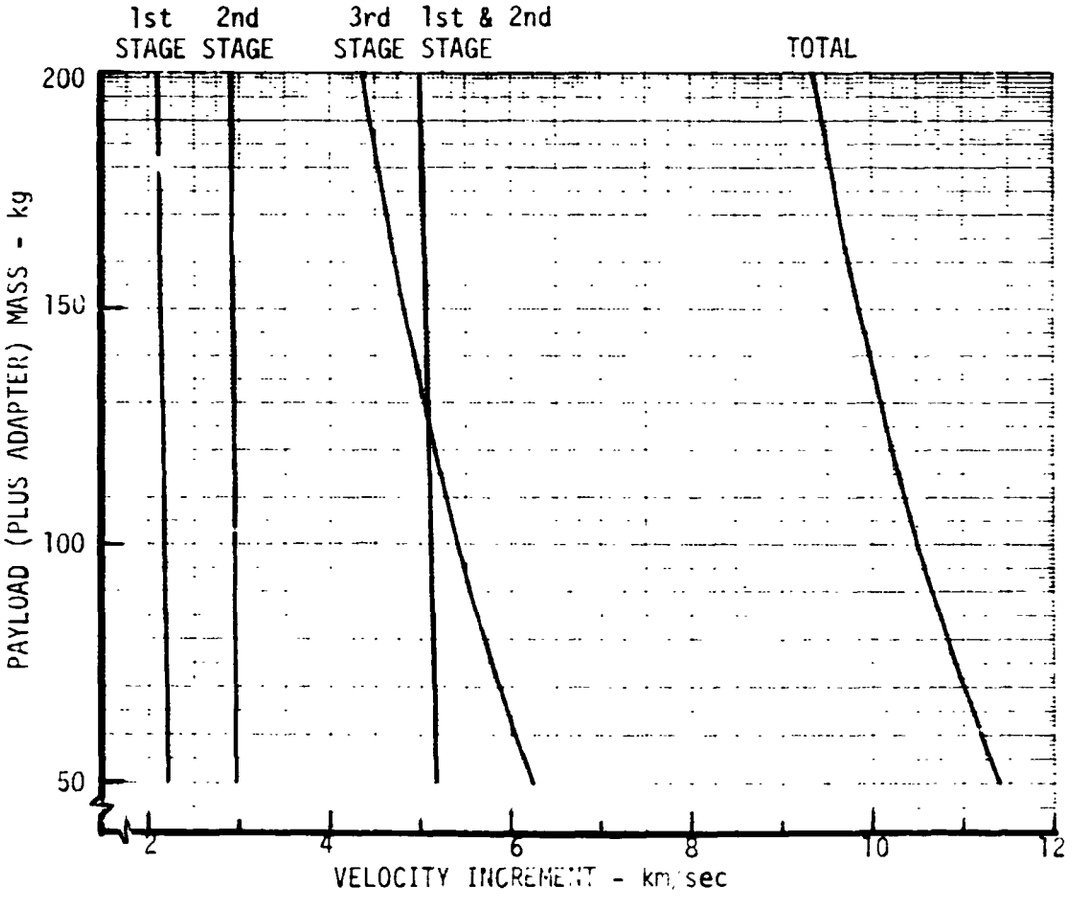

FIGURE 5-11

SOLID IUS/TE364-4 ENTRY CONDITION CAPABILITY

o SINGLE START PER STAGE o IN PLANE MANEUVERS

(a) 100 kg PAYLOAD

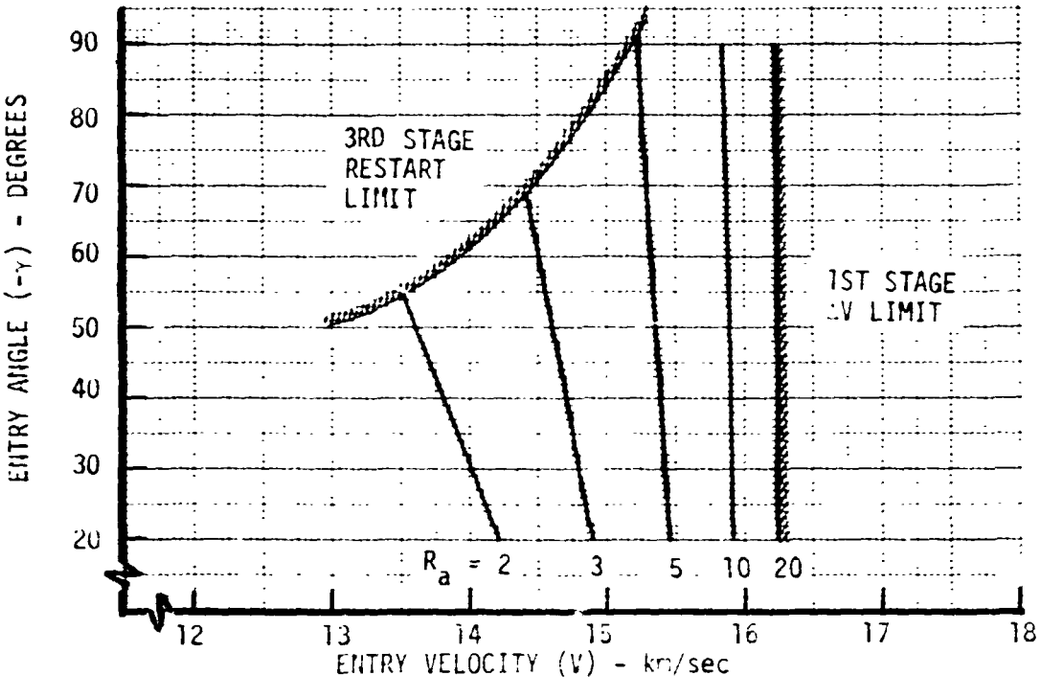

(b) 200 kg PAYLOAD

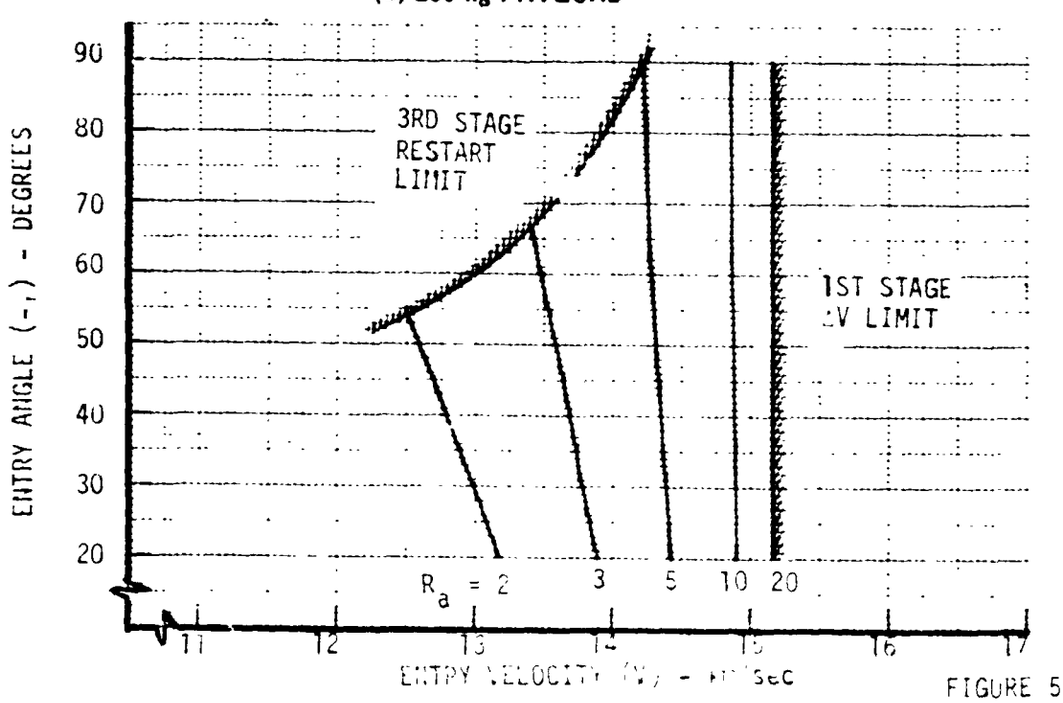

FIGURE 5-12

6.0 REFERENCES

1. Sutton, K., Radiative Heating About Outer Planet Entry Probes, AIAA Paper 75-183.
2. Moss, J. N. and Bolz, C. W. Jr., Viscous-Shock-Layer Solutions with Radiation and Ablation Injection for Jovian Entry, AIAA Paper 75-671.
3. Nicolet, W. E., Aerothermodynamic Environment for Jovian Entry Conditions, AIAA Paper 75-672.
4. The Planet Jupiter (1970), NASA Space Vehicle Design Criteria (Environment), NASA SP-8069, December 1971.
5. The Planet Saturn (1970), Space Vehicle Design Criteria (Environment), NASA SP-8091, June 1972.
6. Myers, H., Models of the Atmosphere of Uranus, McDonnell Douglas Corporation Report E1163 18 October 1974.
7. Saturn/Uranus Atmospheric Entry Probe, McDonnell Douglas Corporation Report E0870, 18 July 1973.
8. Sutton, K., Stagnation Point Radiative Heat Flux for High Speed Earth Entry, received May 1975 (to be published).
9. McNeilly, W. R. (1975), Advanced Shuttle Payloads Sizing Study, MDC E1189 (NAS1-12436), McDonnell Douglas Astronautics Company-East, St. Louis, Mo.
10. Teeter, R. R. et al (1973), Space Shuttle Expendable Upper Stages, BMI-NLVP-TM-73-4, Battelle Columbus Laboratories, Columbus, Ohio.
11. Vetter, H. C., McNeilly, W. R., Siemers, P. M. III, Nachtsheim, P. R., Shuttle Launched Flight Tests: Supporting Technology for Planetary Entry Missions, AIAA Paper 75-1152.